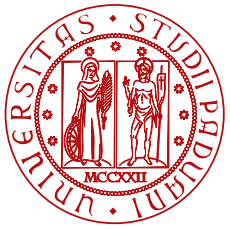

Università degli Studi di Padova

Dipartimento di Ingegneria dell'Informazione

Master Thesis in Bioengineering

Mechanical characterization of a novel dynamic custom ankle-foot orthosis for subjects affected by foot-drop syndrome

Master Candidate

Federica Beghetti

Student ID 2053153

Supervisor

Prof. Zimi Sawacha

University of Padova

Co-supervisor

Ing. Paolo Caravaggi, PhD

Ing. Giulia Rogati

Istituto Ortopedico Rizzoli

Academic Year
2022/2023

Ai miei nonni

Abstract

Ankle foot orthoses (AFOs) are medical devices prescribed to patients with foot drop, a condition consequence to damages or alteration of the central or peripheral nervous system. Foot drop patients show limited or absent active foot dorsiflexion due to weakness of the ankle dorsiflexor muscles. AFOs allow to restore the foot-to-ground clearance in the swing phase of walking and help reducing the risk of stumbling and falling. While standard off-the-shelf AFOs are cost-effective solutions, they can be uncomforatble as they do not always match the patients foot and leg geometry or foot postural alterations, such as severely pronated feet. This can affect the overall quality of life and decrease adherence. Current 3D scanning and manufacturing technologies allow to design and produce custom orthoses that best adapt to the patients morphology.

This thesis was focused on the analysis of a novel passive dynamic custom AFO designed by the researchers of the Movement Analysis Laboratory at the Istituto Ortopedico Rizzoli. The AFO is produced via Selective Laser Sintering of a fiberglass-reinforced polyamide powder. Specifically, this study focused on the mechanical characterization of the novel custom AFOs. The first aim of this thesis was to comprehend which geometrical parameters are associated to AFO stiffness. This objective was addressed by looking for possible correlations between the main AFO dimensions (the predictors) and the experimental-measured AFO stiffness (the outcome variable) in a sample of 8 AFOs produced for 8 patients with foot drop. Eight multiple linear regression analysis models were tested to determine the combination of AFO dimensions most correlated to AFO stiffness. The second aim of this thesis was to estimate the minimum AFO stiffness capable to support the foot and footwear of foot-drop patients in the swing phase of walking. In order to estimate the minimum AFO stiffness, kinematic data from 10 foot-drop patients were used. This data allowed to determine the maximum plantarflexion moment at the ankle in the swing phase of walking. AFO stiffness was here determined as the stiffness allowing a maximum of 1 deg of ankle plantarflexion. All analyses were performed in Matlab.

According to the present study, length, width, and thickness of the AFO calf-shell are the geometrical parameters most correlated to the AFO stiffness. The minimum AFO stiffness to sustain the foot and footwear in the swing phase of walking is about 1.7 N*m/deg.

While data from a larger population are needed to confirm the results of this investigation, this study has the potential to provide useful information to customize the mechanical properties of AFOs according to the degree of deficit of each patient.

Sommario

Le ortesi per piede-caviglia sono dispositivi medici prescritte a pazienti con piede cadente, una condizione conseguente a danni o alterazioni del sistema nervoso centrale o periferico. I pazienti affetti da foot-drop mostrano una limitata o assente dorsiflessione dovuta allinsufficienza dei muscoli dorsiflessori della caviglia. Le ortesi per piede caviglia permettono di ristabilire la distanza piede-terreno nella fase di volo del cammino e aiutano a ridurre il rischio di inciampare e cadere. Sebbene le ortesi per piede caviglia presenti nei modelli standard siano vantaggiose in termini di costi, spesso non si adattano bene alla geometria del piede e della gamba del paziente né alterazioni posturali del piede, come ad esempio piedi affetti da severa pronazione. Ciò può peggiorare la qualità della vita e perciò ridurre lutilizzo. Le tecnologie 3D attuali di scannerizzazione e manifattura permettono di disegnare e produrre ortesi customizzate che si adattano alla morfologia del paziente.

Questo progetto di tesi pone il focus nellanalisi di unortesi piede-caviglia innovativa customizzata progettata dai ricercatori del Laboratorio di Analisi del Movimento dellIstituto Ortopedico Rizzoli. Lortesi piede caviglia è stata realizzata con la tecnica del Selective Laser Sintering a partire da una polvere di poliammide rinforzata con fibre di vetro. In particolare, questo studio si concentra sulla caratterizzazione meccanica di un'innovativa ortesi per piede caviglia customizzata. Il primo obbiettivo di questa tesi è stato comprendere quali parametri geometrici sono associati alla rigidezza dellortesi per piede-caviglia. A questo scopo sono state valutate possibili correlazioni tra le dimensioni dellortesi (parametri predittori) e la rigidezza reale dellortesi (le variabili in uscita) in campione di 8 ortesi per piede caviglia realizzate per 8 pazienti con piede cadente. Sono state testate 8 analisi di regressioni lineare multipla per determinare la combinazione delle dimensioni dell'AFO che sono più correlate alle rigidezza. Il secondo obiettivo della tesi è di stimare la rigidezza minima dellortesi per piede-caviglia affinchè sostenga il piede e la calzatura del paziente nella fase di volo della camminata. Per stimare la rigidezza minima dell'ortesi, sono stati utilizzati i dati di cinematica di 10 pazienti affetti da foot-drop. Questi dati hanno permesso di determinare il massimo momento plantarflettente sulla cavilgia, nella fase di volo del cammino. La rigidezza dell'ortesi è stat determinata come la rigidezza che permette al più 1 grado di plantarflessione della caviglia.

Dallo studio emerge che la lunghezza, larghezza e spessore della parte flettente dell'ortesi sono i parametri geometrici più correlati alla rigidezza dell'AFO. La rigidezza minima dell'ortesi per sostenere il piede e la calzatura nella fase di volo del cammino è di 1.7 N*m/deg.

Nonostante sia necessaria una popolazione maggiore da analizzare, per poter confermare i risultati riportati, questo studio offre importanti informazioni per customizzare le proprietà meccaniche dell'ortesi per piede caviglia, considerando anche il deficit di ogni paziente.

Contents

1 Introduction

1.1 Thesis outline and objective

The foot drop, also known as drop foot, is a syndrome characterised by the inability to lift the foot from the ground. This condition can be caused by various pathologies or alterations of the central and peripheral nervous system such as compressed nerves, brain damages or spinal disorders. This syndrome can cause dragging of the foot and an increase risk of falling due to the weakness of the dorsiflexor muscles. Ankle-Foot Orthoses (AFOs) are orthotic devices often prescribed to foot drop patients to restore a normal foot-to-ground clearance in gait. AFOs are orthotic devices applied to the foot and ankle to sustain the foot during the swing phase of walking. Moreover, dynamic AFOs can be used to reduce the energy cost of walking, storing and releasing energy during the stance phase of gait. Different types of off-the shelf AFOs are available; these are normally available in a limited number of standard sizes, made of wide range of material using standard production technologies. In the last decade, advancements in 3D printing technologies (additive manufacturing), have allowed for the production of custom devices matching the patient's morphology and functional requests. Custom AFOs have been shown to improve comfort and can be designed to address other foot postural alterations and /or ailments.

The "Custom AFO" is a project developed by the Movement Analysis Laboratory of the Istituto Ortopedico Rizzoli in Bologna. The AFO is realized via Selective Laser Sintering, a 3D additive manufacturing technology, using a novel composite fiberglass-reinforced polyamide. Since the AFO has to be customized,

a 3D model of the lower limb and the foot of the patient in weightbearing condition has been used for the production of the custom AFO.

This thesis had two main objectives:

- The first aim was to comprehend which geometrical parameters are associated to AFO stiffness using 8 AFOs designed and produced for 8 foot-drop patients.
- The second aim was to find the minimum AFO stiffness, ddefined as the stiffness required to support the foot in the swing phase of walking.

In order to address the first aim of the thesis, 8 multiple linear regression analysis models were tested to find out the best AFO dimension predictors of AFO stiffness. The best model identified in the analysis will allow to properly dimension the custom AFO according to a specific AFO stiffness prescribed for the patient. . To address the second aim, skin-marker data acquired in static and dynamic conditions in different populations acquired at the Movement Analysis Laboratory were used to estimate the maximum ankle moments in the swing phase of walking.

The thesis is organized as follow. The Introduction section is reporting the anatomy of the ankle-foot complex and its biomechanics, an overview of the movement analysis technique and instrumentations, an explanation of the foot-drop condition, and an overview of the AFO types and of the relevant mechanical properties. The Material and methods section is presenting the populations recruited in the study, the analytical approach to correlate AFO dimensions and AFO stiffness, and the experimental approach for the estimation of the maximum ankle moments in static conditions and in the swing phase of gait. The Results section is reporting all the relevant outcomes of the analyses reported in the previous section. The Discussion is commenting the results and highlights the limits of this study and the future endeavours.

1.2 Anatomy of the foot and ankle joint

The ankle-foot complex is a complicated anatomical region that comprises 28 bones, 33 muscles (both intrinsic and extrinsic), and several tendons and ligaments connecting them. This complex serves crucial functions, including supporting body weight, providing balance, absorbing shock, transferring ground

reaction forces, and compensating for proximal malalignment. A detailed explanation of anatomy and biomechanics of the ankle complex is necessary to comprehend its movements.

Furthermore, the orthotic device investigated in this thesis requires a comprehensive understanding of the ankle joint, its relative bone segments, and the associated muscles to elucidate how an AFO can effectively achieve its goal.

The description of the ankle-foot complex's anatomy is based on 'Gray's Anatomy: The Anatomical Basis of Clinical Practice'. [1].

1.2.1 Anatomical planes

In order to better understand the description of the ankle-foot complex anatomy and its movements, it is useful to explain how we refer to the spatial orientation of the body in space.

Anatomical planes are imaginary planes drawn through the body that divide it into sections. They are helpful for describing movements, positions, and every section of the body objectively. As shown in Figure 1.1, there are three anatomical planes:

- The coronal plane, also known as the frontal plane, is a vertical plane that divides the body into anterior and posterior sections and passes through the body's center of mass.
- The sagittal plane, also known as the anterior-posterior plane, is a vertical plane perpendicular to the coronal plane, dividing the body into left and right sections. It serves as a symmetry plane.
- The transverse plane, also known as the axial plane, is a horizontal plane perpendicular to both the coronal and sagittal planes and parallel to the ground. It divides the body into upper and lower sections.

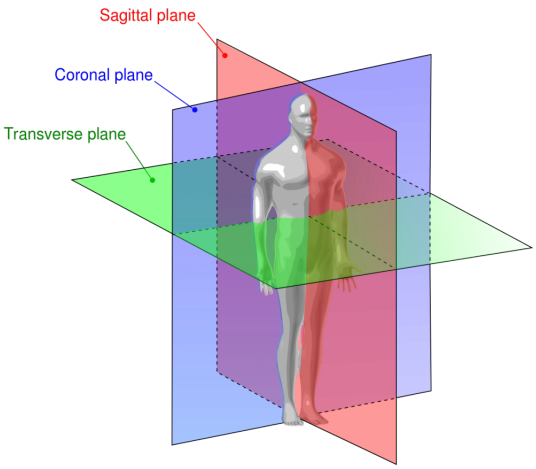

Figure 1.1: Anatomical planes.

There are also three axes around which each body segment can rotate (Figure 1.2). In particular, these are:

- The longitudinal axis, also known as the polar axis, which extends from the top of the head down to the middle of the heels. Around this axis, segments can rotate on the transverse plane.
- The sagittal axis, also known as the anterior-posterior axis, which runs from the anterior part to the posterior part of the body, parallel to the ground. Around this axis, segments can abduct or adduct on the coronal plane.
- The transverse axis, also known as the frontal axis, which passes horizontally from the left to the right section of the body and is parallel to the ground. Around this axis, segments can flex or extend on the sagittal plane..

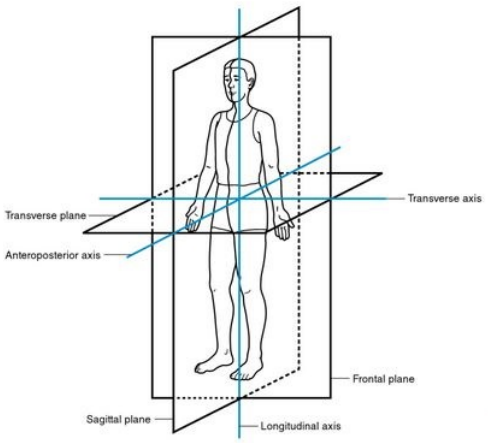

Figure 1.2: Anatomical axis.

1.2.2 Foot bones

The foot is the most distal anatomical district of the body, enabling ambulation and standing while working simultaneously with the other joints of the lower limbthe knee and the hip. Tarsal, metatarsal, and phalanges bones constitute the three main groups of the foot bone skeleton (Figure 1.3). Another crucial anatomical part that requires mention is the lower leg, the area between the knee and the ankle, critical for foot function and the origin of most extrinsic muscles inserting on the foot.

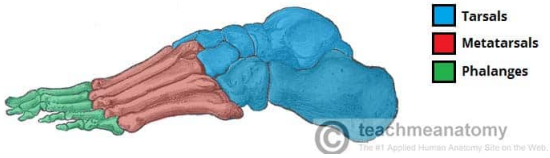

Figure 1.3: Three main groups of the human foot. By ©TeachMeSeries Ltc(2019).

The lower leg consists of two long bones: the tibia and the fibula. These articulate with the talus at the ankle joint and are held together by the tibiofibular syndesmosis, which consists of five ligaments. Typically, the tibia supports about 85% of the body weight, and the fibula supports the remaining 15%

- The **tibia** (Figure 1.4) is a long bone located in the anteromedial part of the leg, being the second longest bone in the human body. Proximally, it articulates with the femur and patella at the knee joint; laterally, it articulates with the fibula at the superior and inferior tibiofibular joints;

distally, it articulates with the talus at the talocrural ankle joint. The tibia has a body and two extremities, proximal and distal. The tibia's proximal extremity is bulkier at the top and has a triangular prismatic shape, with three sides (lateral, medial, and posterior) separated by three margins (anterior, medial, and interosseous). As mentioned earlier, the proximal extremity of the tibia is voluminous and develops in a transversal sense due to the presence of two condyles, lateral and medial. The proximal face of both condyles is coated with hyaline cartilage and constitutes the superior articular face, making contact with femoral condyles. The lateral condyle receives the insertion of the biceps femoris, and the extensor digitorum longus originates from here. Additionally, the tibialis anterior takes origin from the lateral condyle and the upper lateral surface of the fibia, while the semimembranosus takes origin from the medial condyle. Rectus femoris and quadriceps femoris insert proximally on the patella and through the patellar tendon onto the tibial tuberosity, an irregular prominence on the anterosuperior aspect of the tibia. The pes anserinus inserts on the medial upper surface of the tibia, constituting the partially conjoined tendinous insertion of gracilis, sartorius, and semitendinosus. The soleal line, placed posteroproximally, gives origin to the soleus. The popliteus, tibialis posterior, and flexor digitorum insert close to the soleal line. The distal extremity is smaller and ends with a prominence in the medial directionthe medial malleolus. The inferior face of the extremity has a concave articular surface, known as the inferior articular face. The medial face of the malleolus accommodates the flexor tendons, and on the lateral face of the distal extremity, the fibular incision, coated with hyaline cartilage, is visible for the joint with the fibula.

- The **fibula** (Figure 1.4) is a long bone, but it is smaller than the tibia and is located laterally. Its shape is very similar to that of the tibia: it has a body and two extremities, proximal and distal, with a triangular prismatic shape and three sides (lateral, medial, and posterior) separated by three margins (anterior, medial, and interosseous). The proximal extremity is a rounded swelling called the head, with a visible articular surface, the articular face of the head, connected to the lateral condyle of the tibia. In the lateral face of the head, the biceps femoris inserts, while the extensor digitorum

longus inserts onto the anterosuperior surface, and the peroneus tertius originates distally. Between the head and the body, the fibula shows a shrinkage called the neck, where the soleus and the peroneus longus originate. The distal extremity of the fibula forms the lateral malleolus, and the peroneus brevis originates from the lateral aspect of the fibula, near the distal extremity. The extensor hallucis longus has its origin in the middle half of the anterior surface of the fibula and the interosseous membrane. The postero-medial surface of the fibula gives attachment to tibialis posterior and flexor hallucis longus, both ankle flexors.

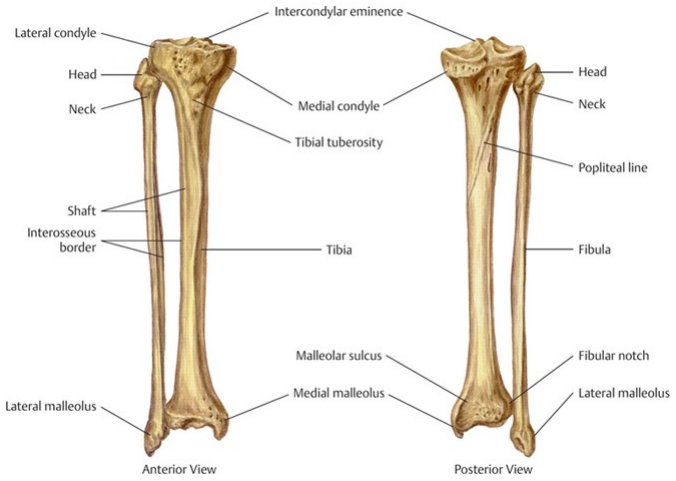

Figure 1.4: The two bones of the lower leg: the tibia and the fibula.

The tarsal is formed by seven irregularly shaped bony elements and constitutes the rearfoot. Tarsals are very important bones since they create a strong weight-bearing platform.

- The **talus** (or astragalus) (Figure 1.5): this short bone transmits body weight to the foot. It has an irregular shape with a visible head, neck, and body. Coated with hyaline cartilage, it articulates superiorly with the tibia and fibula through the tibio-tarsal joint, anteriorly with the navicular through the talonavicular joint, and inferiorly with the calcaneus through the subtalar joint. It has no tendons or muscles attached to it.

- The **calcaneus** (Figure 1.5): this is the largest short bone of the tarsus, with an elongated shape in the anteroposterior direction, forming the posterior

support of the plantar vault. It has six faces allowing articulation with the talus, navicular, and cuboid. The peroneal tubercle on the lateral surface separates the tendons of peroneus longus and peroneus brevis. The Achilles tendon, the largest and strongest tendon in the human body, attaches to the posterior surface. The bone provides attachment to the plantar aponeurosis and other muscles and ligaments.

- The **navicular** (Figure 1.5): this short bone has a flattened oval shape resembling a small boat, placed in the medial side of the tarsal. It articulates proximally with the head of the talus through the talonavicular joint and distally with the three cuneiforms, with the distal articular surface subdivided into three facets, one for each cuneiform bone. The tibialis posterior tendon inserts on the medial side, and the plantar surface is the insertion point for the plantar calcaneonavicular ligament. Other ligaments insert on the superior surface.

- The **cuboid** (Figure 1.5): this short bone, with a cubic shape but six surfaces, articulates proximally with the calcaneus at the calcaneocuboid joint, anteriorly with the fourth and fifth metatarsal bases, and laterally with cuneiforms. The plantar surface has the insertion for peroneus longus and the long plantar ligament.

- Cuneiforms: these are three wedge-shaped short bones placed between the navicular and the first three metatarsal bones. The **medial cuneiform** (Figure 1.5) is the largest cuneiform articulates posteriorly with the navicular, anteriorly with the first metatarsal base, and medially with the middle cuneiform and the second metatarsal base. The peroneus longus tendon inserts on the plantar aspect, as does the base of the first metatarsal, and the tibialis anterior tendon inserts onto the medial surface. The plantar surface, like the other two cuneiforms, is the attachment point for the tendon of the tibialis posterior and the origin of flexor hallucis brevis. The **middle cuneiform** (Figure 1.5) is the smallest of the three cuneiforms articulates posteriorly with the navicular, anteriorly with the second metatarsal base, and medially and laterally with the other two cuneiforms. The **lateral cuneiform** (Figure 1.5), with intermediate dimensions, is the most lateral of the cuneiforms. It articulates posteriorly with the navicular, anteri-

orly with the third metatarsal, medially with the middle cuneiform and the second metatarsal base, and laterally with the cuboid and the fourth metatarsal base.

The metatarsal bones are considered long bones and consist of five units numbered from one to five mediolaterally. They can be divided into three sections: the proximal base, which articulates with the bones of the distal row of the tarsus; the body; and the distal head, which articulates with the proximal phalanges.

- The **fifth metatarsal** (Figure 1.5) is the most lateral metatarsal bone. Its base articulates proximally with the cuboid and the fourth metatarsal base, and distally its head articulates with the base of the proximal phalanx of the fifth toe. The styloid process in the lateral aspect of the base receives the insertion of the tendon of the peroneus brevis, and in the dorsal aspect of the base, there is the insertion of the peroneus tertius tendon.

- The **fourth metatarsal** (Figure 1.5) articulates proximally with the cuboid and the third and fifth metatarsal bases, and distally with the base of the proximal phalanx of the fourth toe.

- The **third metatarsal** (Figure 1.5) articulates proximally with the lateral cuneiform, the second and fourth bases of the metatarsus, and distally with the base of the proximal phalanx of the third toe.

- The **second metatarsal** (Figure 1.5) is the longest metatarsal bone, it articulates proximally with the middle and medial cuneiforms, the first and third metatarsal bases, and distally with the base of the proximal phalanx of the second toe.

- The **first metatarsal** (Figure 1.5) is the shortest metatarsal bone, it articulates proximally with the middle cuneiform and the second metatarsal base, and distally with the base of the proximal phalanx of the hallux. On its base, in the medial side, there is part of the insertion of the tendon of the tibialis anterior, and on the plantar side, there is the insertion for the peroneus longus.

The **sesamoids** are two very small bones located on the first metatarsal, one on the lateral side and the other on the medial side.

The phalanges constitute the skeleton of the fingers and are formed by three bones (proximal, middle, and distal), with the exception of the first toe (or hallux), which is formed by two bones, proximal and distal. This group of bones, considered long bones, has decreasing length and volume from the first toe to the fifth toe. They also have three sections: the head, the body, and the base. In the most distal phalanges, the head is replaced by a wrinkled lamina, the tuberosity, which accommodates the fingernails.

- The **proximal phalanges** (Figure 1.5) articulate proximally with the corresponding metatarsal head through the metatarso-phalangeal joint and distally with the base of the middle phalanges through the interphalangeal joint. The tendon of the extensor hallucis brevis muscle inserts into the dorsal aspect of the proximal phalanx of the hallux. The abductor hallucis muscle has its insertion in the medial aspect of the base of the proximal phalanx of the hallux. The lumbrical muscles have their insertions on the medial surfaces of the proximal phalanges of toes two to five. Dorsal and plantar interossei muscles have their insertions on the medial and lateral sides of the bases of the proximal phalanges of toes two to four. The base of the proximal phalanx of the fifth toe receives the insertion of the abductor digiti minimi on its lateral aspect and that of the flexor digiti minimi on its plantar aspect.

- The **middle phalanges** (Figure 1.5) articulate with the other two phalanges posteriorly and anteriorly through the interphalangeal joint. The tendon of the flexor digitorum brevis muscle inserts onto the medial and lateral sides of the bases and shafts. The central slip of the dorsal extensor expansion inserts onto the dorsal aspect of bases and shafts.

- The **distal phalanges** (Figure 1.5) articulate posteriorly with the middle phalanges through the interphalangeal joint. The tendon of the extensor hallucis longus has its insertion on the dorsal aspect of the base of the distal phalanx of the hallux, while the tendon of the flexor hallucis longus has its insertion on the plantar aspect of the base. The tendon of the flexor digitorum longus has its insertion on the plantar aspect of the bases of the

distal phalanges of toes two to five, while the collateral slips of the dorsal extensor expansion insert onto the dorsal aspect of the same phalanges.

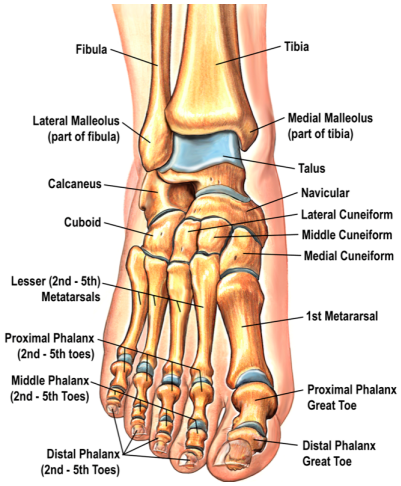

Figure 1.5: Foot bones. Pictures from www.FootEducation.com.

1.2.3 Foot joints

The joints of the foot-ankle complex are as follows: talocrural, intertarsal, tarsometatarsal, intermetatarsal, metatarsophalangeal, and interphalangeal. In total, there are 31 joints that allow connections between the foot bones, even if only a few are considered biomechanically relevant to gait.

The **talocrural joint** (or tibiotarsal joint) is a ginglimo joint, meaning it is a hinge joint that allows plantar and dorsal flexion of the foot in the sagittal plane, which is the main movement. It also allows a small internal/external rotation and adduction/abduction. Connecting the tibia and fibula with the trochlea of the talus, it is commonly known as the ankle joint. Multiple collateral ligaments connecting the tibia with the talus and the calcaneus provide mediolateral stability to the joint.

The intertarsal joints are two joints that allow articulation between the talus and the calcaneus, one placed posteriorly and the other anteriorly. The **subtalar joint** is established between the articular posterior face of the talus and the articular posterior face of the calcaneus, allowing rotation around a single axis. It primarily permits inversion/eversion and dorsiflexion/plantarflexion movements in the transverse plane and some small movements in the sagittal plane.

The second intertarsal joint is the **talocalcaneonavicular joint**, which joins the head of the talus to the superior face of the calcaneus and to the posterior face of the navicular, placed anteriorly. It is a type of enarthrosis joint, allowing inversion/eversion and flexion/extension movements in the transverse plane and small movements in the sagittal one.

The transverse tarsal joint is constituted by a medial portion, the talocalcaneonavicular joint, and a lateral portion, the **calcaneocuboid joint**. This joint is made up by the anterior face of the calcaneus and the posterior face of the cuboid. This saddle joint allows limited rotations, particularly aiding in the medial and lateral rotations of the foot.

Four small arthrodia joints allow small slipping movements. The **cuboidonavicular joint** connects the lateral face of the navicular with the medial face of the cuboid. The **cuneonavicular joint** connects the anterior face of the navicular with the medial face of the cuboid. The **intercuneiform joints** are formed between opposing faces of the three cuneiform bones. The **cuneocuboid joint** connects the medial face of the cuboid with the lateral face of the third cuneiform.

The **tarsometatarsal joints** are arthrodia joints, joining the distal bones of the tarsal (cuboid and cuneiform bones) with the bases of the metatarsal bones. They allow movements of flexion, extension, and small lateral movements of the metatarsal bones, modifying the plantar vault and enabling shape adaptations of the foot.

The **intermetatarsal joints** merge the base of the metatarsal bones, with the exception of the first and second bones bound with an interosseous ligament. They allow small movements of mutual sliding of the metatarsal base.

The **metatarsophalangeal joints** are placed between the metatarsal heads and the base of the proximal phalanges. They are condyle joints, allowing flexion/extension and inversion/eversion of the toes in the sagittal plane. During walking, the main movements of these joints are plantar- and dorsiflexion.

The **interphalangeal joints** are nine trochlea joints (two for each toe except the hallux with one) that join the heads of the phalanges with their base. They allow movements of flexion/extension in the sagittal plane, providing the necessary dorsiflexion range of motion (ROM) for effective grip on the ground at push-off.

1.2.4 Ankle and foot ligaments

Ligaments are strong fibrous structures that bond bones together. Their main function is to stabilize joints and provide support to the foot-ankle complex, working in conjunction with bones, muscles, and tendons. Their crucial role is to prevent excessive movements that could lead to structural rupture.

The ankle includes three groups of ligaments based on their anatomical position: the lateral ligaments, the deltoid ligaments (located on the medial side), and the ligaments of the tibiofibular syndesmosis.

The lateral collateral ligament (LCL) (Figure 1.6) consist of:

- **Anterior talofibular ligament (ATFL)**: made of two bands, originates at the anterior margin of the lateral malleolus and inserts on the talus. Its role is to limit anterior displacement of the talus and ankle plantarflexion.
- **Calcaneofibular ligament (CFL)**; originates from the anterior part of the lateral malleolus and attaches to the posterior region of the lateral calcaneal surface. It allows talocrural joint flexion and extension and subtalar movements.
- **Posterior talofibular ligament (PTFL)**: originates from the malleolar fossa and inserts in the posterolateral talus. It is relaxed in a neutral ankle position and during plantarflexion, and taut in dorsiflexion.

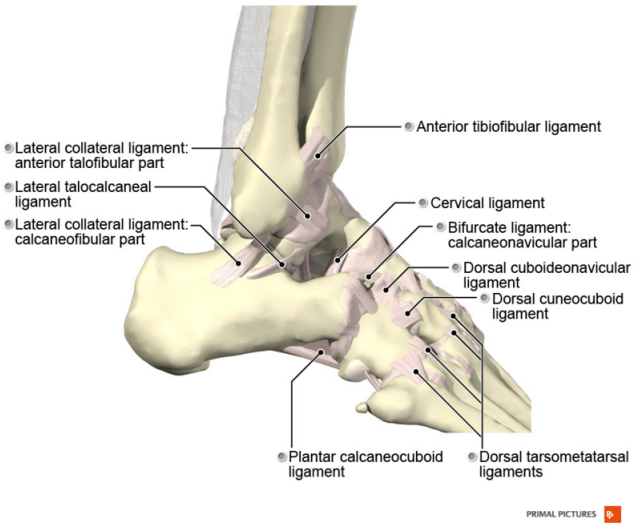

Figure 1.6: Lateral ankle ligament. (Primal Pictures 2020).

The deltoid ligament (Figure 1.7), also known as medial collateral ligaments (MCL), can be divided into a superficial and deep group of fibers as per Milner and Soames [2].

- Superficial: **tibiospring ligament, tibionavicular ligament, superficial posterior tibiotalar ligament, tibiocalcaneal ligament**.
- Deep: **deep posterior tibiotalar ligament, deep anterior tibiotalar ligament**.

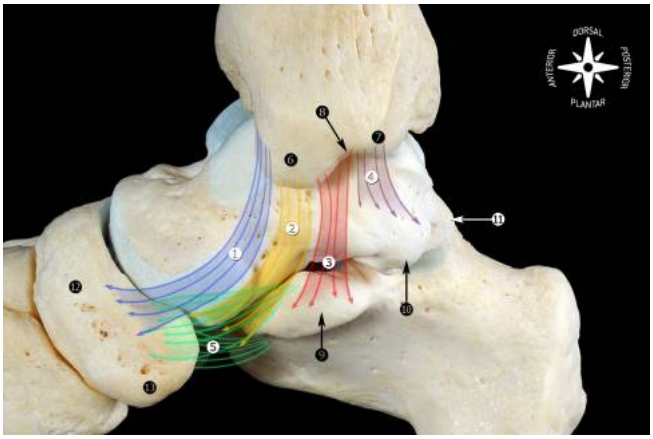

Figure 1.7: The deltoid ligament: 1. tibionavicular ligament; 2. tibiospring ligament; 3. tibiocalcaneal ligament; 4. deep posterior tibiotalar ligament; 5. spring ligament complex (calcaneonavicular ligaments).

The tibiofibular syndesmosis provides medial rotation of the fibula during maximum ankle dorsiflexion and inversion of the fibula during ankle plantarflexion. It also stabilizes the tibia and fibula, including three ligaments:

- **Anteroinferior tibiofibular ligament**: originates at the anterior tubercle of the tibia and inserts at the anterior margin of the lateral malleolus.
- **Posteroinferior tibiofibular ligament**: with the superficial component originating at the posterior edge of the lateral malleolus and inserting at the posterior tibial tubercle, and the deep component originating in the proximal malleolar fossa and inserting at the posterior edge of the tibia.
- **Interosseous tibiofibular ligament**: placed between the tibia and the fibula.

In the foot, three main ligaments are present: the plantar calcaneonavicular ligament (known as the spring ligament), the calcaneocuboid ligament, and the Lisfranc ligaments.

- The **plantar calcaneonavicular ligament** stabilizes the plantar arch in the talocrural joint and supports compression forces. It also limits some movements, such as talus medial rotation, plantar flexion, navicular dorsiflexion, eversion, and abduction.

- The **calcaneocuboid ligament** comprises four ligaments: the medial calcaneocuboid ligament, the dorsolateral calcaneocuboid ligament, the plantar calcaneocuboid ligament, and the long plantar ligament. This complex supports the medial and lateral longitudinal arches.

- The **Lisfranc ligament** originates from the lateral side of the medial cuneiform bone and inserts at the medial side of the base of the second metatarsal bone. It provides stability to the medial column and axial column of the foot arch.

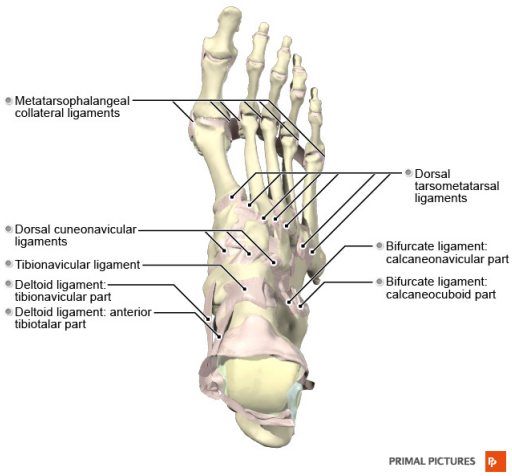

Figure 1.8: Ligaments of the foot-dorsal surface. (Primal Pictures 2020).

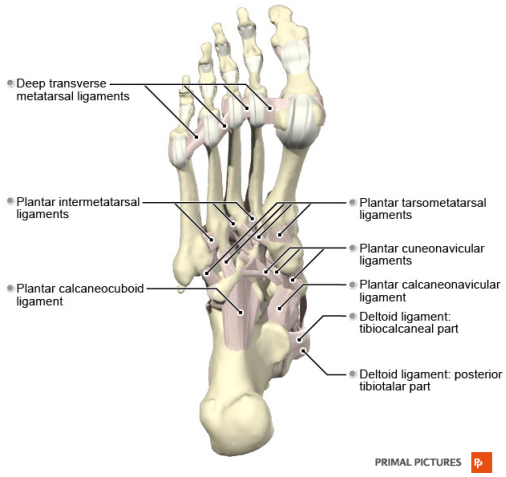

Figure 1.9: Ligaments of the foot-plantar surface. (Primal Pictures 2020).

1.2.5 Plantar fascia

The plantar fascia (or plantar aponeurosis) (Figure 1.10) is a thick fibrous connective tissue that supports the arch of the foot, located beneath the skin on the sole of the foot. It allows flexion of the first metatarsal and provides shock absorption during gait.

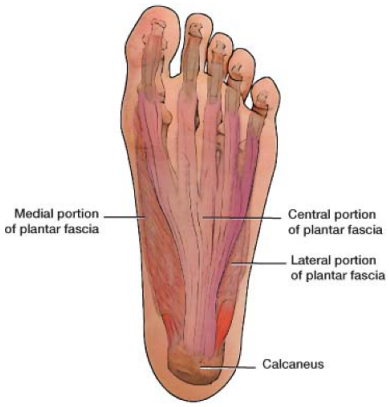

Figure 1.10: Plantar fascia.

The fascia is thicker centrally and thinner along the sides. It can be divided into three parts: the medial, lateral, and central parts. The central part inserts into the tuberosity of the calcaneus and ends in the heads of the metatarsal bones, dividing into five sections. The medial and lateral portions cover the muscles on the sides of the foot.

1.2.6 Intrinsic and extrinsic foot muscles

Foot muscles work with bones, ligaments, and tendons to allow walking, running, and every movement that our foot can perform. They can be divided into two groups: intrinsic and extrinsic muscles.

Intrinsic muscles

The foot has 22 intrinsic muscles that are completely contained within the foot, originating or inserting on the bone, ligaments, or tendons of the foot. Despite being relatively small, these muscles are fundamental for the perfect functioning of the foot [3]. hey are particularly responsible for the fine motor actions of the foot.

Intrinsic plantar muscles are divided into four layers, following the order of exposure during dissection. The first layer (Figure 1.11a), , close to the plantar fascia, includes the abductor hallucis, the flexor digitorum brevis, and the abductor digiti quinti. The second layer (Figure 1.11b)includes the quadratus plantae and four lumbricals. The third layer (Figure 1.11c) includes the adductor hallucis (transverse and oblique), the flexor hallucis brevis, and the flexor digiti quinti brevis. The fourth layer (Figure 1.11d) includes the plantar interossei and dorsal interossei.

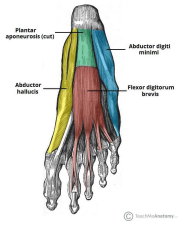

(a) First layer.

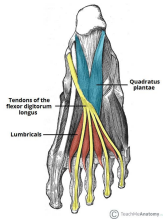

(b) Second layer.

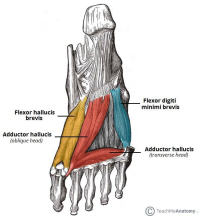

(c) Third layer.

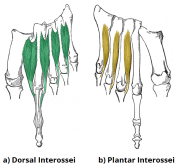

(d) Fourth layer.

Figure 1.11: The four layers of foot intrinsic muscles.

The intrinsic muscles also include dorsal muscles of the foot: the extensor hallucis brevis and extensor digitorum brevis (Figure 1.12).

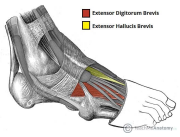

Figure 1.12: The dorsal layer.

Extrinsic muscles

Extrinsic muscles (Figure 1.13) encompass those muscles originating in the leg but are also functional in the movements of the foot and ankle, contributing to the stabilization of the complex. They are grouped according to leg compartments: anterior, posterior, and lateral. These muscles assist in eversion, inversion, plantarflexion, and dorsiflexion of the foot. The anterior compartment includes: anterior tibialis, extensor hallucis longus, extensor digitorum longus, and peroneus tertius. The lateral compartment includes: peroneus longus and peroneus brevis. The posterior compartment includes: gastrocnemius, soleus, plantaris, posterior tibialis, flexor hallucis longus, and flexor digitorum longus.

Figure 1.13: Extrinsic muscles from (a) anterior view and (b) lateral view.

1.3 Biomechanics of the ankle joint

Biomechanics is the science that studies the behaviour of human structures when subjected to forces or moments, in static and dynamic conditions. It is a branch of mechanics that proves useful through the application of mechanical models, specifically a simplified structure that reproduces the anatomical part of interest. This model necessitates the use of rigid bodies, representing segments of the body, connected by mechanical joints that mimic anatomical joints. The union of segments and joints forms the kinematic chain, which is 'open' in the case of the foot because it doesn't have a fixed extremity. Figure 1.14 shows the model of the foot.

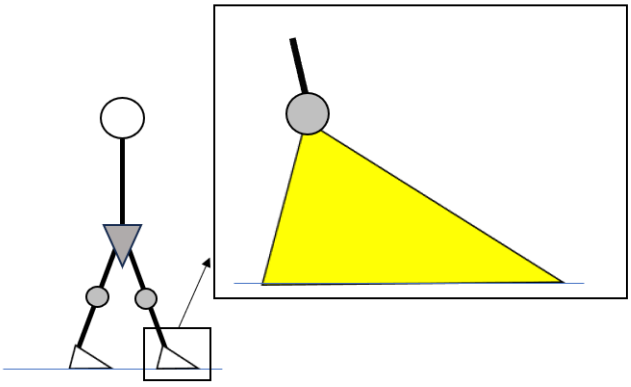

Figure 1.14: Schematic model of the foot.

1.3.1 Ankle forces and moments

The ankle joint plays an important role in walking and maintaining balance, supporting five times body weight during the stance phase of walking and thirteen times body weight during running [4].

Both internal and external forces act on the ankle joint simultaneously. Internal forces result from the action of muscles activated during walking or running. As mentioned earlier, numerous muscles in the foot and leg are involved in gait, each activating at different moments. Figure 1.15 illustrates the muscle activation phases in the lower limb during walking.

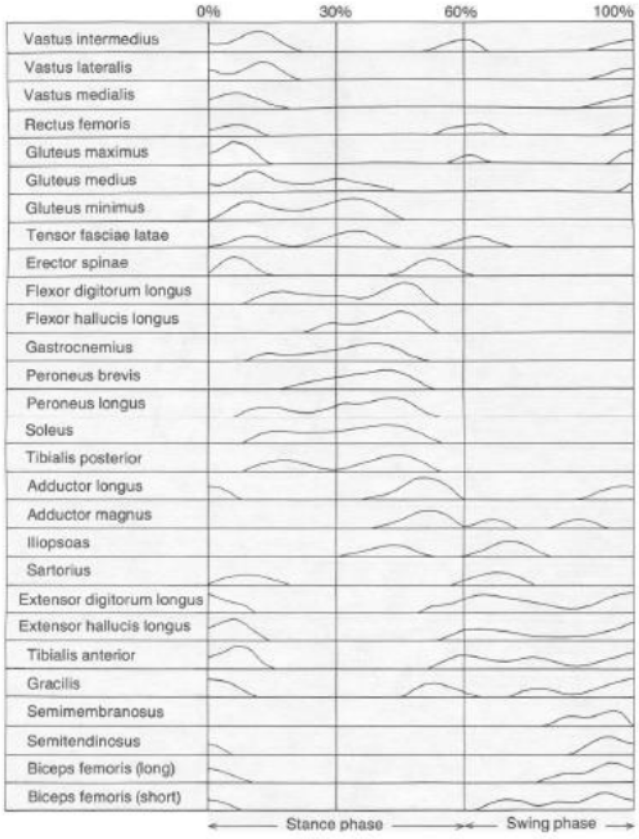

Figure 1.15: Muscle activation in the lower limb during gait. From Vaughan, Davis, & Oconnor, 1999.

External forces arise from the interaction of the foot with the ground, including the force of gravity and acceleration due to inertial forces. The ground reaction force (GRF) is the force exerted by the ground on a body in contact with it. Following Newtons third law, the GRF is equal in magnitude and opposite in direction to the force that the body applies to the ground. The GRF can be split into vertical and tangential components. The tangential components can be further divided into anteroposterior and mediolateral forces, acting respectively along the sagittal or frontal plane. However the tangential component is lower than the vertical component. In Figure 1.16 depicts the trend of the vertical component of the GRF and the centre of pressure (COP) path, where the COP is the point of force application.

During walking, the vertical GRF exhibits two peaks: the first peak, after heel strike, is about 110% of body weight, and the second peak, corresponding to midstance, is around 80% of body weight. The centre of gravity (COG) of

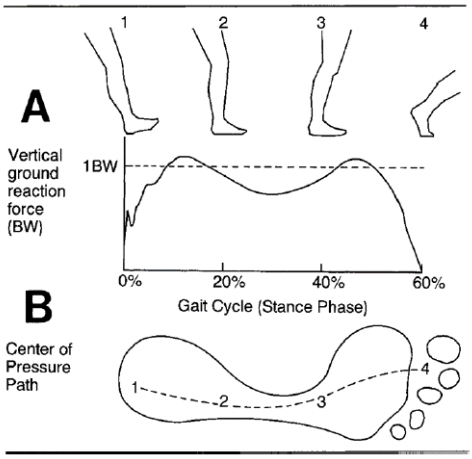

Figure 1.16: A: Graph of vertical GRF during stance phase of gait cycle; B: path of COP. Figure by M. Rodgers in 'Peak Pressure-high Arch during 4 Activities Peak Pressure-flat Arch Durinc' (2008).

the body is lowered during the first peak and lifted during midstance, with the body rotating around the foot. The acceleration due to limb fall occurs when the vertical force exceeds body weight, transferring the weight forward beyond the forefoot. Mathematically:

$$F - w = ma \tag{1.1}$$

where F is the vertical component of the GRF, w is the body weight, m is the mass of the subject and a the acceleration. Now we can express w as the product of m and g, the gravitational acceleration:

$$F = m(g + a) \tag{1.2}$$

In this expression m and g are constant, so the force changes with the acceleration: when $a = 0$, the force is equal to the body weight; when $a > 0$, the force increases, while when $a < 0$ the force decreases. Another important aspect is that the vertical component can be subjected to modification depending on the speed of walking: at high speed the peaks increase and the dips decrease, on the other hand the peaks decrease and the dips became a flattered curve (Figure 1.17).

The GRF is not present during the swing phase since there is no contact of the limb of interest with the ground. During the stance phase, the point of application and direction of the force on the foot are constant in static situations,

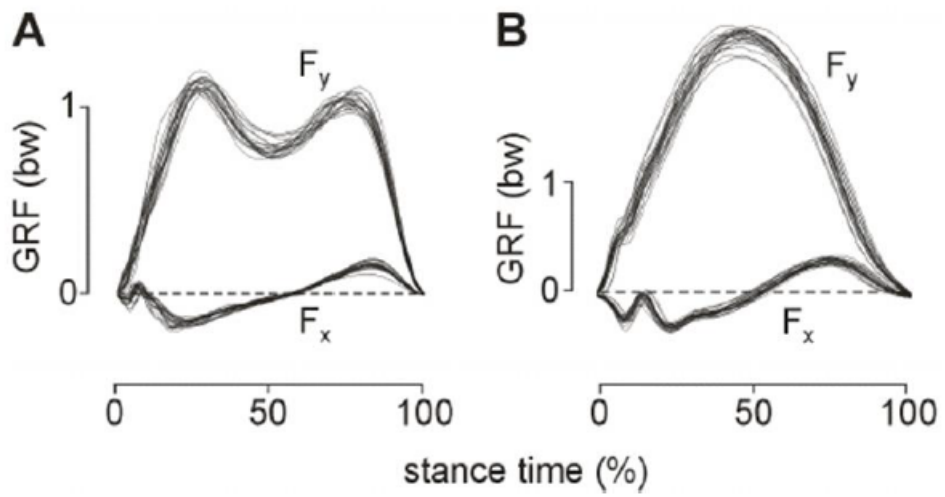

Figure 1.17: A: GRF during walking; B: GRF during running. Figure by Andre Seyfarth in 'Compliant limb behavior: exploiting the basic mechanics of biological legged locomotion for the control of legged systems' (2006).

and the GRF is equal to the body weight. During walking or other activities (dynamic situation) these factors can vary. An external moment occurs when the line of action of the GRF is distant from the centre of rotation of a joint, generating a moment arm or lever arm. The resulting moment increases as the length of the lever arm increases. There is no external moment if the GRF is aligned with the joint center. The equilibrium is achieved when the internal muscle moment balances the external moment, but in dynamic situations, these moments can differ. For instance, during gait, the moment can change, such as from plantarflexion to dorsiflexion, based on the demands of walking (Figure 1.18).

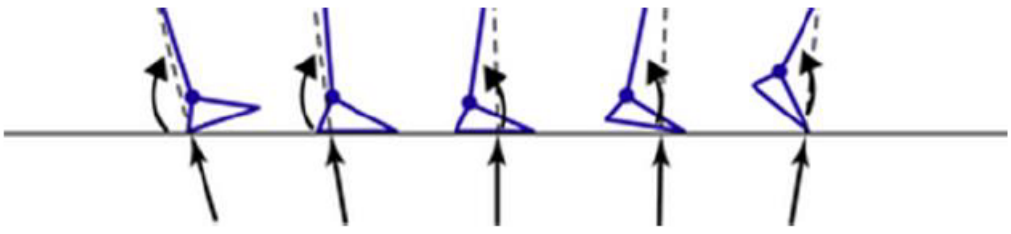

Figure 1.18: Moments at the ankle joint during stance phase.

To minimise the musculoskeletal demand, the GRF should be as close as possible many joints, aiming to minimize external moments as well.

The center of gravity and the axis of rotation of the ankle-foot complex

In the previous paragraphs two important features of the ankle-foot complex have been mentioned: the COG and the axis of rotation of the ankle joint. Both of them are essential for the calculation of forces and moments.

The COG is the point of application of the forces on the foot and it is still a topic of discussion and an open question. Indeed, identifying its position on the foot it is not straightforward and intuitive. In the literature, several studies about body segments characteristics do not report any information about the COG location. Dated articles and books report some information: the location of the COG is a ratio between the distance from the joint axis rotation and the length of the segment length. Clauser et al. [5] reported some values from old papers: Harless et al. [6] (1860) estimated to be between 43.6 and 46, Braume et al. [7] (1889) reported a range of values between 40.4 and 45.3 while Dempstert et al. [8] (1955) reported a value of 42.9. However Clauser et al. in his article positioned the location of the COG considering a ratio of the foot length, in a range between 43.1 and 47.7. According to Dempster et al. [9], Plangenhoef et al. [10] and Drillis and Contini [11], the COG is 28.0% of the foot length from the center of rotation of the ankle, inclined 60.4 deg ° forward from perpendicular to the foots plantar surface.

In more recent years the COG and other inertial parameters are estimated with scaling equations or with multivariate regression equations. Helou et al.[12] propose a multiple non-linear regressions method, using foot length and ankle width. This study leads to a new equation that localize the COG:

$$X_{COG} = K_{COG} + C_{1X\_COG} * L + C_{2\_XCOG} * W \tag{1.3}$$

Where L is foot length, W is ankle width while K_{COG}, C_{1X_COG} and C_{2_XCOG} are the calculated parameters, diversified for male and female.

The axis of rotation is important for kinetic data calculation and it has been studied both in vivo and in cadaveric foot. In this study we are interested in the dorsiflexion and plantarflexion of the foot so the rotation of the ankle in the sagittal plane has been evaluated.

The axis of rotation of the ankle in the sagittal plane is a line that run through the two malleoli as shown in Figure 1.19.

Sometimes subjects present two axis of rotation, one for dorsiflexion and one for plantarflexion [13]. The axis is not parallel to the ground: it is inclined

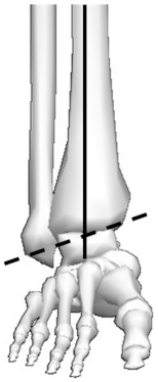

Figure 1.19: The axis of rotation of the ankle joint in the saggital plane

downwards and laterally (Figure 1.20) and downwards and medially (Figure 1.21) [14] in dorsiflexion and plantarflexion, respectively.

Figure 1.20: Inclination of the axis during dorsiflexion

Figure 1.21: Inclination of the axis during plantarflexion

1.3.2 Foot and ankle kinematics

The ankle is a joint that connects the lower limb to the foot and it allows six movements of the foot.

Dorsiflexion and plantarflexion (Figure 1.22) are the most important movements of the foot, crucial for walking. These movements occur in the sagittal plane. During dorsiflexion, the foot moves toward the tibia, with a range of motion (ROM) of 10 deg to 20 deg [4]. Plantarflexion is the opposite movement, where the foot flexes downward away from the tibia. In this case, the ROM is larger due to the involvement of more muscles: 40-55 deg [4]. The axis of rotation for these movements is a line passing through the two malleoli.

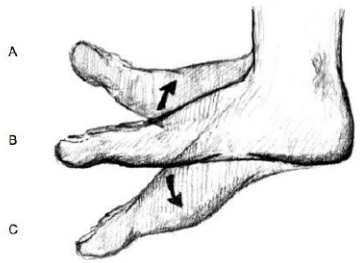

Figure 1.22: A: dorsiflexion; B: neutral position; C: plantarflexion

The foot is capable of side-to-side movements known as inversion and eversion (Figure 1.23), which occur in the frontal plane. Inversion happens when the foot rotates inward and upward, with a maximum movement of 25 deg relative to the neutral position (0 deg), while eversion occurs when the foot rotates outward and upward, with a maximum movement of 15 deg relative to the neutral position.

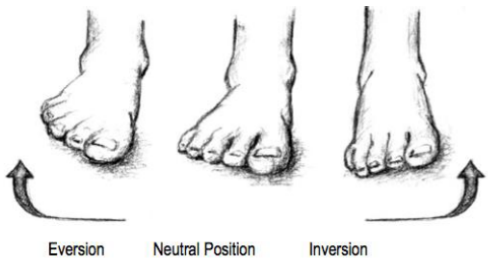

Figure 1.23: Eversion and inversion movements

Abduction and adduction (Figure 1.24) take place in the transverse plane.

Abduction occurs when the foot rotates laterally, moving away from the center, with a maximum movement of 10 degrees relative to the neutral position. Adduction occurs when the foot rotates medially, moving towards the center, with a maximum movement of 20 deg relative to the neutral position.

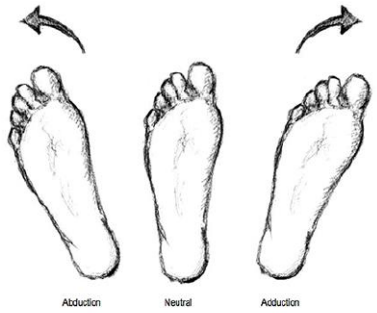

Figure 1.24: Abduction and adduction movements

Supination and pronation are two three-dimensional movements achieved through combinations of the aforementioned movements. Supination is a combination of plantarflexion, inversion, and adduction, with the sole facing medially. Pronation is a combination of dorsiflexion, eversion, and abduction, with the sole facing laterally.

1.4 Gait analysis

Movement analysis is the discipline that describes, analyzes, and defines human movement, with David Winter being a pioneer in this field. His book, "Biomechanics and Motor Control of Human Movement," is widely recognized and popular for movement analysis.

Human movements and posture result from interactions among the nervous, musculoskeletal, and sensory systems, influenced by any forces applied to the body. This precise and coordinated organization makes any small lesion, trauma or injury impactful on movements. Quantitative understanding of each movement can be valuable for studying diseases, evaluating functional limitations, determining treatments, and assessing their effects in patients, making it a crucial tool, especially in clinical applications.

Movement analysis is applicable in various fields, including orthopedic surgery, sports, rehabilitation, physiotherapy, ergonomics, orthotics, and prosthetics. Before the introduction of new technologies facilitating these evaluations, doctors had to rely on visual observation only. However, some dysfunctions may not be easily discernible. Modern technology, such as graphs depicting joint angles or moments, allows doctors to more clearly distinguish between normal and abnormal patterns. It's worth noting that what a patient performs in a laboratory setting may not represent their normality, as they may be focusing on the given task [15].

Walking is the most common motor task and, consequently, the most studied. Gait Analysis (GA) is the methodology that examines body movements and posture, often described as "the systematic study of human walking" [16]. GA typically involves the measurement of joint kinematics (position, velocity, and acceleration) and kinetics (moments and forces). Additional measurements include electromyography (EMG), oxygen consumption, and plantar foot pressures. The main characteristic are [15]:

- Three-dimensionality;
- Non-invasiveness;
- Ability to provide accurate quantitative information;
- Simultaneous acquisition of data on kinematics, dynamics, and muscle activation;

- Ease of use;
- Capability to assess the level of functional limitation and disability due to pathology and its evolution with the growth and/or aging of the individual;
- Evaluation and quantification of the effects of different treatments and monitoring of these effects over time;
- Contribution to treatment planning by drafting a personalized rehabilitation program, allowing objective verification of the patient's clinical status before, during, and after treatment.

1.4.1 Gait cycle

The gait cycle is defined as the period between two successive occurrences of the same event, typically the first contact of one foot with the ground. It can be divided into two main phases:

- The stance phase, beginning when the foot touches the ground and ending when the same foot leaves the ground, comprises 60% of the gait cycle.
- The swing phase, starting when the foot leaves the ground and concluding when the same foot touches the ground again, consists of 40% of the gait cycle.

These phases can be further subdivided into subphases (Figure 1.25) [17]:

- Heel strike, or initial contact, (0-2% of gait cycle): this marks the moment when the foot touches the ground, initiating the first phase of double support. The ankle is dorsiflexed to the neutral position, the knee is extended, and the hip is flexed. Initial contact is made with the heel, while the opposite limb is at the end of terminal stance.
- Foot float, or loading response (2-10% of gait cycle): this occurs as the foot rolls into pronation during double support. The body absorbs the

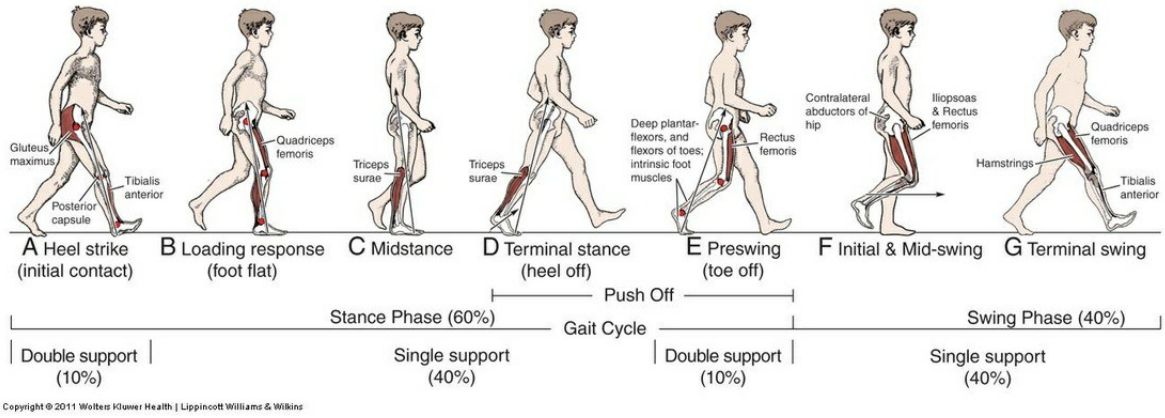

Figure 1.25: The gait cycle. Figure by Physiopedia.

impact with the ground, and body weight is transferred to the limb in the stance phase. The ankle undergoes plantarflexion, the knee flexes to absorb impact, and the hip flexes. The opposite limb is in its pre-swing phase.

- Midstance (10-30% of gait cycle): this marks the first phase of single-limb support, and in the middle of this phase, body weight is entirely supported by one foot. The body starts to move forward with a propulsion force in front of the contact foot. The ankle is dorsiflexed, while the knee and hip are extended. The opposite limb is in its mid-swing phase.

- Heel-off, or terminal stance, (30-50% of gait cycle): this is the second half of single-limb support and begins when the heel leaves the ground. The opposite limb moves forward in the terminal swing phase while the forefoot of the stance leg rolls over. The ankle is plantarflexed, the knee is initially extended and then starts to flex, and the hip is extended.

- Toe off, or pre-swing, (50-60% of gait cycle): this is the second half of single-limb support and begins when the heel leaves the ground. The opposite limb moves forward in the terminal swing phase while the forefoot of the stance leg rolls over. The ankle is plantarflexed, the knee is initially extended and then starts to flex, and the hip is extended.

- Early swing, or initial swing, (60-73% of gait cycle): occurring when the foot is lifted, the limb advances with hip flexion, the knee increases flexion,

and the ankle goes into a neutral position (having a slight dorsiflexion). The opposite limb is in initial midstance.

- Mid-swing (73-87% of gait cycle): this phase occurs as the limb moves forward in front of the centre of pressure. The ankle dorsiflexes to a neutral position, the knee is extended, and the hip increases its flexion. The opposite limb is in late midstance.

- Late swing, or lateral swing, (87-100% of gait cycle): this is the final instant of the swing phase when the swing leg prepares to accept the bodys weight. The ankle remains dorsiflexed to a neutral position, the knee increases its flexion to complete limb advancement, and the hip is flexed. The other limb is in terminal stance.

1.4.2 Gait analysis parameters

The gait cycle is characterized by spatio-temporal parameters that provide important information about the gait and any potential abnormalities. The gait analysis most important spatio-temporal parameters are:

- Stride length [m]: it is the distance between two consecutive heel strikes of the same foot, representing one complete cycle. The stride length should be the same for both feet in a non-pathological subject;

- Step length [m]: it is the distance between the heel strike of one foot and the heel strike of the other foot;

- Stride or step width [m]: it is the distance from the heel to the median line of advancement, considering the frontal plane;

- Foot angle [deg]: it is the angle between the line of advancement and an imaginary line between the midpoints of the calcaneus and the second metatarsal head;

- Step time [s]: it is the interval of time between foot floor contact and foot floor contact of the opposite foot;

- Stride time [s]: it is the duration of the gait cycle, as it is the time interval between two successive foot floor contacts of the same foot;
- Cadence [stride/min]: it is the number of strides per minute;
- Walking speed [m/s]: it can be calculated by multiplying step length by cadence;
- Duration of single and double support [s]: 60% of the gait cycle is characterized by double limb support, while 40% is single limb support. The duration of single support can be helpful in understanding limb support capacity.

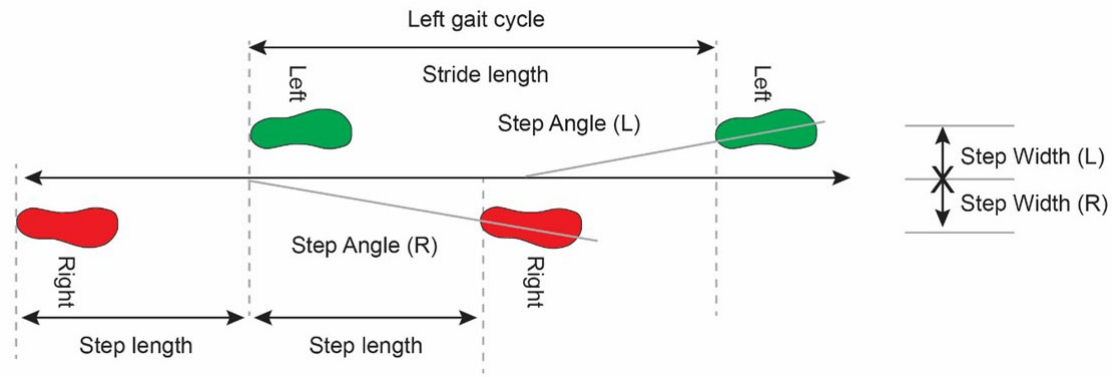

Figure 1.26: Some of the spatio-temporal parameters.

1.4.3 Technology and instrumentation

In the early stages of movement analysis, the only instrumentation used was a camera system, which assisted clinicians in providing qualitative measures. As mentioned earlier, for a precise analysis of human movements and comprehensive study, quantitative analysis is necessary. Even the most advanced camera systems cannot provide information about the forces exchanged with the ground or information on muscular activity. The technologies offered by GA can supply this data objectively, which is another crucial aspect.

The significant advantage is the non-invasiveness of the procedure, making it suitable for children and people with disabilities as well. These technologies are also directly employed in sports fields [18].

Motion Capture (MoCap) is the process of registering human movement (or an object) used not only in medical and sports fields but also in military and entertainment fields. There are different types of MoCap systems [19]:

- Acustical System: it uses sound transmitters positioned on the joints and receptors. The emitters generate frequencies captured by the receptors.
- Mechanical Systems: these systems use electrogoniometers capable of measuring angles, inertial sensors such as accelerometers to measure body acceleration, gyroscopes providing a reference of direction, and optical fibers to detect orientation and displacement of segments. These represent the traditional approach.
- Electromagnetic systems: these systems exploit an external magnetic field generator and electromagnetic sensors positioned on the surface of anatomical segments.
- Hybrid system: this system combines electromagnetic and mechanical systems with a set of accelerometers, gyroscopes, and a portable magnetic system.
- Optical systems: these can be 2D cinema systems or optoelectronic systems. The latter, nowadays the most used in movement analysis laboratories, employs coaxial infrared illuminators with infrared cameras that can detect waves reflected by the markers positioned on a body.

A traditional Movement Analysis Laboratory is equipped with the following instrumentation.

Optoelectronic system based on Stereophotogrammetry (Figure 1.27) has become one of the most utilized systems in a movement analysis laboratory due to its accuracy and precision in reconstructing the instantaneous position of markers. The system uses ground-based cameras and spherical retroreflective markers attached to a body or body region. This is how Vicon (Vicon MX, Vicon, Los Angeles, CA, USA) works, one of the most famous companies that work with optoelectronic systems. Processing software is needed to process the acquired data. The cameras are connected to a computer capable of transforming the emitted signals into spatial coordinates through trigonometric calculations.

Each marker must be simultaneously seen by at least two cameras; however, more than two are recommended. Instrumental errors represent the systematic ones, due to calibration inaccuracies or non-linearity, while random errors can be caused by electronic noise, marker flickering, and marker image shape distortion [20]. Moreover, the accuracy in the detection of markers' position depends on the optical characteristics of the camera system and on the algorithms used for the reconstruction of the markers' trajectories.

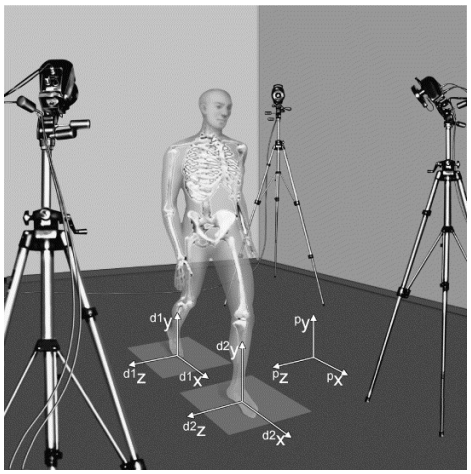

Figure 1.27: Example of optoelectronic stereophotogrammetry

Force platforms (Figure 1.28)) measure the ground reaction forces to the ground produced by the subject during walking. Usually, force platforms are embedded in the floor as not to be visible to the subject, avoiding unnatural movements during walking. Some force platforms give only the vertical reaction; however, the most common platforms provide data on the three components of the force, the coordinates of the center of pressure, and the torque. The system is based on transducers (strain gauges, piezoelectric sensors, capacitance gauges, piezoresistive, etc.); the deformation due to the force applied modifies their electrical properties of the elements and so the electrical output signal, allowing measurements.

Figure 1.28: Force platform

Baropodometry analyzes posture and equilibrium of the subject by acquiring foot plantar pressure data through pressure plates (Figure 1.29). The pressure plates provide the distribution of plantar pressures in a upright position (static) or during walking (dynamic). It also gives the trajectory of the centre of pressure. As with force platforms, different type of sensors can be used: piezoelectric, capacitive, and resistive.

Figure 1.29: Example of pressure platform

Surface electromyography allows the study of muscle activation using electrodes placed on the skin along the muscle fibers. A computerized system acquires the electrical signals of the muscles and provides information about the mechanisms of production of the contractile stimulus and the generation of forces. The exam can be done at rest or during contraction. It is crucial could to understand which muscles are involved in a particular movement.

In brief, the approach to movement analysis is based on inverse dynamics analysis through the analysis of markers' trajectories in space it is possible to estimate the joint angles, while the force plates measure the ground reaction force and the center of pressure; through Newtons laws of motion, it is possible to calculate intersegmental forces and internal moments at the joints.

Figure 1.30: Needle electrodes by Cometa, BTS.

1.4.4 Gait analysis protocols

The protocol for gait analysis defines a biomechanical model and the procedure for data collection, processing, analysis, and reporting of results [21]. It ensures that data acquired and analyzed with the same protocol are comparable, and the measurements are repeatable. It involves the positions of the markers, anthropometric measurements, and the algorithm that calculates the spatio-temporal, kinematic, and kinetic parameters.

Over the years, a few research groups have developed their own protocols to meet their specific requirements. These protocols differ in marker positions, collection procedures, biomechanical models (including degrees of freedom, measured variables, anatomical and technical references), conventions, and terminology. It is clear that comparing data obtained with different protocols can be challenging and, in some ways, incorrect. However, shared data are compared regardless of the protocol applied.

The most widely used protocols to describe the lower limb include:

- Davis protocol used especially in children with cerebral palsy [22].
- C.A.S.T. Protocol (Calibrated Anatomical System Technique) applied to link the estimation of anatomical reference systems with adjacent bone segments [23].

- SAFLo Protocol (Locomotor Functionality Analysis Service) developed at the Bioengineering Center in Milan to obtain kinematics data, joint moments, and powers of the total body [24].
- LAMB Protocol (Laboratory for the Analysis of Movement in Children) developed specifically for subjects in their developmental age[25].
- IOR gait Protocol (Figure 1.31) developed at the IOR research center in Bologna [26].

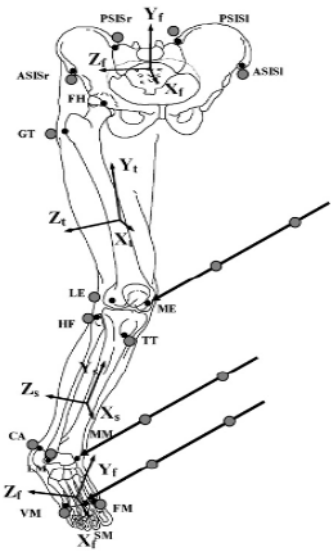

Figure 1.31: The IOR gait Protocol.

- Rizzoli Foot Model also developed at the IRCCS Rizzoli Orthopaedic Institute (IOR) research center in Bologna and focuses on the foot [27].

The protocol used to obtain the gait analysis data used in this project thesis is the IOR gait. A brief description of the anatomical reference systems and measured angles are reported here. The orientation of the anatomical reference system of the anatomical landmarks are defined according to the study of Cappozzo et al. [23] :

- Pelvis (right and left hip bones and sacrum): O_p: the origin is at the midpoint between the anterior superior iliac spines (RASIS and LASIS); z_p: The z axis is oriented as the line passing through the ASISs with its positive direction from left to right; x_p: the x axis lies in the quasi transverse

plane defined by the ASISs and the midpoint between the PSISs and with its positive direction forwards; y_p: the y axis is orthogonal to the xz plane and its positive direction is proximal.

- Right and left thigh: 0_t: the origin is the midpoint between the lateral and medial epicondyles (LE and ME); y_t: the y axis joins the origin with the centre of the femoral head (FH) and its positive direction is proximal; z_t: the z axis lies in the quasi frontal plane defined by the y axis and by the epicondyles with its positive direction from left to right; x_t: the x axis is orthogonal to the yz plane with its positive direction forwards.

- Right and left shank: O_s: tThe origin is located at the midpoint of the line joining the lower ends of the malleoli (MM and LM); y_s: tThe malleoli and the head of the fibula landmarks(HF) define a plane which is quasi-frontal. A quasisagittal plane, orthogonal to the quasi-frontal plane, is defined by the midpoint between the malleoli and the tibia1 tuberosity (IT). The y axis is defined by the intersection between the above-mentioned planes with its positive direction proximal; z_s: the z axis lies in the quasi-frontal plane with its positive direction from left to right; x_s: the x axis is orthogonal to the yz plane with its positive direction forwards.

- Right and left foot (talus + calcaneus + cuboid + navicular + lateral, medial, intermediate cuneiform + metatarsals): O_f: the origin is located at the calcaneus landmark (CA); y_f: the calcaneus and the first and fifth metatarsal heads (FM and VM) define a plane which is quasitransverse. A quasi-sagittal plane, orthogonal to this latter plane, is defined by the calcaneus landmark and the second metatarsal head (SM). The y axis is defined by the intersection of these two planes and its positive direction is proximal; z_f: the z axis lies in the quasi-transverse plane and its positive direction is from left to right; x_f: the x axis is orthogonal to the yz plane and its positive direction is dorsal.

As reported in the article, the convention of Grood and Suntay [28] has been used to describe joint rotations: for the hip and the knee are defined "flexion/extension (Flex/Ext) as the relative rotation about axis e1, taken as the medio-lateral axis (Z) of the proximal segment, internal/external (Int/Ext) rotation

(axis e3) as the relative rotation about the vertical axis (Y) of the distal segment, and abduction/adduction (Abd/Add) as the relative rotation about a floating axis (e2) orthogonal to these two at each collected sample". However for the ankle joint a different terminology is used, respectively dorsiflexion-plantarflexion (Dors/Plan), inversion/eversion (Inv/Ev), and abduction/adduction. Pelvic spatial rotations, including tilt, rotation, and obliquity, adhere to the same convention. This involves computation at the virtual joint formed between the laboratory global frame (considered 'proximal') and the pelvis (considered 'distal'). Beyond the standard calculation of 'absolute angle,' adjustments are made by subtracting the offset derived from the corresponding static posture angle for all joint and pelvic rotations. Joint moments are determined by the vector product of the joint center's position vector and the recorded ground reaction force. The presentation of internal joint moments follows common practice, with the three pertinent components projected within the joint coordinate system (e1, e2, e3).

1.5 Foot drop

Foot drop (also known as 'drop foot') is a foot condition characterized the by insufficient capability or the inability to dorsiflex the foot due to weakness in the dorsiflexor muscles. As a consequence, the patient affected by foot drop cannot lift the forefoot during the swing phase of the walk cycle and has a increased risk for falling. This condition is associated with various pathologies, which will be discussed in detail in the next paragraph. Patients experiencing this issue are compelled to lift their foot off the ground more than normal, leading to compensatory mechanisms at the hip and knee joints. Patients often exhibit hyperflexion at the hip and knee joints and internal rotation of the foot in the transverse plane [29]. These two joints may develop additional conditions due to increased stress and altered mechanics. Furthermore, foot drop can lead to other potentially dangerous consequences, with a significant risk of stumbling and falling.

Foot drop describes weakness in the dorsiflexor muscles of the foot and differs from 'fall foot,' which involves all the muscles below the knee [30].

Figure 1.32: Foot drop.

It can affect individuals of any age, depending on the cause, and both males and females can be equally affected, with an equal likelihood of occurrence. It is referred to as 'bilateral' if the condition affects both feet and 'unilateral' if it affects only one foot.

This condition is not necessarily permanent; it may resolve in days or weeks

if the underlying pathology causing it is treatable. If left untreated, foot drop can cause pain, numbness, and/or tingling.

1.5.1 Etiology

The causes of the foot drop are now described.

Compressive nerves

Foot drop is a condition induced by various pathologies, ranging from muscular to neurological disorders. However, a lesion of the peroneal nerve is the most likely cause of foot drop [30]. This nerve innervates the tibialis anterior, which is the main dorsiflexor muscle. Undoubtedly, a malfunction of this nerve prevents the correct functioning of the muscle. The peroneal nerve, originating as a branch of the sciatic nerve, courses from the back of the knee to the front of the shin and is superficial, near the head of the fibula, making it susceptible to injury. Sports injuries, diabetes, surgery, childbirth, and prolonged improper sitting can damage the nerve.

Other reported nerve compressions include compression palsies in the intensive care unit and sciatic nerve compression, both of which can result in foot drop. Lumbar radiculopathy, especially L5 radiculopathy, the most common lumbar radiculopathy, is another cause of foot drop [31].

Traumatic injuries

Traumatic injuries, such as joint dislocation, fractures, trauma, and general musculoskeletal injuries, can lead to sciatic neuropathy, resulting in foot drop. Lumbosacral plexopathies, caused by traumatic injuries, complications after pelvic surgery, neoplasm complications, or radiation therapy, can also affect nerves in the lumbar or sacral plexus, with some patients exhibiting signs of foot drop [32].

Brain or spinal disorders

Various brain or spinal disorders can also contribute to foot drop:

- Stroke, caused by a blocked blood vessel supplying the brain, affects 1 in 4 people according to the World Health Organization (WHO), with an incidence of foot drop at 3.3% [33].

- Multiple Sclerosis, a chronic inflammatory disease involving progressive demyelination of nerves in the brain and spinal cord, affecting 2.8 million people worldwide [34].
- Cerebral palsy, a condition affecting children in their early years, causes stiff and/or weak muscles, tremors, and other difficulties. It occurs in 4 per 1000 children [35].
- Charcot-Marie-Tooth disease, a group of disorders causing peripheral nerve damage, which can directly affect the nerves controlling muscles, impacting 1 in 3300 people worldwide [36].
- Amyotrophic Lateral Sclerosis (ALS), which occurs when motor neurons degenerate, leading to weakness and eventually muscle atrophy. It affects 1.9 per 100,000 people worldwide [37].

Since the foot drop is not a pathology but a condition due to a more complex disease, it is not possible to talk about 'symptoms.' From a medical standpoint, it is better to discuss the 'signs' of foot drop. These signs can vary widely between patients, depending on the cause, and may appear suddenly or occur gradually. Generally, patients exhibit a different gait, quantitatively visible with gait analysis of the three joints of the lower limb.

The most common signs among patients are as follows:

- Inability to hold footwear, which can occasionally worsen symptoms due to the addition of weight to the foot.
- Tripping, which can occur when the patient is unable to properly lift the foot due to muscle weakness.
- Falls, as well as tripping, are very common and may cause further dangerous consequences.;
- High steppage gait due to compensatory movements, which consist of raising the thigh up in an exaggerated way to avoid hitting the floor while walking.
- Circumduction gait is another compensatory movement to avoid tripping and falls.

- Limp foot ;
- Numbness;
- Often unilateral, particularly if caused by a pinched nerve
- Decrease in muscle mass since patients try to use the affected leg as little as possible and rely on the non-affected leg to support themselves.
- Rombergs sign, which is positive if the patient can stand with his feet placed together and eyes open but falls with his eyes closed [38].

All these signs are mainly due to muscle weakness, which can be evaluated by a physiatrist via manual and visual assessment according to the Medical Research Council (MRC) scale for strenght. The operator grades the patient's foot weakness as follows:

0 = complete paralysis,
1 = flicker contraction,
2 = contraction with gravity eliminated alone,
3 = contraction against gravity alone,
4 = contraction against gravity and some resistance,
5 = contraction against powerful resistance (normal power).

However, this method is not entirely objective, even with a well-trained physiatrist. This prompted the researchers of the Movement Analysis Laboratory of the IOR to set up an apparatus to measure ankle dorsiflexor and plantarflexor forces in a quantitative way. This apparatus, was presented at the 8th International Foot and Ankle Biomechanics (iFAB) congress in Bordeaux, with an abstract titled 'An easy-to-use apparatus to measure ankle dorsiflexor and plantarflexor forces in non-weightbearing conditions: a pilot study in a sample of healthy subjects' Figure 1.33. The apparatus is based on a uniaxial load cell (1 kN) designed to measure dorsiflexion and plantarflexion force in non-weightbearing and quasi-isometric conditions.

During the acquisition, the patient lies supine with the ankle unsupported, and the forefoot is constrained between two rods connected to the load cell. The apparatus was tested on 30 healthy subjects, each applying the maximum voluntary ankle plantarflexion and dorsiflexion force. Two conditions were tested: one with the knee fully extended and one with the knee flexed around 15

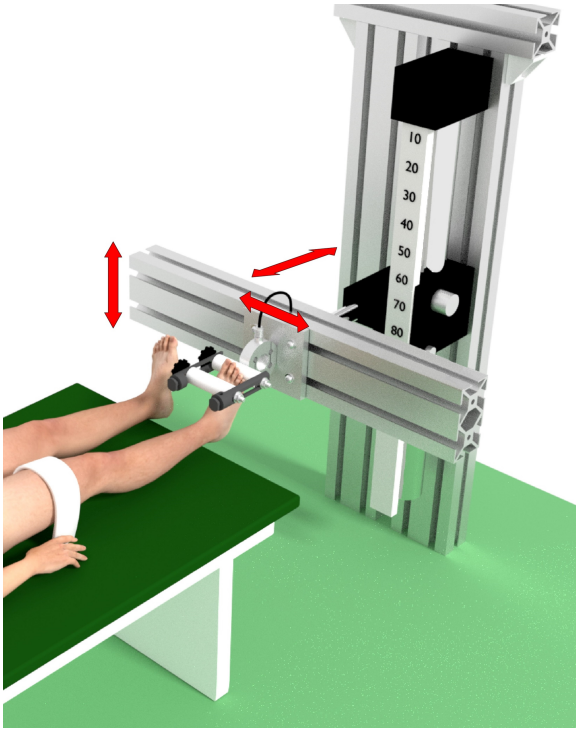

Figure 1.33: The apparatus to test ankle plantaflexion and dorsiflexion forces.

degrees. The dorsiflexion forces measured with this apparatus were comparable to a similar setup, and it was found to be reliable and simple to use.

1.5.2 Treatments

Each patient requires appropriate evaluation and treatment tailored to their specific needs. Nowadays, patients can be treated with different therapies based on the severity of their pathological conditions and the findings from evaluation and diagnosis. In some patients, if the cause of foot drop is successfully treated, the condition might improve or even disappear.

Conservative management

In cases of mild conditions, patients can be treated with a conservative approach to avoid surgeries. The purpose of this approach is to stabilize gait, prevent falls, and minimize further loss of range of motion.

Conservative management includes physical therapy, splinting, or pharmacological therapy to manage pain. Physical therapy is recommended as a conservative approach also after surgery and serves several objectives: reducing

muscle fiber atrophy, preserving ankle mobility, promoting reinnervation after nerve surgery, and improving overall gait steadiness.

In 1961, Liberson et al. [39] demonstrated that electrical stimulation of dorsiflexor muscles might improve foot drop arising from stroke. Taylor et al. [40] expanded on this technique and created an FES-based orthosis, the Odstock Dropped Foot Stimulator (ODFS) . This orthotic has been modified and upgraded and is now known as PACE, a small electrical stimulator. Recently, more wireless devices have been developed. These devices aim to lift the foot at the ankle (similar to other orthotic devices) and provide therapeutic effects.

Different types of orthotics can be employed, such as various braces or splints. Splinting is used to avoid contractures, and the AFO is the most utilized orthosis for drop-foot.

Surgical options

Surgical intervention is necessary in severe trauma cases. In cases of nerve reconstruction or transection, autologous nerve grafts are often performed. In instances of nerve compression, surgeons may prefer to perform neurolysis and nerve decompression, resulting in about 97% of patients showing a restoration of full motor function. The worst-case scenario, involving complete nerve dysfunction, may require nerve and/or tendon transfers.

1.5.3 Biomechanics of foot drop

As previously stated, patients often perform compensatory movements in order to avoid falling and tripping. Compensation is a strategy whereby one aims to counteract, consciously or unconsciously, certain weaknesses, frustrations, desires, or feelings of inadequacy or incompetence in one life area through gratification or excellence in another area [41]. Biomechanically, compensation involves certain actions performed by patients to counteract deficiencies and adapt to the environment with this condition. The degree of compensation depends on the severity of the condition causing these unusual movements.

In general, foot drop patients exhibit indirect compensation, particularly evident in their gait analysis, which shows an increase in the angles of the hip and knee joints. In a study by Simonsen et al. [42] involving 6 male subjects with unilateral foot-drop and 14 healthy subjects (6 males and 8 females), differences

in kinematic parameters of the knee (Figure 1.34) and the hip joint (Figure 1.35) were observed.

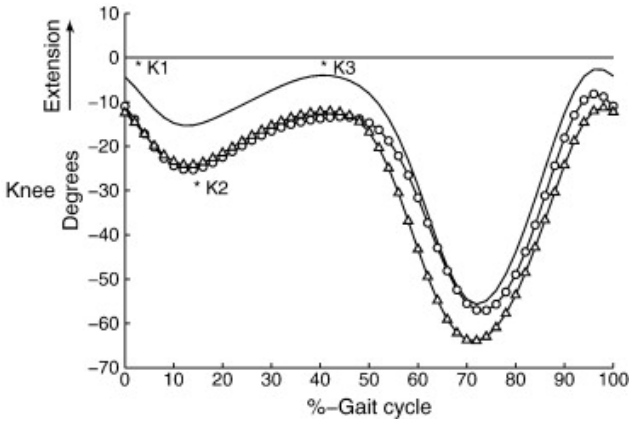

Figure 1.34: Knee joint angles in the saggital plane. Full line denotes healthy subjects, triangles the affected leg of the patients and circles the unaffected leg of the patients.

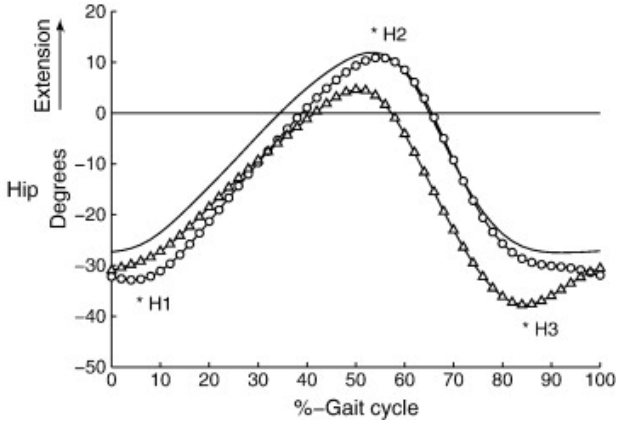

Figure 1.35: Hip joint angles in the saggital plane. Full line denotes healthy subjects, triangles the affected leg of the patients and circles the unaffected leg of the patients.

Focusing on the knee, it is evident that patients with foot drop experience increased flexion of the knee joint, resulting in an elevated knee joint extensor moment. This aspect of the condition is significant, as an increased extensor moment about the knee joint directly leads to heightened bone-on-bone forces in the knee joint [43], potentially leading to osteoarthritis.

Another natural consequence of foot drop is a higher flexion of the hip joint to prevent the toe from striking the ground.

A more interesting approach could involve comparing affected and non-affected joints of the same patient. A study of the Movement of Analysis Laboratory, still under review, has been presented at the XXIII SIAMOC (Società Italiana di Analisi del Movimento in Clinica) in Rome in October 2023, with a cohort of 10 patients with unilateral foot drop to demonstrate the effect of the functionality of a custom AFO during gait. They obtained similar results to Simonsen, showing that patients exhibit higher knee and hip joint flexion in the affected limb as a result of compensation.

1.6 Ankle Foot Orthoses (AFOs)

An orthotic device is defined as an 'externally applied device used to compensate for impairments of the structure and function of the neuro-muscular and skeletal systems' (ISO 8549-1:2020, 3.1.2). There are different classes of orthoses, divided into lower limb orthoses, upper limb orthoses, spinal orthoses, and head orthoses. Orthoses are described with reference to body segments and joints. In Table 1.1, the classification of orthoses with their abbreviations is provided.

Orthoses, regardless of the body section for which they are intended, serve several functions:

- Manage a deformity (prevent, reduce, or hold a deformity).
- Change the range of motion of joint(s) (limit or increase the range of motion).
- Change the dimension of a limb segment(s) (add to the length or improve the shape of a segment).
- Manage abnormal neuromuscular function (compensate for weak muscle activity or control muscle hyperactivity).
- Reduce or redistribute the load on tissues.

To achieve the best results for patients, the use of an orthotic device should be complemented with physiotherapy.

Orthosis can be custom-fabricated namely ' a device that is designed and manufactured to meet the functional requirements of the individual user based

DEVICE	ABBREVIATION
Classes of lower limb orthosis	
Toe orthosis	TO
Foot orthosis	FO
Ankle-foot orthosis	AFO
Knee orthosis	KO
Knee-ankle-foot orthosis	KAFO
Hip orthosis	HO
Hip-knee orthosis	HKO
Hip-knee-ankle-foot orthosis	HKAFO
Classes of upper limb orthosis	
Finger orthosis	FO
Thumb orthosis	TO
Hand orthosis	HO
Wrist-hand orthosis	WHO
Elbow orthosis	EO
Elbow-wrist-hand orthosis	EWHO
Shoulder orthosis	SO
Shoulder-elbow orthosis	SEO
Shoulder-elbow-wrist-hand orthosis	SEWHO
Classes of spinal orthosis	
Cervical orthosis	CO
Cervico-thoracic orthosis	CTO
Cervico-thoraco-lumbo-sacral orthosis	CTLSO
Thoracic orthosis	TO
Thoraco-lumbo-sacral orthosis	TLSO
Lumbo-sacral orthosis	LSO
Sacro-iliac orthosis	SIO
Classes of head orthosis	
Facial orthosis	FO
Cranial orthosis	CO

Table 1.1: Terminology defined in ISO 8549-3

on information such as moulds, models, measurements and images' or prefabricated (off-the-shelf) namely 'a device that has been designed to meet particular functional requirements and is normally available in a range' (ISO 13404:2007).

This thesis focuses on lower limb orthoses, specifically those developed for the ankle joint and foot, known as AFOs. These orthotic devices are prescribed to patients with drop foot and, more broadly, to patients with neuromuscular dysfunctions related to the lower limb and foot. AFOs play a crucial role in controlling ankle joint motion, compensating for muscle weakness, improving

gait functions, and aiding walking [44]. Additionally, AFOs may reduce energy costs and decrease pathological moments at the ankle and knee joints [45].

AFOs are braces that encompass the foot, ankle joint, and lower leg to provide stability and assist in the push-off phase of walking. Typically, patients with drop foot cannot fully lift the foot off the ground due to weakness of dorsiflexor muscles. Moreover, AFOs can potentially store energy of deformation during midstance and release it at the foot-off [46].

In the market, various types and designs of AFOs are available to treat different dysfunctions. Flexibility is a crucial aspect of these devices, and AFO stiffness will be further discussed in the following section.

AFO components are depicted in Figure 1.36. The shoe insert, which constitutes the plantar aspect of the AFO, is designed to fit inside the shoe. The calf shell is secured to the leg with a calf strap.

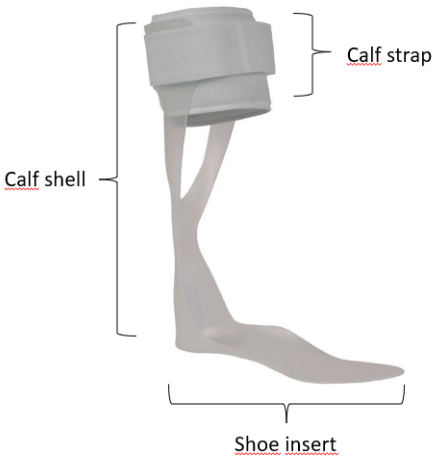

Figure 1.36: AFO components.

1.6.1 Classification

AFOs are classified into three main groups: passive, semiactive and active [47].

- Passive AFO: it lacks electrical or electronic elements or other power sources but can have mechanical elements like dampers or springs..
- Semiactive AFO: it can vary the flexibility of the AFO itself.

- Active AFO: it has a power source, control system, sensor, and actuators that assist ankle movements.

However, passive AFOs are the most commonly employed nowadays due to their simple handling. Semiactive and active AFOs are often heavier due to their power supply and control system, as illustrated in Figure 1.37. Active and semiactive AFOs are primarily used for rehabilitation purposes, while passive AFOs can be used daily with greater ease.

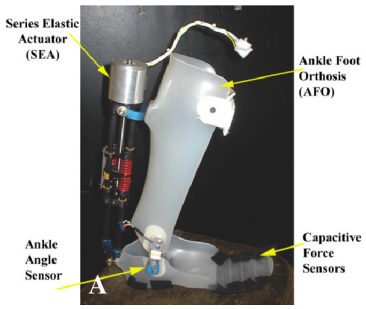

Figure 1.37: Example of an active AFO.

Passive AFOs can be further classified into three more groups: rigid (or solid), hinged and dynamic

Rigid AFO

This type of AFO (Figure 1.38) is characterized by a stiff shell that does not allow any movements, immobilizing the ankle joint completely. Additionally, it prevents all movements of the subtalar and midfoot joints. It is a non-articulated orthosis designed to prevent any movements, covering the back of the lower leg from below the fibular head to the heel. Usually, this type of AFO is prescribed to patients with severe conditions, as the complete locking of the ankle may prevent further pain.

Rigid AFO, one of the first AFO models, supports the foot during the swing phase and does not allow dorsiflexion. While it secures the ankle joint completely, this is also a negative aspect of the device as it can lead to inappropriate contact in the next stance phase [48].Furthermore, Delafontaine et al. [49] demonstrated that rigid AFOs have other side effects, disturbing gait parameters and balance control, and deteriorating the vertical braking action during single-stance.

Figure 1.38: Rigid AFO.

Hinged AFO

Hinged AFO (Figure 1.39) is constituted by two parts hinged together: the calf shell, where the lower limb adheres and is usually locked by a strap, and the shoe insert where the foot rests. This type of AFO allows some movements, preventing excessive ankle plantarflexion during the swing phase but allowing ankle dorsiflexion in the stance phase. The dorsiflexion movements can be adjusted by screwing the hinge in a desirable way.

Figure 1.39: Hinged AFO.

Balaban et al. [50] eported in a study with eleven children affected by hemiplegic cerebral palsy that this type of AFO reduces energy consumption and can control dynamic equinus deformity, an alteration of ankle joint motion. However, hinged AFO is expensive to fabricate, and patients often find it difficult to tolerate due to its shape, which necessitates modifications to the footwear.

Dynamic AFO

The dynamic AFO (Figure 1.40) is the most utilized model due to its simple design, making it comfortable to use. Compared to the other two types of AFOs, its design appears less invasive. A dynamic ankle-foot orthosis was first described by Hylton in 1989 as 'a very thin, flexible supramalleolar orthosis with a custom contoured soleplate to include support and stabilization to the dynamic arches of the foot' [51]. It is called dynamic because, unlike the other two models, it allows some degree of ankle eversion, inversion, plantar and dorsiflexion.

Dynamic AFOs are capable of providing maximum midline stability and movement control while permitting freedom of movements [52]. It is recommended for those patients who have mild foot drop.

Figure 1.40: Dynamic AFO.

It can be compared to a spring: it stores energy during the stance phase, which is then released in the pre-swing phase. There are two types of dynamic AFO: the posterior leaf spring AFO and the ventral shell spring. In the first one, the calf shell supports the lower limb from behind, while in the latter, the support of the leg is in contact with the front part of the tibia.

A study by Erel et al. [53] demonstrated that dynamic AFO allows for a more evenly distributed weight, secure medial-lateral stability, and midline positioning, resulting in better ankle plantar and dorsiflexion. Some types of hinged AFO can also be classified as dynamic AFO, such as spring-hinged posterior shell AFO and spring-hinged ventral shell AFO. Figure 1.41 shows the main types of passive-dynamic AFOs.

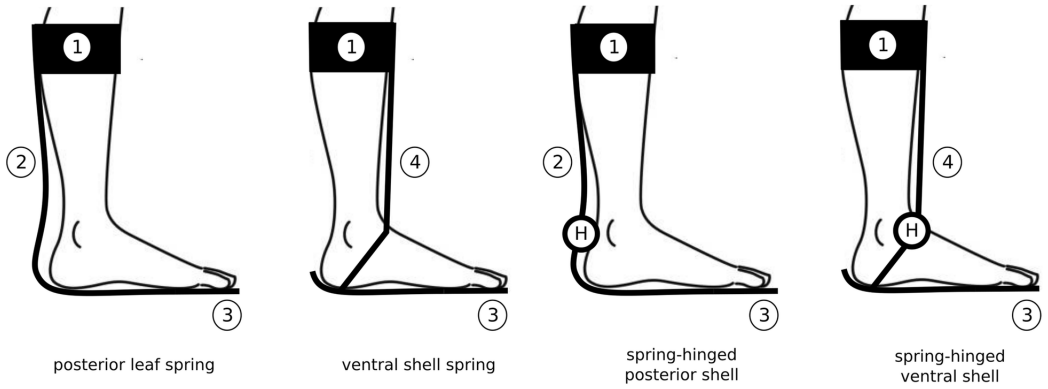

Figure 1.41: The four main type of passive dynamic AFOs. (1) is the calf strap; (2) is the calf shell; (3) is the foot plate; (4) is the ventral shell. H is the fixed-stiffness hinge joint.

1.6.2 Orthotic materials

One of the crucial aspects when designing an AFO, besides its shape, is the material. It influences the stiffness of the orthosis, as well as its durability, fatigue, strength, and corrosion resistance. The choice of material also influences comfort, an important aspect in AFO design as it affects whether a patient will be able to wear the AFO. Material also affects the weight of AFO, which is a crucial conisderation for AFOs designed for children.

An AFO should meet the following requirements [54]:

- Strong enough to provide support
- Flexible to provide comfort while walking
- Breathable to reduce or prevent excessive sweating
- Lightweight to reduce energy exerted while walking
- Thin orthosis to enhance aesthetic looks and easier fitting into clothes
- Easily mouldable for custom made orthosis

It is important to find the perfect material capable of achieving all these aspects.

The materials used for AFO production are:

- Composite materials: these materials are made with fibers submerged in a matrix, usually made with resin. The aim of composite materials is to achieve the best mechanical and physical properties derived from the materials they are composed of. They are the most commonly utilized materials for fabricating AFOs. A study by Sarma et al. [55] selected Kevlar Fiber Reinforced UHMWPE-based composite material as the best option to fabricate AFOs. Two important examples of composites are carbon fiber and fiberglass, even if the former is the most employed according to the review by Rogati et al. [56]. Its stiffness, strength, resistance to temperature and corrosion combined with low density make it the perfect material, particularly for passive dynamic AFOs. Moreover, these materials can be easily used for additive manufacturing (AM), which is the most common method of processing.

- Thermoplastic materials: These materials can be processed with common processing techniques and are easy to work with, making them widely used in producing AFOs. The main advantage of this class of material is that they are deformable but can return to their initial shape when the force causing the deformation stops. They are also resistant and durable. Among thermoplastic materials, some preferred ones include polyamide ([57], [58], [59]), polyurethane ([60], [61]), polycarbonate ([62]) and polypropylene ([63], [64]).

- Metallic materials: these materials are strong and malleable, but due to their high density, they are not suitable for building an AFO. Titanium, stainless steel, etc., are employed for small parts like screws..

- Leather: like metallic materials, leather is used for small parts.

The correct choice of AFO material is crucial and must be considered in terms of functional demands, including flexibility, durability, weight, comfort, and aesthetic acceptability, which is an aspect often neglected.

1.6.3 Manufacturing

Following the choice of the material, it is fundamental to select the proper manufacturing process. Moreover, the entire process must be affordable, fea-

sible, and quick. Clearly, as with any other manufacturing process, AFO fabrication technology has evolved over the last few decades, from conventional manufacturing to 3D printing AM, introduced in the last 20 years. AM has improved the possibility to create more complex shapes that can perfectly replicate patients' lower limb and foot shapes.

AFOs can be prefabricated or custom-made. Prefabricated AFOs are usually available in different sizes to fit a range of patients. However, they do not provide solutions for any deformities or specific requests of patients. This led to the production of custom-made AFOs that can help with a patients specific condition, such as altered foot posture.

The most 3D-printed AFOs are manufactured with two methods: Selective Laser Sintering (SLS) and Fused Deposition Modeling (FDM). There are two other methods, less used by far: Stereolithography (SLA) and Multi Jet Fusion (MJF). These techniques are better described below.

- Selective Laser Sintering consists of fusing or sintering selected areas of successive powder layers using a laser beam. This system is equipped with a deflection system that makes the beam scan the powder according to the CAD model [65]. The object is realized layer by layer, transforming the three-dimensional problem into a bi-dimensional one. The type of powder (plastic, ceramic, etc.), the size of the powder, and the power of the laser beam are factors that can influence the result. In particular, the morphology and granulometry of the powder have an effect on the powder bed density and flowability [66]. This method has important advantages. First of all, the object does not need support, since the powder itself can do it. Moreover, it is a fast and economical process, and durable, functional, and complex parts can be produced. On the other hand, objects are not as smooth as SLA-manufactured objects. The most used materials with this technique are polymers. However, glass, ceramics, and even metals can be employed.

- Fused Deposition Modeling has been applied for commercial purposes since the beginning of the 1990s by Stratasys Inc., USA. The material is melted in a liquid state inside a liquefier head and then deposited through a nozzle following the CAD model, building the object layer by layer [67]. Like other AM manufacturing processes, there are process parameters to

optimize to obtain the desirable final object. This method has similar advantages to SLS: fast production, cost-efficiency, different materials can be used, production of complex components [68]. Despite these advantages, FDM needs a support structure, which means longer production time and waste of material. Moreover, it is less accurate than SLS.

- Stereolithography is a technique introduced in the late 1980s and, besides the numerous AM methods, is one of the most versatile and prevailing [69]. It is widely used in the biomedical field to build patient-specific models, aids for complex surgery, tailor-made parts, and scaffolds for tissue engineering. SLA also uses CAD files to produce parts layer by layer (usually 25-100 μm). This method is based on the solidification of a resin through photopolymerization with a laser beam. One of the biggest limits of the process is the restricted number of resins available for SLA, as they should have precise characteristics: they have to be liquid but with a short time of solidification, with a low molecular weight, with multifunctional monomers, and highly crosslinked.

- Multi Jet Fusion is one of the most recent techniques, emerging in 2014. It is similar to SLS, but it utilizes infrared lamps, instead of a laser beam, to fuse the selected area based on a CAD model; it also needs the use of a fusing agent [70]. MJF is characterized by high printing velocity, dimensional precision, and high quality in printed parts [71].

1.6.4 AFO MECHANICAL PROPERTIES

Certainly, an AFO improves the ambulation of foot drop patients, avoiding dragging of the foot and reducing the risk of falls. However, the orthosis must be comfortable and easy to fit inside the shoe, to ensure good adherence from the patients. Stiffness plays an important role in this context since an increase in the AFOs stiffness often leads to discomfort. Moreover, dynamic passive AFOs are designed for patients with mild foot drop, with the aim of supporting the foot during the swing phase of walking, and an excess of stiffness would lead to improper walking.

Stiffness can be defined as "resistance to sagittal plane rotation, described by the slope of the ankle torque vs. ankle angle curve of an AFO" [72], and it is one of the key aspects when designing this type of orthosis. It is affected by AFO material, shape, and geometry. However, until today, there are no guidelines about the choice for the optimal AFO stiffness for the specific patient. Moreover, AFO stiffness should take into account the deficit of the conditions and patients requests. Commonly, an AFO with higher rigidity is suggested for patients with a severe deficit, but there are no quantitative standards. Moreover, rigid AFOs promote medio-lateral stability but less energy return than more compliant AFOs.

In the literature, stiffness appear to be a less important feature: a review by Eddison et al. [73] reported that only 3.6% of publications about AFOs for children with cerebral palsy inform on stiffness aspects. Nevertheless, AFO stiffness has great relevance, as reported by Totah et al. [72] in a recent review. Increased AFO stiffness may result in reduced ankle range of motion and an increase in knee flexion. The researchers proposed guidelines for future studies:

- Researchers should provide the type, material, pitch, manufacturing method, and torque-angle curve for each AFO used. They should also cite the measurement instrument and technique used to obtain those curves.

- AFO stiffness should be measured in both plantarflexion and dorsiflexion directions, and the speed of flexion testing should be reported.

- Participants should be tested at both prescribed and self-selected walking speed to facilitate inter-subject comparisons.

- Detailed descriptions of subject characteristics should be provided, including noting any contractures.

- Each subjects raw data, including preferred walking speed, rather than across-subject averages, should be provided to allow deeper analyses for individual stiffness effects.

- Considering AFO-footwear interaction effects, authors should note the type, make, and model of the footwear used with the AFO. When possible, we recommend standardizing footwear across participants.

In conclusion, we can say that stiffness must meet specific patient biomechanical needs.

In the literature, several methods for the AFO stiffness evaluation have been proposed.

The Bi-articular Reciprocating Universal Compliance Estimator (BRUCE) is a device that can determine AFO characteristics [74]. The design is based on a rappresentation of the human leg and foot, and it can manually replicate ankle dorsiflexion and plantarflexion movements to deform the AFO. Meanwhile, forces and deformation are recorded and post-processed. The AFO angle-moment relationship is implemented with a linear model, and ankle stiffness is determined through a linear fit of the mean of the moments.

The AFO Stiffness Measurement Apparatus (SMApp) [75] is a different device that measures torque and angle while the AFO is moved at a certain speed in a defined range of motion. Stiffness is obtained from the torque-angle curve. Shuman et al. [76] compared five methods for evaluating AFO stiffness: the already mentioned BRUCE and SMApp with the Kentucky Stiffness Tester (KST) and the device for Evaluating Mechanical Properties In Rotating Exoskeletons (EMPIRE). The last method is manual. First of all, the authors underline how fixtures and alignment can differ between the five methods and could affect stiffness. Other aspects such as the footplate clamping block, the surrogate shank height, and total deflection were different among methods and contributed to inter-method differences in AFO stiffness. However, these limitations do not appoint one method better than another.

At the Movement Analysis Laboratory of IOR, an apparatus to determine AFO mechanical properties has been implemented [77]. This device uses a servo-hydraulic machine and allows applying a displacement-controlled rotation of to AFO shell, to simulate dorsiflexion and plantarflexion movements. Stiffness is then calculated as the slope of the torque/angle curve. The apparatus resulted easy to use, adaptable to different AFO models, and appeared as an improvement with respect to other devices presented in the literature. This device will be further explained in detail in the Materials and Methods chapter.

As stated before, there are no precise guidelines to design the optimal stiffness for the specific patient. Usually, stiffness is assigned taking into consideration the patient's body weight and is based on the experience of the clinicians.

In some studies, the optimum AFO stiffness was defined by analyzing kinematics, kinetics, and gait parameters of patients wearing AFO with different

stiffness levels. However, this method is neither cost-effective nor time-saving. The goal is to determine the optimal AFO stiffness for the specific patients before its production, based on a gait analysis evaluation. Alternatively, an AFO with adjustable stiffness could be used, but it is possible with hinged AFO only.

Waterval et al. [78] developed an optimization method to select the correct AFO stiffness. They analysed kinematic data of patients wearing AFOs with varying stiffness levels. Using the gait results and patient characteristics, they developed a musculoskeletal model capable of calculating the optimal AFO stiffness for a new patient.

AFO stiffness values are still an open question even if it is an extremely important aspect of an AFO that could influence, as we have seen, a lot of factors. Further investigation needs to be done in this field.

2

Material and methods

In this section, the main steps to produce a custom-made passive dynamic AFO (PD-AFO) using a fiberglass reinforced polyamide (Windform®GT, CRP Technology, Modena) will be explained in detail. Subsequently, the mechanical properties of the AFO will be analyzed, focusing on the stiffness and the determination of the minimum stiffness. A brief description of the laboratory instrumentation used to obtain the gait analysis data will be also provided.

2.1 Foot-drop patients

The study received approval from the Ethical Committee of the hosting institution (No. 0016384, 23 December 2019), and patients provided informed consent to participate to the study. Patient selection was based on the following inclusion criteria: foot-drop condition due to nerve compression at the lumbosacral region of the spine, insufficiency of the ankle dorsiflexor muscles, and an agreement to wear the custom AFO for at least 6 months. Exclusion criteria encompassed severe degenerative disease, disorders of the central nervous system, and/or BMI>30 kg/m^2. Information about the selected patients is presented in Table 2.1.

2.1.1 Clinical evaluation

Clinical evaluations of patients were conducted through a questionnaire on ankle or foot discomfort and general conditions. This was performed before the

Patient ID	Age [years]	Height $[cm]$	Weight $[kg]$	BMI $[kg/m^2]$	Shoe size	Affected foot
2	68.2	180	83	25.6	44	left
3	77.5	195	96	25.2	45	right
4	50.3	184	95	28.1	45	left
6	49.5	183	97	29.0	45	left
8	57.3	183	85	25.4	45	left
9	63.0	178	94	29.7	43	left
10	69.9	175	76	24.5	40	left
11	73.6	172	80	27.0	44	right
13	56.9	178	77	24.3	41	left
14	82.9	159	59	23.3	39	left
Mean ± std	64.9 ± 11.4	178.7 ± 9.3	84.2 ± 12.0	26.2 ± 2.1	43.1 ± 2.3	/

Table 2.1: The patients of the project study.

gait analysis and before wearing the custom-made AFO. The Manchester Oxford Foot Questionnaire (MOxFQ) [79], a 16-question validated patient-recorded outcome measure (PROM) for foot and ankle surgery, was used. Each answer was scored from 0 to 4, and scores for each item were categorized into three domains: walking/standing problems (seven items), foot pain (five items), and issues related to social interaction (four items). The scores were then converted into a new scale ranging from 0 to 100.

2.2 Custom AFO production

Modern additive manufacturing technologies are utilized to produce a custom AFO, relying on the three-dimensional model of the orthosis. The scanning of the foot and leg of the subject is crucial for the AFO design. The goal is to create a lightweight and comfortable AFO that supports the foot during the swing phase of gait while being easy to wear. To adress the specific patient's needs, the AFO footplate can be customized to conform to the sole of the foot, in order to correct foot posture issues such as hyper-pronation or supination. The calf shell is curved on the transverse plane to provide rigidity and ensuring a rigid

rotation around an axis aligned and close to the real ankle joint axis. Furthermore, the cross-section of the calf shell is designed to offer sufficient stiffness to support the foot during the swing phase of gait, with a thicker section at the bottom. The lower part of the calf shell is equipped with a hole to avoid interference with the posterior aspect of the calcaneus.

The AFO must withstand ankle joint plantarflexion moments caused by weight and inertial forces acting on the foot and footwear to support the foot in the swing phase during walking.

The following sections describe the main steps for custom AFO production, while the feasibility of the procedure has been tested in a previuos study [80].

2.2.1 3D scanning of the foot and lower limb

Since the three-dimensional design of the custom AFO relies on the morphology of the patient's foot and leg, the initial step in the production process involves scanning the patient's affected foot and leg in a weight-bearing condition. The scanner utilized is based on the low-cost Microsoft Kinect depth sensor [81]. The Kinect sensor is an RGB-depth camera (Figure 2.1) that can simultaneously capture depth and color images of the environment. It employs a laser emitter, an infrared camera, and an RGB camera to generate a 300,000-point cloud 3D image of the scanned object at a maximum of 30 frames per second (fps).

Figure 2.1: The Kinect sensor camera.

The sensor is positioned inside a box, with a scanning glass at the top where the patient stands (Figure 2.2). The sensor is situated above a rotating plate, manually rotated during scanning to provide a complete visualization of the sole of the foot. The acquisition time is approximately 25 s.

To acquire and post-process the raw 3D data, the software Skanect for Windows was utilized. The Kinect is then used to scan the patient's leg by manually

Figure 2.2: The Kinect-base 3D scanner.

moving the sensor around the leg. To create the complete scan, the scans of the feet and legs are merged (Figure 2.3).

Figure 2.3: The scan of the foot and the leg combined together.

2.2.2 AFO 3D DESIGN: MORPHOLOGICAL APPROACH

The 3D model of the patient's leg is imported into Blender (Blender Foundation, Amsterdam, Europe), an open-source 3D software used for modeling, animation, and rendering. In particular, the WASP Med Blender Add-on, designed for modeling orthoses in the medical sector, is used for designing the orthosis. Blender allows both manual and real-time control of freeform geometries, enabling the operator to refine the device with parametric and manual editing to achieve a fully customized design based on the patient's anatomy.

The AFO is adapted to the morphology of the patient's lower limb, which is imported as a .stl file. This enables the design of a fullt customized AFO for the patient.

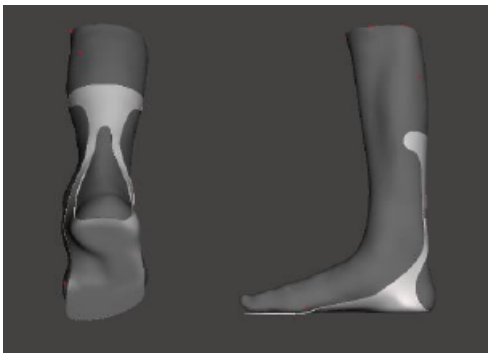

Figure 2.4: From left to right: posterior and lateral view of AFO with lower limb.

In this stage, careful attention to specific details of the AFO structure is crucial to prevent discomfort and pain for the patient. First and foremost, meticulous consideration should be given to the footplate, ensuring it accurately reproduces the sole of the patient's foot and addresses any supination or pronation issues. Another critical aspect is the posterior hole, which could potentially cause skin irritation through friction. Ensuring a perfect anatomical fit at the calf strap is also essential to guarantee the proper fixation of the AFO to the leg.

The .stl file of the 3D model of the AFO is then utilized to produce the orthosis using AM.

2.2.3 AFO Manufacturing via Selective Laser Sintering

The .stl file of the custom AFO is sent to CRP Technology (Modena), a company specialized in producing high-performance products through AM, primarily for the automotive and aerospace sectors. Currently, their only medical application is the Custom AFO.

The custom AFO is produced via SLS using an innovative fiberglass-reinforced-polyamide-based powder (Windform®GT, CRP Technology). This material is primarily utilized in the automotive and motorsport sectors for applications requiring flexibility and impact resistance. The material has obtained safety certification for contact with the skin, a crucial factor in a medical application. It is also ductile, waterproof, and non-electrically conductive. The main parameters of the material are reported in Figure 2.5. The flexibility of the material

makes it suitable for the application. Furthermore, the AFO must withstand fatigue cycles resulting from walking. However, this type of material is capable of enduring such cycles, as long as the AFO is used appropriately.

WINDFORM® GT

Technical Specifications & conformity

	Test Method	SI Unit	US Unit
General Properties			
Density (20 °C/68 °F)		1,19 g/cc	1.19 g/cc
Colour		BLACK	BLACK
Thermal Properties			
Melting point	ISO 11357-2	193,0 °C	379 °F
HDT, 1.82 Mpa	ASTM D 648 TYPE B	169,4 °C	337 °F
Vicat 10N	ASTM D1525-09	188,9 °C	372 °F
Flamability Properties			
Burning Test - HB 1mm	UL 94	HB	HB
Burning Test - HB 3mm	UL 94	HB	HB
Mechanical Properties			
Tensile Strength	UNI EN ISO 527-1	56,21 Mpa	8150 psi
Tensile Modulus	UNI EN ISO 527-1	3289,80 Mpa	477 ksi
Elongation at break	UNI EN ISO 527-1	14,82 %	14.82 %
Flexural Strength	UNI EN ISO 14125	87,90 Mpa	12700 psi
Flexural Modulus	UNI EN ISO 14125	3227 Mpa	468 ksi
Impact Strength Unnotched (Charpy 23°C)	UNI EN ISO 179-1	54,28 KJ/m²	25.8 ft-lb/in²
Impact Strength Notched (Charpy 23°C)	UNI EN ISO 179-1	8,69 KJ/m²	4.14 ft-lb/in²
Hardness Shore D	UNI EN ISO 868	79	79
Compression Strength	ASTM D695-10	90,8 Mpa	13169.43 psi
Compression Elastic Modulus	ASTM D695-10	4,00 Gpa	580.15 ksi
Electrical Properties			
Resistivity, Volume	ASTM D257	2,62 x 10^15 ohm*cm	2.62 x 10^15 ohm*cm
Resistivity, Surface	ASTM D257	1,02 x 10^16 ohm	1.02 x 10^16 ohm
Surface Finish			
After SLS Process		6,20 Ra µm	6.20 Ra µm
After manual finishing		1,45 Ra µm	1.45 Ra µm
After CNC machining		1,15 Ra µm	1.15 Ra µm
Properties per Density Unit			
UTS per density unit		47,24 Mpa/(g/cc)	6850 psi/(g/cc)
Tensile Modulus per density unit		2764,54 Mpa/(g/cc)	401 ksi/(g/cc)
Flexural Strength per density unit		73,87 Mpa/(g/cc)	10700 psi/(g/cc)
Flexural Modulus per density unit		2711,76 Mpa/(g/cc)	393 ksi/(g/cc)

Figure 2.5: Technical sheet of the Windform®GT

2.3 Custom AFO mechanical properties

Before being used for the patients gait analysis functional evaluation, the custom AFO is mechanically evaluated at the Medical Technology Laboratory of IOR to etimate AFO stiffness.

2.3.1 Experimental measurements of AFO stiffness

To determine AFO stiffness, a new setup has been developed at the Medical Technology Laboratory of IOR in collaboration with the Movement Analysis Laboratory [77].

Figure 2.6: The new setup to determine AFO stiffness with an AFO positioned.

The apparatus is based on an axial-torsional testing machine (Biaxial 858 Mini-Bionix, MTS System Corp., Eden Prairie, MN, USA), which simulates the AFO during the midstance phase of walking (Figure 2.6). The footplate of the AFO is fixed to a rigid wall, while the actuator is aligned to the ideal ankle joint axis. The anatomical proportions considered are: the vertical distance from the footplate is 21% of the foot length, and the horizontal distance from the calf shell plane is 25% of foot length [82]. The actuator replicates the leg and consists of an aluminum rod with a plastic cylinder, which is free to translate and rotate around the rod in frictionless conditions. The AFO calf strap constricts the superior part of the AFO calf shell on the cylinder. The apparatus works in angular displacement control, with a maximum of 15 deg° in flexion. The actuator is connected to a torque cell that measures the AFO-resisting torque. The test is repeated five times in dorsiflexion and five times in plantarflexion

with a 15 deg° rotation applied at 15 deg°/sec speed. The stiffness is calculated as the slope of the angle-torque curve.

2.3.2 Correlation between AFO dimensions and AFO stiffness

The first aim of this thesis is to correlate the AFO stiffness with its dimensions, so it is important to understand which are the relevant dimensions of the AFO. In order to correlate the geometric characteristics to the mechanical properties, a simplified model of the AFO has been created: the AFO support (calf shell) is considered as a cantilever beam fixed at one end, where a force can be applied at the free end. However, this method leads to values of AFO stiffness inconsistent with those measured in the laboratory using the dedicated apparatus (the 'real stiffness'). This is due to the fact that the proposed scheme does not consider the curvature of the calf shell in the transverse plane, a curvature that allows the AFO to flex around the ankle axis.

Considering that developing a model with these characteristics can be complicated due to the shape of the calf shell and the two rods, a new method has been developed in order to correlate AFO stiffness and its dimensions (reverse engineering). The only dimension that is not correlated to the length of the foot is the maximum thickness of the calf shell. This section will explain a method to quantify this dimension.

Until now the dimensions are determinated as described below:

- the length of the calf shell is 60% of the length of the foot;
- the width of the calf shell is 20% of the length of the foot;
- the thickness of the foot plate goes from 2 mm at the forefoot to 2.5 mm at the rearfoot.

For this purpose, 8 AFOs which were already produced for 8 patients have been selected. Over the years, the design of the custom AFO developed at IOR has been modified: in the list below, the different versions developed during the years are reported with their main properties and differences. Version 2.2 has been taken into consideration for this study.

- Version 1.0: It is characterized by an anterior or posterior calf shell; the calf shell is curved in the transverse plane, and it has a large longitudinal opening in the calf shell.

- Version 2.0: It is characterized by a posterior calf shell for better comfort in the contiguous tissues; the calf shell is curved in the transverse plane, and it has a small longitudinal opening in the calf shell to improve strength and stiffness.

- Version 2.2: It is characterized by a posterior calf shell; the calf shell is curved in the transverse plane, and the opening of the calf shell is 40% of the calf shell itself so that the bending axis is closer to the ankle joint axis. Foot plate thickness varies from 2.5 mm at the rearfoot to 2.0 mm at at forefoot for good posterior strength and larger anterior flexibility.

- Version 3.1: It is characterized by a posterior calf shell with a straight squared section to facilitate the calculation of the bending stiffness, and the opening of the calf shell is 40% of the calf shell itself. Foot plate thickness varies from 2.5 mm at the rearfoot to 2.0 mm at at forefoot for good posterior strength and larger anterior flexibility.

- Version 3.2: It is characterized by a posterior calf shell with a straight squared section; the opening of the calf shell is 40% of the calf shell itself. Foot plate thickness varies from 2.5 mm to 2.0 mm.

- Version 3.3: It is characterized by a posterior calf shell and a larger leg fixation shell to increase stability and comfort. The width of the calf shell is 20% the length of the foot for aesthetic purposes and to facilitate fit. Foot plate thickness varies from 2.5 mm at the rearfoot to 2.0 mm at at forefoot for good posterior strength and larger anterior flexibility.

AFOs from patients 2, 9, 10, 11, 13, and 14 have been used, considering that patient 2 developed bilateral foot-drop. The eighth AFO was produced for a new patient external to the clinical trial, which was already concluded. This patient presents unilateral foot drop due to Amyotrophic Lateral Sclerosis. Her information is reported in Table 2.2.

Plantarflexion stiffness has been taken into consideration since patients apply plantarflexion movements on the AFO because they are not able to dorsiflex the foot. AFO stiffness has to oppose the force and moment caused by this movement.

Patient ID	Age $[years]$	Height $[cm]$	Weight $[kg]$	BMI $[kg/m^2]$	Shoe size	Affected foot
15	57	158	56	22.43	38	right

Table 2.2: Information of patient 15

AFOs dimensions

The first step of the procedure was to measure the dimensions of each orthosis. The software Rhinoceros (version 7, Robert McNeel & Associates) was utilized to measure the AFO's dimensions from the CAD model used for manufacturing. This software allows the measurement of the section or length of interest. For some dimensions, multiple measurements were taken, and the mean was calculated. In Figure 2.7 , the .stl file of an AFO imported into Rhino 3D is shown.

Figure 2.7: Visualization of an AFO on Rhino 3D

The measured dimensions, considered relevant for calculating the stiffness, include the length of the calf shell (Figure 2.8), width of the calf shell (Figure 2.9), maximum thickness of the calf shell, width of the rods, and thickness of the rods (Figure 2.10). To measure the width and thickness of the rods consistently across all AFOs, measurements were taken 5 mm below the posterior hole.

With these dimensions, other relevant parameters have been calculated: the moment of inertia of the calf shell and the moment of inertia of the rods. Additionally, to understand if there is a linear, quadratic, or cubic correlation between the dimensions and the AFO stiffness, the quadratic and cubic values of the calf shell maximum thickness and the rod thickness have been calculated.

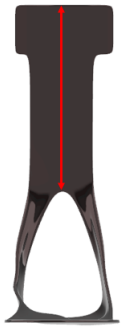

Figure 2.8: Length of the calf shell.

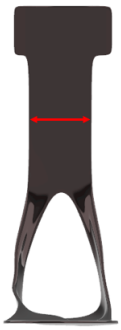

Figure 2.9: Width of the calf shell.

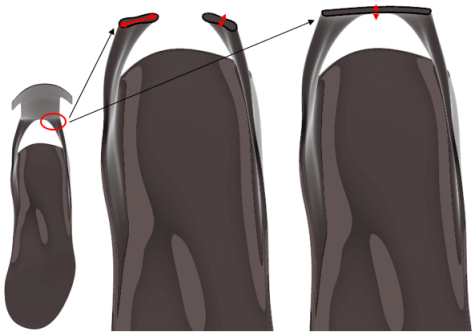

Figure 2.10: From left to right: width of the rod, thickness of the rod and the maximum thickness of the calf shell.

Different models have been tested to determine the best one.

- The **linear model**: in this model all dimensions are linear.
- The **quadratic model**: in this model, the calf shell maximum thickness and the rod thickness are quadratic, while all other dimensions are linear.
- The **cubic model**: in this model, the calf shell maximum thickness and the rod thickness are cubic, while all other dimensions are linear.
- The **moment of inertia of the rod model (A)**: this model, the rod thickness is cubic since it is the measure that is cubic while calculating the moment of inertia of the rod; all other dimensions are linear.
- The **moment of inertia of the rod model (B)**: in this model the moment of inertia of the rod has been included, calculated as:

$$BM = \frac{1}{12} * t_{rod}^3 * w_{rod} \tag{2.1}$$

  Where t_{rod} is the thickness of the rod and w_{rod} is the width of the rod. All the other dimensions are linear.

- The **moment of inertia of the calf shell model (A)**:in this model, the calf shell maximum thickness is cubic since it is the measure that is cubic while calculating the moment of inertia of the calf shell; all other dimensions are linear.
- The **moment of inertia of the calf shell model (B)**: in this model the bending moment of the calf shell has been included, calculated as:

$$BM = \frac{1}{12} * t_{shell}^3 * w_{shell} \tag{2.2}$$

  Where t_{shell} is the maximum thickness of the calf shell and w_{shell} is the width of the calf shell. All the other dimensions are linear
- The **moments of inertia model**: in this model, both the moment of inertia of the rod and the calf shell have been included, calculated as already shown; all other dimensions are linear.

Both the moment of inertia of the rod and the moment of inertia of the calf shell have been considered because the AFO bends in a region near the superior part of the hole. However, the exact point is not clear. Therefore, the stiffness could be correlated with both of these quantities.

Linear and multilinear regression analysis

The objective is to create a model that can predict the AFO stiffness based on the dimensions of the orthosis. The equation of the model would be similar to the following one:

$$Y = \beta + \alpha_1 * x_1 + \alpha_2 * x_2 ... + \alpha_n * x_n \tag{2.3}$$

Where Y is the AFO stiffness, β is the intercept, α are the coefficients and x are the dimensions or the calculated quantities.

Through a multilinear regression analysis, the intercept and the coefficients α have been calculated, using the FITLM function on MATLAB. This analysis has been done for each model explained before. This function receives the real stiffness and the dimensions as input parameters. The output of the function are the intercept and the coefficients α.

The MATLAB code used is reported in Appendix A.

Statistical analysis

The FITLM function in MATLAB allows for the calculation of some important parameters related to statistical analysis to choose the best model. The selected parameters include the percentage error of the predicted stiffness with respect to the real stiffness estimated in laboratory, the root-mean-square error (RMSE), the p-value, the R^2 and the adjusted R^2 of the model.

The percentage error of the real stiffness and the predicted one helps understand 'how far' the calculated stiffness is from the real one. The RMSE indicates the mean quadratic discrepancy between the observed stiffness and the calculated one. The p-value of the model indicates the level of significance of the model itself, determining if the obtained data are repeatable; generally, significance is high if the p-value is lower or equal to 0.05. The coefficient of determination R^2 indicates if the linear regression model chosen can be further used to predict different data; if R^2 is close to 1, it means that the independent

variables can fully explain the dependent variable. The R^2 is used when the model has too many independent variables.

2.4 Gait analysis of foot-drop patients

In order to analyze the AFO functional outcome in terms of comfort for the patients and spatiotemporal, kinematic, and kinetic data, a gait analysis session is necessary. Once the AFO has been produced and its mechanical properties have been tested, each patient in the study is asked to walk along a 10 m pathway, in the Movement Analysis Laboratory, in three different conditions: wearing the footwear (without AFO), referred to as the 'shod' condition, wearing a Codivilla spring (Ottobock), and wearing the custom AFO. The next section will discuss the procedure and instrumentation employed for the AFO functional evaluation.

2.4.1 Laboratory instrumentation

IOR's Movement Analysis Laboratory is equipped with a Vicon 612 stereophotogrammetric system (Vicon Motion Capture, Oxford, UK), comprising eight M2 optoelectronic cameras sampling at 100 Hz. Reflective markers are applied to the patient on anatomical landmarks following the IOR gait kinematic protocol [26], specifically designed for the lower limb. The cameras are strategically positioned to ensure that each reflective marker is visible to at least 2 cameras simultaneously. The system registers the 3D trajectories of each marker. These data are post-processed to obtain angles, torque, and power of joints. It is important to note that these measurements may be influenced by imprecise marker positioning on the subject's anatomical landmarks and soft tissue artifacts, potentially leading to inaccurate kinematic data.

Two force platforms (Kistler Instruments, Winterthur, Switzerland), model 9281, equipped with piezoelectric sensors sampling at 2000 Hz, have been used to measure ground reaction forces during gait. These platforms are embedded in the floor to ensure that patients do not make any forced movements over them. These provide information on the vertical, medio-lateral, and antero-posterior forces components of the ground reaction force, as well as moments and coordinates of the center of pressure. Throughout the gait cycle, both the right and left feet step over the two force platforms.

Figure 2.11: IOR movement analysis laboratory.

A set of wireless surface electromyographic sensors (Zerowire, Cometa, Milan, Italy) sampling at 2000 Hz is utilized to quantify muscular activation during walking. These sensors are applied to both lower limbs to record the myoelectric activity of the tibialis anterior, gastrocnemius, rectus femoris, and biceps femoris muscles.

During a gait analysis, all of this instrumentation is employed, and data on kinematics, forces, and myoelectric activity are collected. However, in this thesis, since the objective is to determine the forces during the swing phase to calculate the moment on the ankle joint, the focus is primarily on kinematic data.

2.4.2 Experimental data collection

As explained in section 1.6.2, patients are clinically evaluated by clinicians according to the MRC scale. The patient is instructed to exert maximum force in ankle plantarflexion and dorsiflexion against the resistance applied manually by the clinician. In this way, plantarflexion and dorsiflexion residual forces are evaluated. The scale ranges from 0 (no contraction) to 5 (normal muscle activity). According to inclusion criteria, patients must be evaluated with a dorsiflexion muscular force $\leqslant 3$.

Since the AFO is completely customized, it is important to evaluate the plantar foot shape and morphology. For this purpose, a podoscope highlighting patients' footprint in weight-bearing is used. This evaluation allows assesing the foot shape and classifiying the foot as cavus, normal, or flat. This assessment is

necessary to identify any potential foot posture alterations that can be addressed by shaping the AFO footplate.

The first step of the gait analysis is to record the static position of the markers while the patient is standing still in an upright position for a few seconds. The neutral angles at all joints are calculated.

The patient is then asked to walk at self-selected speed along the pathway in the laboratory in three different conditions: shod, wearing a Codivilla spring, and wearing the custom AFO. For each condition, five trials are executed. The patient is required to complete a visual analog scale (VAS) to assess comfort at the plantar foot-plate, the calf shell, the overall comfort, and the perceived support during the pushing phase while wearing the two AFOs.

For the purpose of this thesis, the gait analysis of the shod condition only has been evaluated.

2.4.3 Data processing

After the acquisition, gait analysis data are organized into .csv files, subdivided for each walking trial and each condition. Each file includes spatiotemporal data, trajectories of the markers in the three spatial directions, electromyographic muscular activation data, and ground reaction forces. For this study, trajectories of the markers and spatiotemporal data related to the custom AFO condition and the static data have been utilized.

Converting .csv file

All data for each trial of each patient are collected in a .csv file, the most popular format for exchanging data. It represents data in a table where each row corresponds to a specific instant, and each column corresponds to a specific marker. While this format is very suitable for displaying data, it can be a little confusing because data representing different aspects (kinematics, muscular activity, etc.) are all grouped together and can be dispersed due to the large file size.

A new script has been developed by Ing. Paolo Caravaggi and Ing. Silvia Tamarri to organize data in a more structured manner. They created a structure in Matlab where, for each selected .csv file, data are subdivided into spatiotemporal data, gait events, kinematics data, force plate data, and EMG data (Figure 2.12) .

Fields	name	SPATEM	GAITEVENTS	KIN	FORCEPLATE	EMG
1	'C:\Users\fe...	*1x1 struct*	*1x1 struct*	*1x1 struct*	*1x1 struct*	*1x1 struct*
2	'C:\Users\fe...	*1x1 struct*	*1x1 struct*	*1x1 struct*	*1x1 struct*	*1x1 struct*
3	'C:\Users\fe...	*1x1 struct*	*1x1 struct*	*1x1 struct*	*1x1 struct*	*1x1 struct*
4						

Figure 2.12: Example of the structure created with the script.

Spatiotemporal data contain information about the time of stance, time of swing, stride length, and other important gait analysis parameters. The gait events section reports the instant of foot strike and foot off. Kinematics data are reported in the 'KIN' section, which includes marker trajectories, joint angles, torque, and power. Force plate data report the forces in the three spatiotemporal directions. 'EMG' contains the signal of each muscle activation.

For the purpose of this project thesis, some modifications have been made. In order to determine the minimum stiffness, it is necessary to calculate forces and moments during the swing phase of walking (the complete procedure will be explained in the following section). The script has been modified so it is possible to obtain each marker trajectory of the complete gait, of the stance phase only, or of the swing phase only, the one that has been used.

With this script, it is also possible to normalize trajectories to compare different trials of one patient or trials from different patients.

2.5 Estimation of the minimum AFO stiffness

Until now, AFOs have been produced with the aim of ensuring comfort for the patients, with a careful analysis of the AFO design considering the geometrical and morphological aspects, without a primary focus on stiffness. The hypothesis is that there exists an optimal AFO stiffness specific to each patient, dependent on geometrical characteristics, functionality, the nature of the condition, functional requests of the patient, and the need for stability. However, considering all these aspects together could be challenging, so it is better to proceed step by step. The aim of this thesis is to find the minimum stiffness, specifically the AFO stiffness that can support the foot during the swing phase of walking. Therefore, the functional aspect is now a priority, without neglecting patient comfort.

AFO stiffness can assume a range of values, with the lower limit being the minimum stiffness below which the AFO does not achieve its goal of supporting

the foot. The upper limit is infinite stiffness, representing a high value of stiffness. However, in this case, the AFO is considered rigid and does not allow any movement of the foot, which can be challenging for severe cases of foot drop or other conditions. The Custom AFO should not be rigid; instead, it should allow normal movements of the foot, and patients should be able to wear it inside the shoe without feeling it. It is an elastic dynamic orthosis suitable for patients with mild foot drop and a deficit limited to the ankle joint. Its purpose is to support the foot without addressing problems arising from other pathologies. Both MATLAB scripts that have been developed to estimate the AFO stiffness in static and gait conditions are reported in Appendix A.

2.5.1 Ankle moments in static conditions

Firstly, the static condition has been taken into consideration. The foot is lifted from the ground but does not perform any movements. The only force acting in this condition is the gravitational force due to the weight of the foot and the footwear (Figure 2.13).

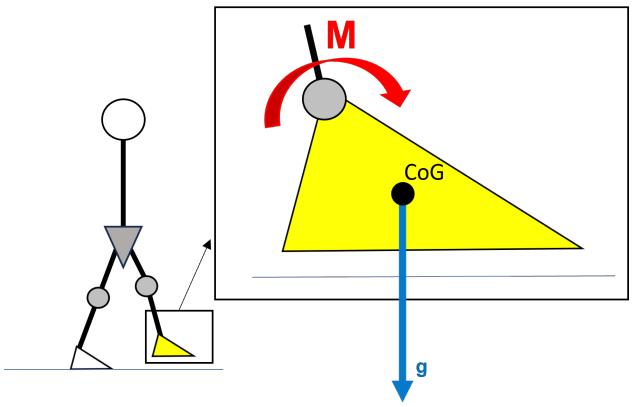

Figure 2.13: Schematic representation of the gravitational force acting on the foot in a static state

Mathematically, the moment at the ankle joint can be calculated as the cross product between the force acting on the foot and the lever arm of the force:

$$\vec{M} = a\vec{r}m \times \vec{F}_g \tag{2.4}$$

$$\vec{F}_g = (m_{foot} + m_{footwear})\vec{g} \tag{2.5}$$

Where $\vec{M}$ is the resultant moment of the ankle joint due to the gravitational force; $\vec{F_g}$ is the gravitational force obtained considering both the weight of the foot, m_{foot}, and the footwear, $m_{footwear}$; arm is the lever of the force, namely the distance between the point of application of the force, the COG and the ankle joint; g is the gravitational acceleration.

The moment at the ankle joint axis $\vec{M_{axis}}$ is calculated as the dot product between $\vec{M}$ and the unit vector of the axis $\vec{u}$:

$$\vec{M_{axis}} = \vec{M} \cdot \vec{u} \tag{2.6}$$

The assumption is that the axis of the ankle passes through the two malleoli, identified by the two markers LM and MM (Figure 2.14) which corresponds to the lateral malleolus and the medial malleolus.

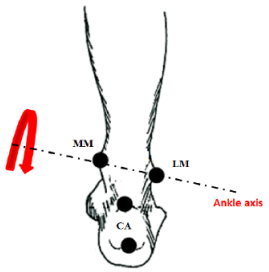

Figure 2.14: The ankle axis through the lateral and medial melleoli.

The COG has been calculated as the mean of the position of three markers: FM, VM and CA (Figure 2.15), positioned respectively at the first metatarsal head, the fifth metatarsal head and at the calcaneus . The position of the COG seems consistent with what can be found in the literature, as cited in section 1.4.1.

The arm of the force is considered the distance between the COG and the middle point between the two markers LM and MM.

$$arm = |COG - middlepoint(LM - MM)| \tag{2.7}$$

Another important step is to calculate the weight of the foot and the footwear. In the literature, various methods exist for calculating the foot weight. One approach is to consider the foot weight as a percentage of the body weight: Clauser et al. [5] considered the mass of the foot as 1.6% of the body weight,

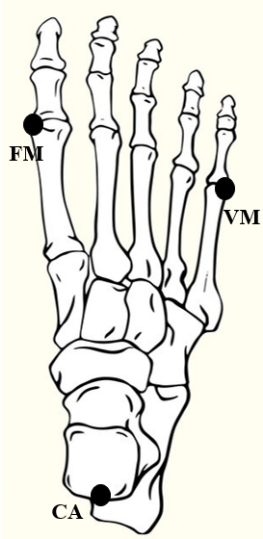

Figure 2.15: Position of the three markers VM, FM and CA used to calculate the COG.

while Durkin et al. [83] considered it as 1.3%. However, these methods may lead to inaccurate values: 'Generally, because of individual differences, it is preferable to use a mathematical model rather than a simple proportion' [84]. Other method have been introduced over the years. For example, Elou et al. [12] predicted foot weight with an equation that takes into consideration the length of the foot, the width of the ankle, and the sex of the patient. Pavol et al. [85] used an equation that considers not only the length of the foot and the width of the ankle but also the height of the ankle and the body weight. These four methods lead to similar values of foot weight; however, the latter is the one that has been chosen. The first two methods have been excluded because they reduce the calculation to a simple percentage without considering the anatomical features of the patient's foot. The equation of Pavol et al. appears better than the equation developed by Helou et al. because it also includes the body weight of the patient. Moreover, the study carried out by Pavol et al included 79 patients, while the study of Helou et al. included only 6 patients, so it does not cover a wide range of the population. The equation of Pavol et al. is the following:

$$m_{foot} = 0.0083 * m_{body} + 254.5 * l_{foot} * h_{ankle} * w_{ankle} - 0.065 \tag{2.8}$$

Where m_{body} is the body weight of the patient; l_{foot} is the length of the foot; h_{ankle} is the height of the ankle, value obtained using static data of gait analysis of the LM marker; w_{ankle} is the width of the ankle, calculated as the distance

between the two malleoli.

Regarding the weight of the footwear, two types of shoes have been considered to analyze different scenarios: a lightweight shoe and a safety shoe. After weighing several shoe sizes, a mean has been calculated, as the weights of different shoe sizes were quite similar. The weight of the two type of footwear are:

- 0.164 kg for the lightweight shoe;
- 0.496 kg for the safety shoe.

The plantarflexion moment can be calculated as follows:

$$M_{axis} = K * \theta \tag{2.9}$$

Where K is the stiffness and θ is the angle displacement. To obtain the equation, a rearrangement has been performed:

$$K = \frac{M_{axis}}{\theta} \tag{2.10}$$

The angle displacement can be arbitrarily imposed: with $\theta = 0$, the stiffness will be theoretically infinite, making the AFO rigid. On the other hand, if a high value of θ is imposed, the stiffness will be lower, and the AFO may be too elastic. For the purpose of this thesis, θ has been set to 1 because the objective is for the AFO to support the foot during the swing phase without any displacement.

The MATLAB code used is reported in Appendix B.

To generalize this concept and find the minimum stiffness for a specific patient with an imposed body weight, the ratio between the obtained stiffness and the patient's body weight has been calculated for each patient. A mean of the obtained values has been calculated.

$$value = mean(\frac{K_i}{m_{body_i}}) \tag{2.11}$$

Where K_i is the stiffness obtained for the patient i and m_{body_i} is the body weight of the patient i.

With this value it is possible to calculate the minimum stiffness for the specific patient using the body weight only.

$$K_j = value * m_{body_j} \tag{2.12}$$

For each patient, the median, the 25th and 75th percentiles of the five trials (three trials for patients 2, 3, and 6) for the plantarflexion moment and for the stiffness have been calculated.

In order to validate this process, the same script has been applied to the data of a different population, acquired in static conditions population was composed by healthy subjects and people with diabetes (n=99; age=56.6 ± 11.2; BMI=28.0 ± 6.3 ;). The method has been applied to both feet.

2.5.2 Ankle moments in gait

It is more interesting to analyze the dynamic condition since it is during walking that the AFO exerts its function. Each patient has to walk in shod condition up to five times.

If we consider the dynamic condition, there are other forces applied to the COG of the foot:

- Gravitational forces, due to the weight of the foot and the shoe;
- Inertial forces, due to the acceleration of the foot caused by walking.

Both of these forces cause a moment on the ankle joint axis. Moreover, there is another term that needs attention: the contribution of the inertia of the foot considering circular motion. Figure 2.16 is a schematic representation of forces and moments during gait.

Mathematically:

$$\vec{M} = a\vec{r}m \times (\vec{F_g} + \vec{F_a}) \tag{2.13}$$

Compared to the static state, the contribution of the inertial forces F_a becomes noticeable here. In this case, the mass of the foot utilized is that of the lightweight shoe, as the gait analysis has been performed only with this type of shoe.

As seen before, to calculate the moment on the ankle joint axis, the dot product is needed:

$$\vec{M_{axis}} = \vec{M} \cdot \vec{u} \tag{2.14}$$

Finally, the moment on the ankle joint can be calculated as follows:

$$\vec{M_{axis\_total}} = \vec{M_{axis}} + I_{ankle} * \vec{\alpha} \tag{2.15}$$

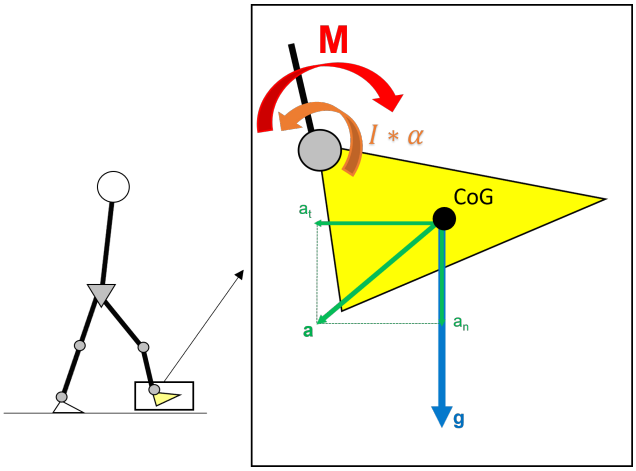

Figure 2.16: Schematic representation of the gravitational force, the inertial forces and the contribution of the inertia due to circular motion acting on the foot in a dynamic state

The contribution $I_{ankle} * \vec{\alpha}$ is the contribution of inertia due to circular motion, where I_{ankle} is the moment of inertia of the foot with respect to the ankle axis, α is the angular acceleration.

In order to calculate the moment of inertia of the foot, a brief literature review has been conducted. Similar to the mass of the foot, inertia parameters can be calculated in various ways. However, the moment of inertia appears to be more complex than other features. Articles often report the values of the moment of inertia of the foot, and these have been considered as references. Hinrichs et al. [86] reported the following equation to calculate the moment of inertia of the foot with respect to the COG:

$$I_{COG} = 6.7508 * l_{foot} - 4.2725 * h_{ankle} - 105.42 \tag{2.16}$$

The Huygens-Steiner theorem is then used to obtain the moment of inertia of the foot with respect to the ankle axis:

$$I_{ankle} = I_{COG} + m_{foot} * d^2_{ankleCOG} \tag{2.17}$$

Where $d_{ankleCOG}$ is the distance between the COG and the axis of the ankle. Since the patients walked with their shoes on, specifically the lightweight shoe (mass of the lightweight shoe is 0.164 kg), this has to be taken into consideration

in the previous calculations. The equation 2.17 becomes:

$$I_{ankle} = I_{COG} + m_{tot} * d^2_{ankleCOG} \tag{2.18}$$

Where m_{tot} includes the weight of the foot and the weight of the shoe.

In order to validate these values, the moment of inertia with respect to the ankle axis has been calculated using nmsBuilder [87], , a software developed to create musculoskeletal models for OpenSim. For this purpose, it has been utilized to calculate the moment of inertia starting from the CAD model of the foot of each patient (Figure 2.17). The reference system has been positioned in a manner such that the moment of inertia is calculated with respect to the ankle axis. The density used is 1.18 g/cm^3, which is a mean between the density of the bone (1.30 g/cm^3) and the density of the soft tissues (1.06 g/cm^3). It was not possible to calculate the moment of inertia of the non-affected foot since the CAD model of the foot available was for the affected foot only. Moreover, the CAD model of the affected foot of patient 2 was not available.

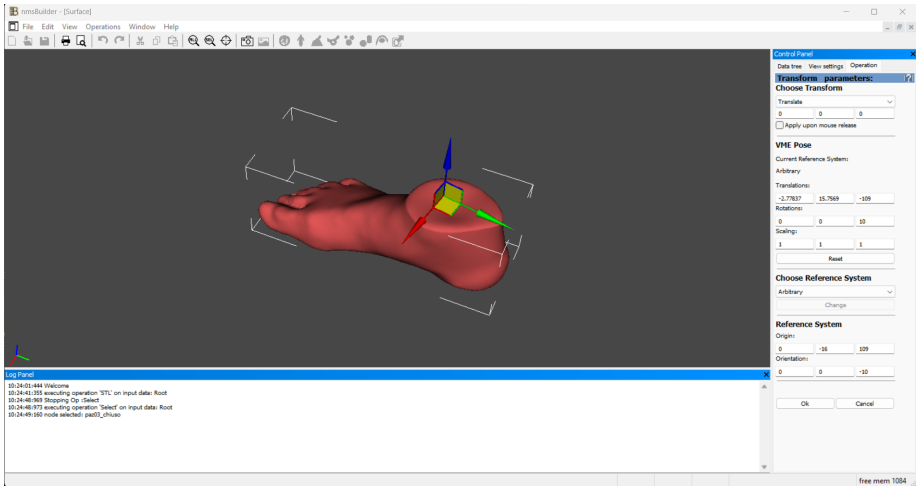

Figure 2.17: Screenshot of the software nmsBuilder with a cad model of a foot and the reference system used.

The minimum stiffness for the specific patient has been considered as the maximum plantarflexion moment, and, as observed in the static case, we consider a displacement of one degree. Considering the convention used, with plantarflexion represented by negative values and dorsiflexion represented by positive values, the maximum plantarflexion moment is the minimum value of

$\vec{M_{axis\_total}}$.

$$M_{planta} = min(M_{axis\_total}) \tag{2.19}$$

As we seen for the static case, the minimum plantarflexion moment can be calculated as follows:

$$M_{planta} = K * \theta \tag{2.20}$$

Then to obtain the stiffness:

$$K = \frac{M_{planta}}{\theta} \tag{2.21}$$

In order to obtain the minimum stiffness for the specific patient in the dynamic state, the same reasoning applied to the static state has been done:

$$value = mean(\frac{K_i}{m_{body_i}}) \tag{2.22}$$

$$K_j = value * m_{body_j} \tag{2.23}$$

For thoroughness, the maximum value of the M_{axis_total} has been calculated and represents the maximum dorsiflexion movement.

$$M_{dorsi} = max(M_{axis\_total}) \tag{2.24}$$

For each patient, the median and the 25th and 75th percentiles of the five trials (three trials for patients 2, 3, and 6) for the minimum moment, the maximum moment, and the stiffness have been calculated.

3 Results

In this section, the main outcomes of this study are reported. The results are divided into paragraphs as follows: custom AFO mechanical properties, which include the evaluation of real AFO stiffness and the correlation between the AFO stiffness and the AFO dimensions, and the evaluation of the AFO minimum stiffness, which pertains to both static and dynamic conditions. The results are then discussed in the following section, 'Discussion'.

3.1 Custom AFO mechanical properties

This paragraph pertains to the mechanical properties of the AFO, with a particular focus on stiffness, which is one of the main characteristics that influences the functional outcome of an AFO.

3.1.1 Experimental measurements of AFO stiffness

The mean values of the stiffness for both dorsiflexion and plantarflexion in each AFO (version 2.2) are reported in Table 3.1, based on the five trials.

Patient ID	Dorsiflexion stiffness [Nm/deg]	Plantarflexion stiffness [Nm/deg]
2 (right)	0.1270	0.2219
2 (left)	0.1320	0.2243
9	0.0857	0.1546
10	0.0898	0.2143
11	0.0966	0.1539
13	0.1293	0.2352
14	0.1279	0.2334
15	0.0994	0.1891

Table 3.1: Experimentally measured AFO dorsiflexion and plantarflexion stiffness from laboratory testing for the eight AFO examinated. The mean of five trials are here reported.

3.1.2 Correlation between AFO dimensions and AFO stiffness

The dimensions correlated to the stiffness of the AFO, obtained with Rhino 3D software, are reported in Table 3.2. The measurements for the thickness of the calf shell and the rod were repeated three times, and the mean values are presented. These measurements were conducted for the AFO version 2.2.

In Table 3.3, the moments of inertia for the rod and the calf shell are reported. These values were obtained using the dimensions of the AFOs as reported in Table 3.2.

The intercept β and the coefficients α of each dimensions are calculated using the FITLM function in MATLAB. The regression analysis has been performed for each model. Table 3.5 is to understand which α is linked to the dimensions.

Patient ID	Length of the calf shell [mm]	Width of the calf shell [mm]	Maximum thickness of the calf shell [mm]	Width of the rod [mm]	Thickness of the rod [mm]
2 (right)	168.91	53.87	2.97	22.53	3.07
2 (left)	168.58	54.40	2.99	22.90	3.10
9	161.63	46.88	2.75	21.71	3.69
10	143.26	48.66	2.43	20.45	3.42
11	159.42	52.3	2.52	19.76	2.57
13	157.61	49.63	2.86	19.30	3.58
14	143.1	45.92	2.56	19.63	3.38
15	148.11	47.66	2.48	18.59	2.76

Table 3.2: Dimensions of the eight AFOs obtained with Rhino 3D

Patient ID	Moment of inertia of the rod $[mm^2]$	Moment of inertia of the calf shell $[mm^2]$
2 (right)	54.32	118.01
2 (left)	56.68	120.78
9	90.64	80.95
10	68.38	58.18
11	27.96	69.47
13	73.59	97.09
14	63.35	63.95
15	32.45	60.58

Table 3.3: Moment of inertia of the rod and moment of inertia of the calf shell. The moments of inertia are obtained with the dimensions of the eight AFO.

Model	β	α_1	α_2	α_3	α_4	α_5	α_6	α_7	α_8	α_9	α_{10}	α_{11}
1	0.2636	-0.0072	0.0069	0.2575	/	/	0.0003	-0.0075	/	/	/	/
2	0.624	-0.0070	0.0065	/	0.0502	/	-0.003	/	-0.0010	/	/	/
3	0.7414	-0.0068	0.0060	/	/	0.0122	-0.009	/	/	-0.0002	/	/
4 (A)	0.2477	-0.0072	0.0069	0.2736	/	/	0.0001	/	/	-0.0002	/	/
4 (B)	-0.8368	-0.0028	0.0027	0.1270	/	/	0.0130	0.3577	/	/	-0.0069	/
5 (A)	0.7546	-0.0068	0.0061	/	/	0.0122	-0.0008	-0.0049	/	/	/	/
5 (B)	-0.1162	-0.0078	0.0099	0.4370	/	/	0.0021	-0.0135	/	/	/	-0.0016
6	-0.8689	-0.0030	0.0032	0.1553	/	/	0.0130	0.3480	/	/	-0.0067	-0.0002

Table 3.4: Coefficients β and α for each model calculated with the FITLM function on MATLAB.

Length of the calf shell	α_1
Width of the calf shell	α_2
Maximum thickness of the calf shell	α_3
Maximum thickness of the calf shell (quadratic)	α_4
Maximum thickness of the calf shell (cubic)	α_5
Width of the rods	α_6
Thickness of the rod	α_7
Thickness of the rod (quadratic)	α_8
Thickness of the rod (cubic)	α_9
Moment of inertia of the rod	α_{10}
Moment of inertia of the calf shell	α_{11}

Table 3.5: The dimensions used and and the relevant $alpha$ obtained from the multiple linear regression analysis.

'Model 1' corresponds to the linear model; 'Model 2' corresponds to the quadratic model; 'Model 3' corresponds to the cubic model; 'Model 4 (A)' corresponds to the moment of inertia of the rod model (A); 'Model 4 (B)' corresponds to the moment of inertia of the rod model (B); 'Model 5 (A)' corresponds to the moment of inertia of the calf shell model (A); 'Model 5 (B)' corresponds to the moment of inertia of the calf shell model (B); 'Model 6' corresponds to the moments of inertia model.

Additionally, the function returns the statistics of the model. To choose the best model, the following parameters have been evaluated: the percentage error of the real stiffness and the predicted one, the RMSE, the p-value of the model, the R^2 and the R^2_{adj}.

Model	%error	RMSE	p value	R^2	R^2_{adj}
1	0.7469	0.0041	0.010473	0.9958	0.9853
2	0.9378	0.0046	0.013239	0.9947	0.9814
3	1.1127	0.0052	0.017132	0.9931	0.9759
4 (A)	0.7508	0.0040	0.010381	0.9958	0.9854
4 (B)	0.0520	3.4747e-04	0.0073555	1.0000	0.9999
5 (A)	1.1112	0.0052	0.017134	0.9931	0.9759
5 (B)	0.5029	0.0052	0.10989	0.9965	0.9758
6	1.0319e-13	0	NaN	1	-Inf

Table 3.6: The statistical analysis for each model calculated with FITLM function on MATLAB.

3.2 Estimation of the minimum AFO stiffness

In this paragraph, the results obtained for the estimation of the minimum stiffness of the AFO for specific patients in both static and dynamic conditions are reported.

3.2.1 Ankle moment in static conditions

In the static conditions, the force of gravity due to the mass of the foot and the footwear has been considered, including both lightweight and safety shoes (respectively 0.164 kg and 0.496 kg). Various studies have been consulted to calculate the mass of the foot. Table 3.7 presents a comparison of four studies for the calculation of the mass for the affected foot.

Patient ID	Mass of the foot [kg]			
	Clauser et. al	Durkin et. al	Pavol et. al	Helou et. al
2	1.33	1.08	1.06	1.14
3	1.54	1.25	1.32	1.74
4	1.52	1.24	1.32	1.59
6	1.55	1.26	1.28	1.57
8	1.36	1.11	1.21	1.52
9	1.50	1.22	1.21	1.54
10	1.22	0.99	1.052	1.36
11	1.28	1.04	1.09	1.246
13	1.23	1.00	1.09	1.33
14	0.96	0.78	0.82	1.056

Table 3.7: Comparison of the mass of the affected foot of the four mentioned studies.

After selecting the equation reported by Pavol et al. [85], the mass of both feet was calculated. The results are reported in Table 3.8.

Patient ID	Mass of the foot [kg]	
	Affected foot	Non affected foot
2	1.06	1.06
3	1.32	1.41
4	1.32	1.33
6	1.28	1.28
8	1.21	1.26
9	1.21	1.28
10	1.05	1.12
11	1.09	1.12
13	1.09	1.11
14	0.82	0.86

Table 3.8: Estimated mass of both the affected and non affected foot for the 10 foot drop patients, using the equation reported by Pavol et al..

Following the procedure explained in section 2.5.1, the moment at the ankle axis has been calculated for both the affected and non affected foot, with lightweight and safety shoes. Figure 3.1 displays the boxplot of the moment at the ankle axis, while Table 3.9 provides the median along with the 25th and 75th percentiles. The ankle moments for each patients are reported in the Appendix B.

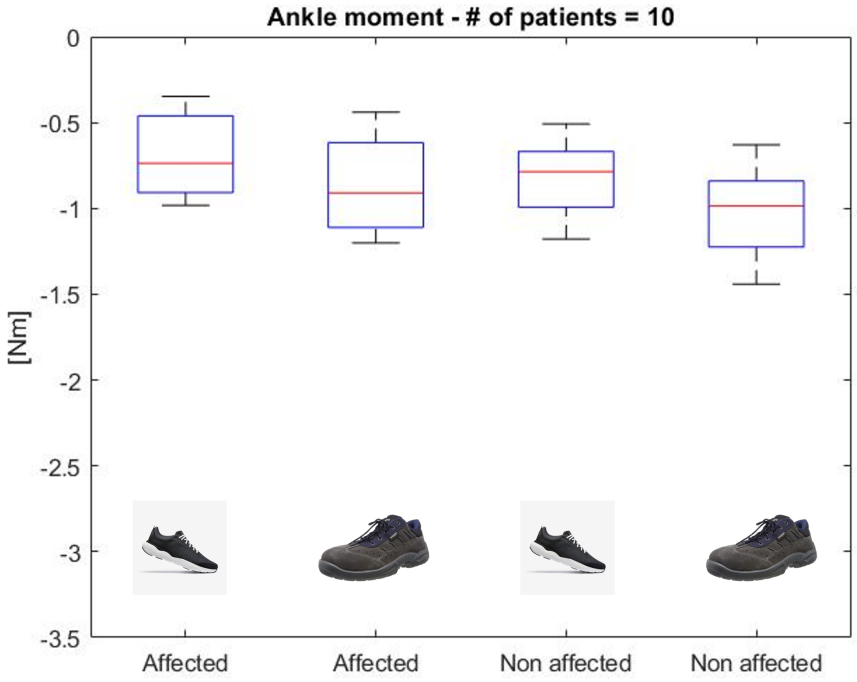

Figure 3.1: Boxplot of the distribution of the moment at the ankle axis for both affected and non affected foot, with lightweight shoe and safety shoe, across the 10 foot drop patients.

	Moment at the ankle axis [Nm]			
	Affected foot		Non affected foot	
	Lightweight shoe	Safety shoe	Lightweight shoe	Safety shoe
Median (25th, 75th)	-0.74 (-0.91, -0.46)	-0.91 (-1.11, -0.62)	-0.79 (-0.99, -0.67)	-0.99 (-1.22, -0.84)

Table 3.9: Median and 25th and 75th percentile of the moment at the ankle axis for both affected and non affected foot for the 10 foot drop patients.

The AFO stiffness was estimated by assuming a maximum 1 deg of plantarflexion at the ankle during the swing phase of gait. Figure 3.2 shows the boxplot of the estimated minimum AFO stiffness, and Table 3.10 presents the median, 25th, and 75th percentiles. The AFO minimum stiffness for each patient are reported in the Appendix B.

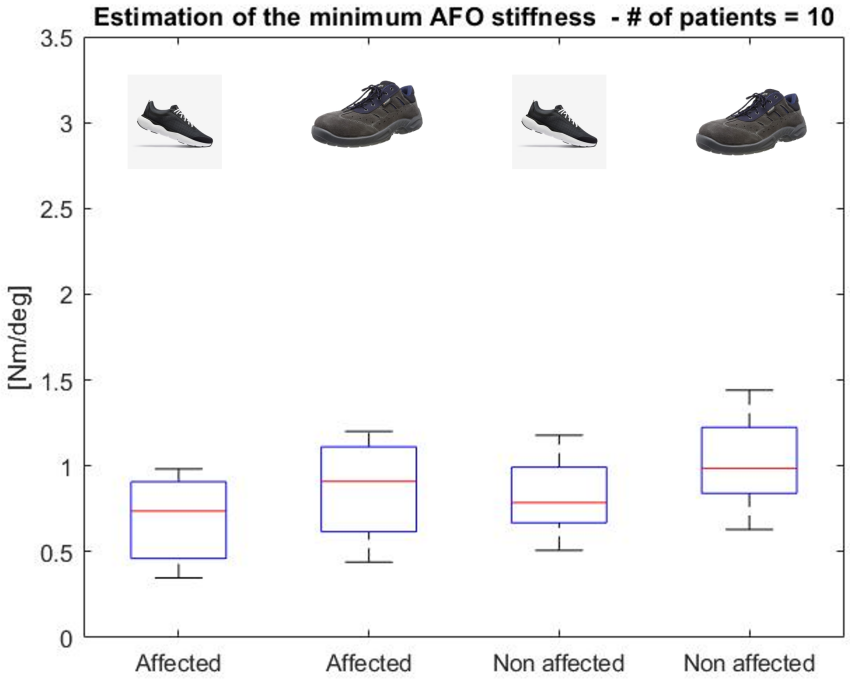

Figure 3.2: Boxplot of the distribution of the minimum AFO stiffness estimated across the 10 foot drop patients, for both affected and non affected foot, with lightweight shoe and safety shoe.

	Minimum AFO stiffness [Nm/deg]			
	Affected foot		Non affected foot	
	Lightweight shoe	Safety shoe	Lightweight shoe	Safety shoe
Median (25th, 75th)	0.74 (0.46, 0.91)	0.91 (0.62, 1.11)	0.79 (0.67, 0.99)	0.99 (0.84, 1.22)

Table 3.10: Median and 25th and 75th percentile of the estimated minimum AFO stiffness for both affected and non affected foot for the 10 foot drop patients.

To validate the process, the script has also been applied to a different study that includes diabetic patients and a control group. The evaluation has been conducted for both feet, with lightweight shoes and safety shoes. Figure 3.3 displays the boxplot of the moment at the ankle axis, while Table 3.11 presents the median, 25th, and 75th percentiles for both feet with the two different types

of shoes.

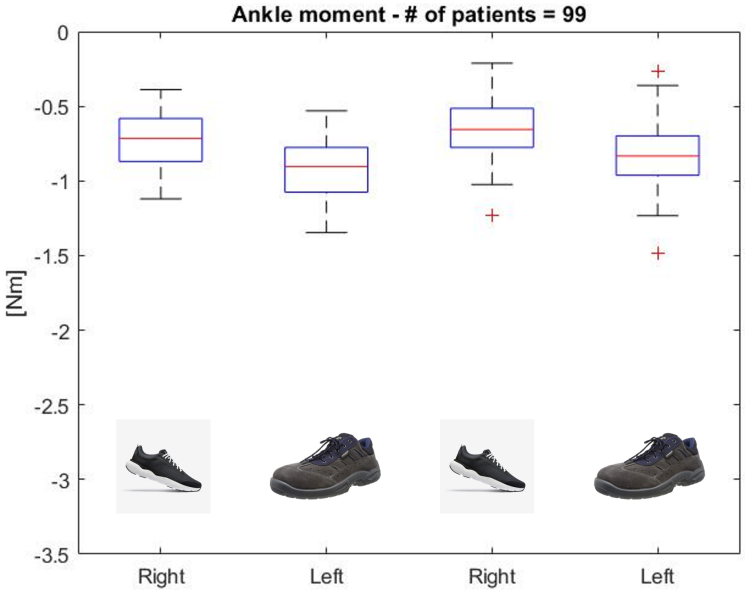

Figure 3.3: Boxplot of the distribution of the moment at the ankle axis for both right and left foot, with lightweight shoe and safety shoe, across the 99 patients.

	Moment at the ankle axis [Nm]			
	Right foot		Left foot	
	Lightweight shoe	Safety shoe	Lightweight shoe	Safety shoe
Median (25th, 75th)	-0.72 (-0.87, -0.58)	-0.90 (-1.07, -0.78)	-0.66 (-0.78, -0.51)	-0.83 (-0.96, -0.70)

Table 3.11: Median and 25th and 75th percentile of the moment at the ankle axis for both right and left foot for the 99 patients.

As seen before with the moment at the ankle axis, the estimated minimum AFO stiffness has been calculated, considering a displacement of 1 degree. Figure 3.4 displays the boxplot for both feet with lightweight and safety shoes, while Table 3.12 presents the median, 25th, and 75th percentiles.

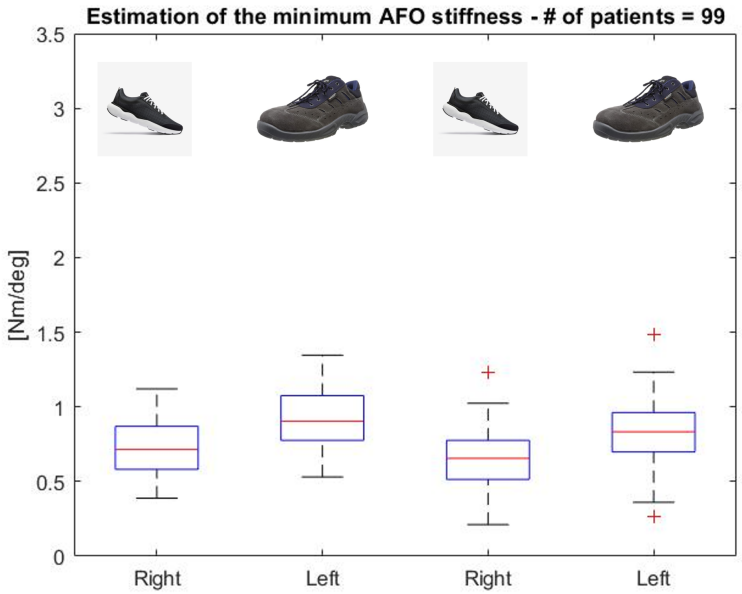

Figure 3.4: Boxplot of the distribution of the minimum AFO stiffness estimated across the 99 patients, for both right and left foot, with lightweight shoe and safety shoe.

	Minimum AFO stiffness [Nm/deg]			
	Right foot		Left foot	
	Lightweight shoe	Safety shoe	Lightweight shoe	Safety shoe
Median (25th, 75th)	0.72 (0.58, 0.87)	0.90 (0.78, 1.07)	0.66 (0.51, 0.78)	0.83 (0.70, 0.96)

Table 3.12: Median and 25th and 75th percentile of the estimated minimum AFO stiffness for both right and left foot for the 99 patients.

The ratio of the estimated minimum AFO stiffness and the bodyweight of each patient calculated through Equation 2.11 is:

- affected foot, lightweight shoe: 0.0082 Nm/deg kg
- affected foot, safety shoe: 0.0102 Nm/deg kg
- non affected foot: 0.0096 Nm/deg kg

- non affected foot, safety shoe: 0.0120 Nm/deg kg

3.2.2 Ankle moments in gait

In the dynamic case, the forces due to the foot accelerations and inertial components in the swing phase are taken into consideration. These forces are obtained by processing the kinematic data from the gait analysis performed by each patient in 'shod' condition. Additionally, to calculate the moment at the ankle axis, it is necessary to determine the contribution of inertia due to the motion of the foot around the ankle axis. In Table 3.13 , the moments of inertia with respect to the ankle axis for both the affected and non-affected foot with a lightweight shoe are reported. The moment of inertia of the feet have been calculated using an equation reported by Hinrichs et al. [86].

Patient ID	Moment of inertia of the foot [kg m^2]	
	Affected foot	Non affected foot
2	0.0109	0.0097
3	0.0157	0.0178
4	0.0162	0.0178
6	0.0158	0.0184
8	0.0164	0.0154
9	0.0132	0.0136
10	0.0099	0.0099
11	0.0129	0.0153
13	0.0121	0.0144
14	0.0101	0.0089

Table 3.13: Moment of inertia for both affected and non affected foot with a lightweight shoe of the 10 foot drop patients. The moment of inertia has been estimated with the equation presented by Hinrichs et al..

To validate the value of the moment of inertia of the foot, the software nmsBuilder has been used. In Table 3.14, the moment of inertia of the foot, calculated with the equation of Hinrichs and using nmsBuilder, are reported without the shoe for each patient.

	Moment of inertia of the foot [kg m^2]		
Patient ID	Affected foot		Non affected foot
	Hinrichs eqaution	nmsBuilder	Hinrichs equation
2	0.0095	/	0.0085
3	0.0144	0.0113	0.0162
4	0.0149	0.0066	0.0163
6	0.0146	0.0063	0.0169
8	0.0149	0.0060	0.0140
9	0.0121	0.0057	0.0124
10	0.0089	0.0045	0.0088
11	0.0115	0.0059	0.0136
13	0.0109	0.0059	0.0129
14	0.0088	0.0032	0.0078

Table 3.14: Moment of inertia for both affected and non affected foot of the 10 foot drop patients, calculated with the equation presented by Hinrichs et al. compared with the moment of inertia of the affected foot of the 10 foot drop patients estimated with nmsBuilder.

As observed in the static case, calculating the stiffness requires determining the moment at the ankle axis. Figure 3.5 displays the graphs of the moment at the ankle axis for the 10 foot drop patients in each trial for the affected foot, while Figure 3.6 represents the graphs of the moment at the ankle axis for the 10 foot drop patients in each trial for the non-affected foot.

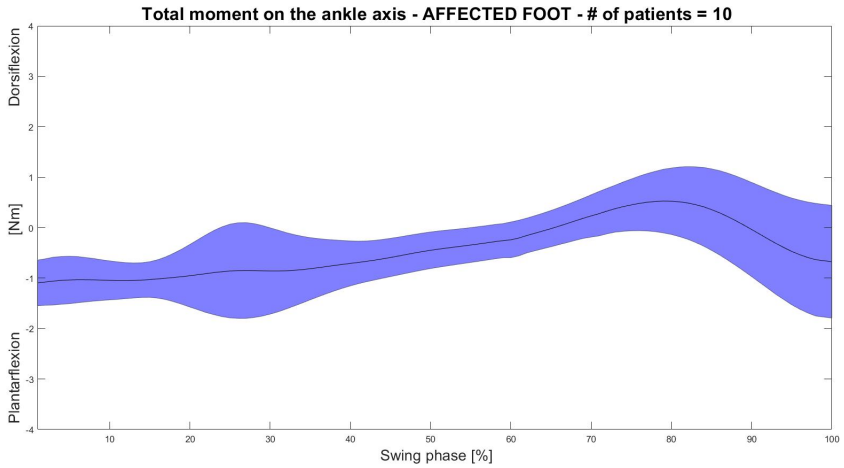

Figure 3.5: Mean temporal profile (± 1SD) of the ankle moment (Nm) for the 10 foot-drop patients in the affected foot across normalized swing phase duration.

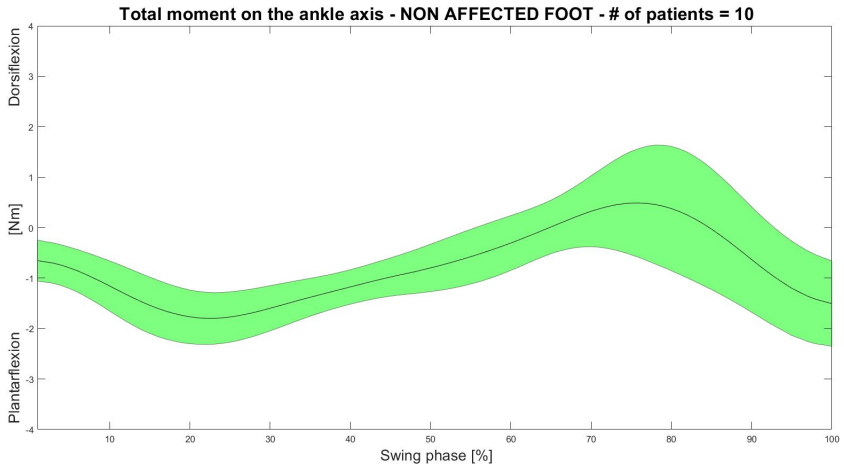

Figure 3.6: Mean temporal profile (± 1SD) of the ankle moment (Nm) for the 10 foot-drop patients in the non affected foot across normalized swing phase duration.

The mean value and standard deviation of the trials for each patient were considered. In the Appendix B, the graphs for each patient are provided.

From the moment at the ankle axis, the minimum and maximum values were extracted, representing the plantarflexion and dorsiflexion moments, respectively. For both of these quantities, the boxplot (Figure 3.7 and Figure 3.8), the median and the 25th and 75th percentiles (Table 3.15 and 3.16) are reported. Both plantarflexion and dorsiflexion for each patient are included in the Appendix B.

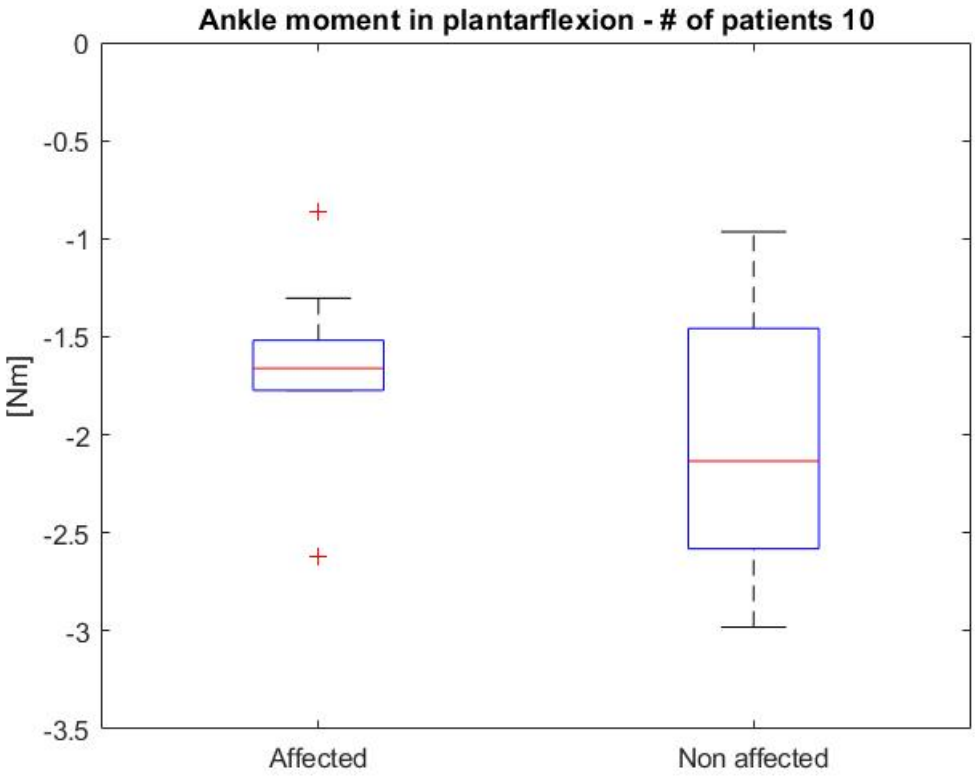

Figure 3.7: Boxplot of the distribution of the plantarflexion moment at the ankle axis for both affected and non affected foot, across the 10 foot drop patients.

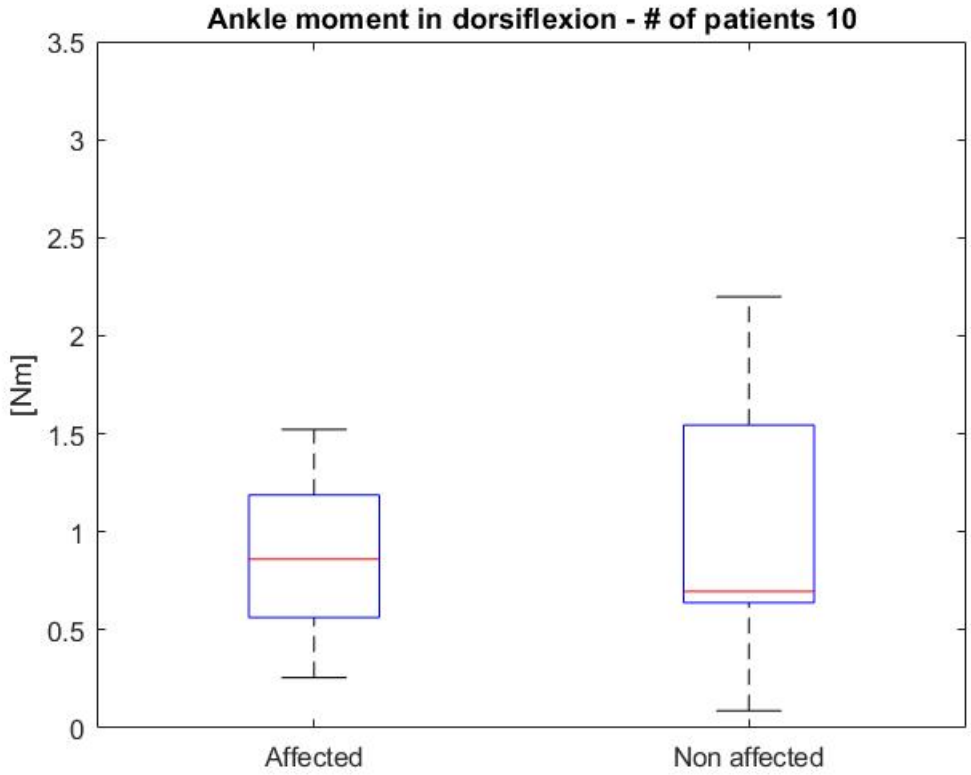

Figure 3.8: Boxplot of the distribution of the dorsiflexion moment at the ankle axis for both affected and non affected foot, across the 10 foot drop patients.

	Maximum plantarflexion moment [Nm]	
	Affected foot	Non affected foot
	Lightweight shoe	
Median (25th, 75th)	-1.66 (-1.77 -1.52)	-2.14 (-2.58, -1.46)

Table 3.15: Median and 25th and 75th percentile of the plantarflexion moment for both affected and non affected foot for the 10 foot drop patients.

As mentioned in paragraph 2.5.3, the plantarflexion moment is necessary to calculate the minimum stiffness of the AFO. The results in Figure 3.9 and in Table 3.17 are reporting the estimated minimum AFO stiffness required to allow a maximum 1 deg of plantarflexion in the swing phase of gait. The minimum stiffness for each patient are provided in the Appendix B.

	Maximum dorsiflexion moment [Nm]	
	Affected foot	Non affected foot
	Lightweight shoe	
Median (25th, 75th)	0.86 (0.56, 1.19)	0.70 (0.64, 1.54)

Table 3.16: Median and 25th and 75th percentile of the dorsiflexion moment for both affected and non affected foot for the 10 foot drop patients.

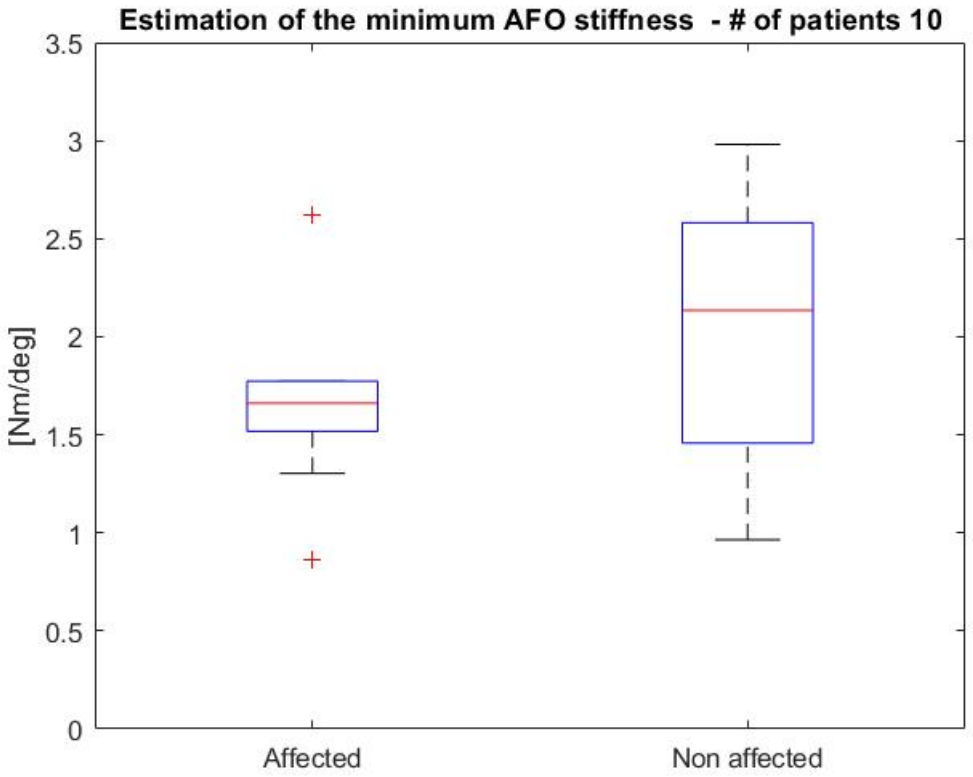

Figure 3.9: Boxplot of the distribution of the minimum AFO stiffness estimated across the 10 foot drop patients, for both affected and non affected foot.

The ratio of the estimated minimum AFO stiffness and the body weight of each patient calculated through Equation 2.22 is:

- affected foot, lightweight shoe: -0.0194 Nm/deg kg
- non affected foot, lightweight shoe: -0.0243 Nm/deg kg

	Minimum AFO stiffness [Nm/deg]	
	Affected foot	Non affected foot
	Lightweight shoe	
Median (25th, 75th)	1.66 (1.52, 1.77)	2.14 (1.46, 2.58)

Table 3.17: Median and 25th and 75th percentile of the estimated minimum AFO stiffness for both affected and non affected foot for the 10 foot drop patients.

4

Discussion

This thesis conducted at the Movement Analysis laboratory of the Istituto Ortopedico Rizzoli was focussed on the characterization of the mechanical properties of a novel custom passive-dynamic Ankle Foot Orthosis developed by the team of researchers of IOR. This project follows a number of studies from the same research group which aimed at defining the design principles, and reporting on the functional evaluation of the novel fiberglass-reinforced polyamide custom AFO in a population of foot-drop patients.

One of the objectives of this thesis was to determine the correlation between the dimensions of the AFO and its stiffness. Using dimensions and stiffness of 8 AFOs, multiple linear regression analysis has allowed to determine an equation that best predict the AFO stiffness. In addition, the minimum AFO stiffness required to sustain the foot in static and dynamic conditions was determined by the analysis of the lower-limb static and kinematic data in a population of foot-drop patients. Gait analysis was performed at the Movement Analysis Laboratory using the IOR gait protocol. The patients were asked to walk with the footwear at a comfortable speed along a 10 m pathway. The kinematic data allowed to estimate the maximum plantarflexion and dorsiflexion moments due to the gravitational and inertial forces acting on the ankle axis in the swing phase of walking.

This section pertains with the discussion of the results presented in Section 3, as follows: the correlation between AFO dimensions and AFO stiffness, and the estimated minimum AFO stiffness in static and dynamic conditions. The last two paragraphs will explain the limitations of this study and any potential

future developments aimed at improving the functional aspects of the custom AFO.

4.1 Correlation between AFO dimensions and AFO stiffness

Eight models have been proposed to describe the relationship between the relevant AFO dimensions and AFO stiffness. The outcomes of the 8 multiple linear regression models are reported 3.6.

It is important to point out that Model 4B (the model based on the moment of inertia of the rod) and Model 8 (model based on the moments of inertia) were the best models in terms of RMSE and R^2 and R^2 adjusted. However, both models were discarded as the outcome of the statistical analysis showed abnormal values probably due to the limited number of samples.

As far as the statistical outcome of the other models, Model 1 (the linear model) and Model 4A (moment of inertia of the rod) showed an RMSE of 0.004 which is the lowest error calculated. Moreover, these two models showed the lowest p-values ($p \approx 0.01$). While it is difficult to determine which model is better representing the mechanical behaviour of the calf-shell, it is sensible to consider model 4A to be superior as it includes the thickness of the rod raised to the cube. Thus, this model seems to be more realistic in describing the bending properties of the AFO, since these are correlated to the moment of inertia of the relevant cross section. Using model 4A, it is possible to estimate the AFO dimensions for a specific AFO stiffness, with the error reported above. The main limitation of this analytical approach is in the limited number of samples (n=8) used for the regression analysis, which could be responsible for inaccurate results.

4.2 Estimation of the minimum AFO stiffness

The mass of the affected foot for the ten patients, calculated with different methods, are reported in Table 3.7. Even though the methods resulted in similar foot masses, those by Clauser et al. [5] and Durkin et al. [83] are too simple as they merely consider the mass of the foot as a percentage of the body weight (1.6% and 1.3%, respectively). These methods have therefore been excluded. According to J.G. Reid et al. [84], more anatomical features of the patients foot

must be considered. Pavol et. al [85] include body weight, length of the foot, and width and height of the ankle in their equation, while Helou et al. [12] consider only the length of the foot and the width of the ankle. Therefore, the equation proposed by Pavol et al. was preferred since it was also based on a larger sample size.

Table 3.8 reports the masses of both feet for each patient. The small differences between the two feet can be explained by the non-perfect symmetry in the human body anthropometry between left and right side. Moreover, the positioning of the skin-markers on anatomical landmarks is always subjected to some error and this may also have affected the differences in foot mass between left and right side.

As expected, for both affected and non-affected foot, the moment at the ankle (and thus the resulting minimum AFO stiffness) is higher when wearing the safety shoe rather than with a lightweight shoe. The median ankle moment in the affected foot was estimated to be 0.74 Nm and 0.91 Nm when wearing a lightweight shoe and a safety shoe, respectively. The median ankle moment in the non-affected foot, was estimated to be 0.79 Nm and 0.99 Nm when wearing a lightweight shoe and a safety shoe, respectively. Very similar results were obtained by the static analysis of the ankle moments in a population of 99 subjects (people with diabetes and control subjects). Therefore, wearing a safety shoe results in an increase of ankle plantarflexion moment in static conditions of about 25% due the heavy safety components present in this footwear such as the steel toe cap. As a limitation of this analysis, to simplify the estimation of the ankle moment, it should be highlighted that the centre of gravity (COG) of both shoes was assumed to be coincident with that of the foot; this was also estimated from the position of the three skin-markers used for the kinematic analysis and thus it is also affected by some error. The position of the COG, even if the result seems consistent with what has been found in literature, may not be accurate.

Table 3.13 reports the moments of inertia of both the affected and the non-affected foot. Similar to what observed in the estimation of the mass of the foot, a difference in the moment of inertia between feet was observed probably due to morphological differences and the positioning of the markers. The choice of the equation to calculate the moment of inertia of the foot was challenging. Methods based on the measurement of cadaver feet or other complex methods can be found in the literature. The moments of inertia estimated by the equation developed by Hinrichs et al. [86] seemed to be consistent with those calculated

with nmsBuilder (Table 3.14), which is a reliable method often reported in the literature.

Figure 3.5 is reporting the temporal profile of ankle moment in the affected foot during normalized swing phase duration. The rather small standard deviation indicates a consistent data distribution, except for a restricted region between 20% and 35% of the swing phase. This represents the initial instances of the swing phase, and the variability can be explained by patient-specific kinematic compensatory movements due to the pathological condition. Figure 3.6 is reporting the temporal profile of ankle moment in the non-affected foot during normalized swing phase duration. This pattern is more consistent throughout the entire swing phase and is characterized by rather small standard deviations.

It was observed that the median plantarflexion moment in the affected foot is about -1.66 Nm and -2.14 Nm in the non-affected foot. The larger total moment in the non-affected foot can be explained by the higher acceleration on the non-affected side. The distribution of the maximum ankle plantarflexion moment is reported in Figure 3.7, whereas the corresponding minimum AFO stiffness is presented in Figure 3.9. While the non- affected foot shows a symmetrical boxplot (with a slight tendency towards the 25th percentile), the affected foot shows that data is compressed to the 25th percentile and presents two outliers. This seems to indicate a larger variability in biomechanical data in the affected side.

Table 3.16 is reporting the maximum dorsiflexion moment during the swing phase. Similar to what observed for the plantarflexion moment, larger moments were estimated on the non-affected side (about 0.86 Nm) with respect to the affected side (about 0.70 Nm). It should be highlighted that some patients walked with a walking stick, which can affect gait kinematics and speed. As a general limitation of this dynamic analysis, the use of skin-markers is intrinsically affected by skin motion artifacts. These may have affected the location and orientation of the ankle axis and thus biased the estimation of the ankle moments. In addition, the AFO minimum stiffness was here determined to be that allowing a maximum of 1 deg plantarflexion in the swing phase. A less conservative approach to estimate the AFO stiffness may consider the maximum plantarflexion angle in the swing phase recorded in a healthy population.

4.3 Future endeavours

To enhance the precision in the estimation of the COG position it could be useful to consult the anthropometric table by De Leva [88], which is a dataset that provides anthropometric data for various segments of the human body. This type of data is often used in biomechanics and ergonomics to understand the physical characteristics of individuals and to estimate parameters like the COG.

As for the model correlating the AFO dimensions with the AFO stiffness, a larger dataset is needed improve the accuracy. The regression analysis functions, such as FITLM implemented in MATLAB, work more efficiently with larger datasets.

In order to improve the customization of the AFO mechanical properties, future endeavours should include the patients degree of deficit and functional demand. Finally, the AFO stiffness in dorsiflexion is correlated to that in plantarflexion but was not investigated in the present study. This property affects the dynamics of the foot and ankle during the stance phase and should be optimized to improve walking stability and efficiency.

4.4 Conclusions

To conclude, this thesis project has allowed to correlate the dimensions of the new passive dynamic custom AFO with its stiffness. This information will allow for a more accurate dimensioning of the AFO.

In addition, the minimum AFO stiffness required to support the foot of foot-drop patients has been estimated for two types of shoes (lightweight and safety shoe). This information is critical to determine the basic specification of the orthosis also with respect to the type of footwear usually worn by the patient.

Matlab scripts

```
%CORRELATION BETWEEN AFO DIMENSIONS AND AFO STIFFNESS
% The function 'rigidAFO' has been implemented to determine the
%coefficients of the function that express the AFO stiffness as a function
%of the AFO dimensions. To obtain this has been used the function 'fitlm'.
%In order to determine the optimal model this function determine the
%statistical analysis of the model

%The function input are the stiffness and a vector with the dimensions; the
%functiion output are the coefficients, the R^2 and R^2 adjusted, the RMSE,
%the 'mean error' and K which is a simple table to visualize the calculated
%stiffness and the experimental stiffness and their relative error

function [alpha, Rsquared, RsquaredAdj, meanError, RMSE, meanError, K]=rigidAFO(stiffness, dimension);

fitlm_fun=fitlm(dimension, stiffness); %the function 'fitlm' create the linear regression model
alpha=table2array(fitlm_fun.Coefficients); %extraction of the table with the coefficients
%Extraction of the R^2 and R^2 adjusted
Rsquared=fitlm_fun.Rsquared.Ordinary;
RsquaredAdj=fitlm_fun.Rsquared.Adjusted;
```

```
%With the function 'anova' the p-value of the model can be extracted
summary=anova(fitlm_fun, 'summary');

%The following for cycle calculate the stiffness using the
    coefficients
%calculated above and saved in the first column of the table 'alpha'
K=[];
for i=1:size(dimension, 1); % the cylce iterates for each set of AFO
    dimensions and its relative experimental stiffness
     %The equation uses the intercept (the first value of the colum)
    and the
     %dimensions multiplied for their respective coefficient.
     k_fitlm=alpha(1,1)+dimension(i,:)*alpha(2:end,1);
     K(i,1)=k_fitlm;
     %Calculation of the relative error between the experimental
    stiffness
     %and the calculated one
     err_fitlm=(stiffness(i)-k_fitlm)/stiffness(i)*100;
     K(i,2)=err_fitlm;
     errore_fitlm(i)=err_fitlm;
end

meanError=mean(abs(errore_fitlm));

RMSE=fitlm_fun.RMSE;

K=[K stiffness];

end
```

```
% CORRELATION BETWEEN AFO DIMENSIONS AND AFO STIFFNESS

close all
clear all
clc

%% Loaad of the data
%The data are imported from an excel table into a MATLAB table
data=readtable('dimensioniSETT.xlsx');

%For each model an array withe the dimension is created and the it
    has
%been applied the function 'rigidAFO'
%% Uso la funzione rigidAFO per-GRANDEZZE LINEARI
```

```
dimensionp=[data.lenght(1:end-2) data.width(1:end-2) data.cstmax(1:
    end-2) data.w5rod(1:end-2) data.t5rod(1:end-2)];
[alpha1, Rsquared1, RsquaredAdj1, meanError1, RMSE1, meanError1, K1]=
    rigidAFO(data.StiffnessPlanta(1:end-2), dimensionp);

%% Uso la funzione rigidAFO per-GRANDEZZE QUADRATICHE
dimension2p=[data.lenght(1:end-2) data.width(1:end-2) (data.cstmax(1:
    end-2).^2) data.w5rod(1:end-2) data.t5rod2(1:end-2)];
[alpha2, Rsquared2, RsquaredAdj2, meanError2, RMSE2, meanError2, K2]=
    rigidAFO(data.StiffnessPlanta(1:end-2), dimension2p);

%% Uso la funzione rigidAFO per-GRANDEZZE CUBICHE
dimension3p=[data.lenght(1:end-2) data.width(1:end-2) (data.cstmax(1:
    end-2).^3) data.w5rod(1:end-2) data.t5rod3(1:end-2)];
[alpha3, Rsquared3, RsquaredAdj3, meanError3, RMSE3, meanError3, K3]=
    rigidAFO(data.StiffnessPlanta(1:end-2), dimension3p);

%% Uso la funzione rigidAFO per-AGGIUNGO MOMENTO D'INERZIA ASTICELLE(
    SINGOLE MISURE)
dimensionRODp=[data.lenght(1:end-2) data.width(1:end-2) data.cstmax
    (1:end-2) data.w5rod(1:end-2) data.t5rod3(1:end-2)];
[alphaROD, RsquaredROD, RsquaredAdjROD, meanErrorROD, RMSEROD,
    meanErrorROD, KROD]=rigidAFO(data.StiffnessPlanta(1:end-2),
    dimensionRODp);

%% Uso la funzione rigidAFO per-AGGIUNGO MOMENTO D'INERZIA ASTICELLE
dimensionRODmp=[data.lenght(1:end-2) data.width(1:end-2) data.cstmax
    (1:end-2) data.w5rod(1:end-2) data.t5rod(1:end-2) data.
    inertia_momentROD(1:end-2)];  %lascio comunque le altre misure al
    cubo?
[alphaRODm, RsquaredRODm, RsquaredAdjRODm, meanErrorRODm, RMSERODm,
    meanErrorRODm, KRODm]=rigidAFO(data.StiffnessPlanta(1:end-2),
    dimensionRODmp);

%% Uso la funzione rigidAFO per-AGGIUNGO MOMENTO D'INERZIA PARTE
    FLETTENTE (SINGOLE MISURE)
dimensionFLETTp=[data.lenght(1:end-2) data.width(1:end-2) (data.
    cstmax(1:end-2).^3) data.w5rod(1:end-2) data.t5rod(1:end-2)];
[alphaFLETT, RsquaredFLETT, RsquaredAdjFLETT, meanErrorFLETT,
    RMSEFLETT, meanErrorFLETT, KFLETT]=rigidAFO(data.StiffnessPlanta
    (1:end-2), dimensionFLETTp);

%% Uso la funzione rigidAFO per-AGGIUNGO MOMENTO D'INERZIA PARTE
```

```
    FLETTENTE
dimensionFLETTmp=[data.lenght(1:end-2) data.width(1:end-2) data.
    cstmax(1:end-2) data.w5rod(1:end-2) data.t5rod(1:end-2) data.
    inertia_momentFLETT(1:end-2)];
[alphaFLETTm, RsquaredFLETTm, RsquaredAdjFLETTm, meanErrorFLETTm,
    RMSEFLETTm, meanErrorFLETTm, KFLETTm]=rigidAFO(data.
    StiffnessPlanta(1:end-2), dimensionFLETTmp);

%% Uso la funzione rigidAFO per-AGGIUNGO ENTRAMBI I MOMENTI D'INERZIA
dimensionmmp=[data.lenght(1:end-2) data.width(1:end-2) data.cstmax(1:
    end-2) data.w5rod(1:end-2) data.t5rod(1:end-2) data.
    inertia_momentROD(1:end-2) data.inertia_momentFLETT(1:end-2) ];
[alphamm, Rsquaredmm, RsquaredAdjmm, meanErrormm, RMSEmm, meanErrormm
    , Kmm]=rigidAFO(data.StiffnessPlanta(1:end-2), dimensionmmp);
```

```
%ESTIMATION OF AFO MINIMUM STIFFNESS IN STATIC CONDITIONS
% This script has been developed to calculate the minimum stiffness
    in static conditions, for the
% specific patient using its static data

close all
clear all
clc

%Import of the static data
file=uigetfile('*.csv','Select CSV files','MultiSelect','on');

%The cycle iterates as many times as the number of file selected
for i=1:size(file,2);
    %the imported table is converted into an array
    dataTable = readtable(string(file(i)));
    data=table2array(dataTable);

    %ID patient is useful in order to selected the correct
    informations
    %about each patient reported in an excel file
    IDpaz=input('Inserire l''ID del paziente: ');

    %The ID patient numerical order does not respect the order in the
     excel
    %table
    if IDpaz == 2;
        IDpaz=1;
    elseif IDpaz == 3;
```

```
        IDpaz=2;
    elseif IDpaz == 4;
        IDpaz=3;
    elseif IDpaz == 6
        IDpaz=4
    elseif IDpaz == 8
        IDpaz=5
    elseif IDpaz == 9;
        IDpaz=6;
    elseif IDpaz == 10;
        IDpaz=7;
    elseif IDpaz == 11;
        IDpaz=8;
    elseif IDpaz == 13;
        IDpaz=9;
    elseif IDpaz == 14;
        IDpaz=10;
    end

    %Import of the table with the necessary patients data
    datiPaz=readtable('info_paz.xlsx');
    info=table2array(datiPaz);
    bodyweight=info(IDpaz,2); %kg
    lenghtFoot=info(IDpaz,3)/1000; %m

    %Affected foot
    if IDpaz == 1 | IDpaz == 3 | IDpaz == 4  | IDpaz == 5 | IDpaz ==
    6 | IDpaz == 7 | IDpaz == 9 | IDpaz == 10;  %left foot affected
        %find the indices of the position of the necessary markers
        posLLM=find(strcmp(dataTable.Properties.VariableNames, 'LLM')
    );
        posLCA=find(strcmp(dataTable.Properties.VariableNames, 'LCA')
    );
        posLVM=find(strcmp(dataTable.Properties.VariableNames, 'LVM')
    );
        posLFM=find(strcmp(dataTable.Properties.VariableNames, 'LFM')
    );
        posLMM=find(strcmp(dataTable.Properties.VariableNames, 'LMM')
    );
        LMMM=MM-LM;
        %conversion in meters
        LM=data(:,posLLM:posLLM+2)/1000; %m
        CA=data(:,posLCA:posLCA+2)/1000;
```

```
64          VM=data(:,posLVM:posLVM+2)/1000;
65          FM=data(:,posLFM:posLFM+2)/1000;
66          MM=data(:,posLMM:posLMM+2)/1000;
67
68      else  %rigth foot affected
69          posRLM=find(strcmp(dataTable.Properties.VariableNames, 'RLM')
    );
70          posRCA=find(strcmp(dataTable.Properties.VariableNames, 'RCA')
    );
71          posRVM=find(strcmp(dataTable.Properties.VariableNames, 'RVM')
    );
72          posRFM=find(strcmp(dataTable.Properties.VariableNames, 'RFM')
    );
73          posRMM=find(strcmp(dataTable.Properties.VariableNames, 'RMM')
    );
74
75          LM=data(:,posRLM:posRLM+2)/1000; %m
76          CA=data(:,posRCA:posRCA+2)/1000;
77          VM=data(:,posRVM:posRVM+2)/1000;
78          FM=data(:,posRFM:posRFM+2)/1000;
79          MM=data(:,posRMM:posRMM+2)/1000;
80          LMMM=LM-MM;
81      end
82
83      %% Determination of the mass of the foot
84      %Calculation of the ankle width, which is the distance between
    the 2
85      %malleoli
86      ankleWidth=mean(sqrt((MM(:,1)-LM(:,1)).^2+(MM(:,2)-LM(:,2)).^2+(
    MM(:,3)-LM(:,3)).^2)); %m
87      %Calculation of the ankle height, which is the height of the
    lateral
88      %malleolo; it has been subtracted 2 cm since the static data has
    been
89      %collected with the shoes on
90      ankleHeight=mean(LM(:,3))-0.02; %m
91      %The following equation to calculate the mass of the foot has
    been
92      %implemented by Pavol et al.
93      mfoot=0.0083*bodyweight+254.5*lenghtFoot*ankleHeight*ankleWidth
    -0.065; % kg
94
95      %% Determination of the force of gravity
```

```
96  %For this calculation  both the mass of the foot
97  %and the mass of the shoe, in this case a lightweight shoe, has
    been considered
98  mshoe=0.164; %kg  (with the safety shoe: mshoe=0.496)
99  mtot=mfoot+mshoe;
100 %We imposed, as convention, that the acceleration of gravity is
101 %directed downwards
102 g=-9.81; %m/s^2
103 %Creation of the array with the gravity force, which has one
104 %compenent along the z axis
105 Fg=mtot*g; %N
106 prova=ones(length(MM),1);
107 Fg=Fg*prova;
108 Fgxy=zeros(length(Fg),2);
109 Fg=[Fgxy Fg];
110
111 %% Determination of the ankle axis moment
112 %Determination of the COG through a function that calculate the
    mean
113 %position of the three markers
114 COG=GravityCenter(CA, VM, FM);
115 middlepoint=((LM+MM)./2);
116 arm=abs(COG-middlepoint); %lever arm of the force of gravity
117 M=cross(arm, Fg); %cross product
118 %Determination of the unit vector of the ankle axis
119 modLMMM=sqrt((LM(:,1)-MM(:,1)).^2+(LM(:,2)-MM(:,2)).^2+(LM(:,3)-
    MM(:,3)).^2);
120 LMMM=(LM-MM);
121 unitvector=(LMMM/mean(modLMMM));
122 M_axis=dot(M, unitvector, 2); %dot product, to calculate the
    component of the moment along the ankle axis
123 M_AXIS(i)=mean(M_axis);
124
125 M_axis_normalizedweight=M_axis/bodyweight; %Nm/kg
126 M_max_nw=max(M_axis_normalizedweight); %max ankle moment
    plantarflex
127
128 %% Determination of the stiffness
129 displacement=1; %deg
130 stiff_p=M_AXIS(i)/displacement;  %Nm/deg
131
132 stiff_p_bw=stiff_p/bodyweight;
133 STIFF_P_BW(i)=stiff_p_bw;
```

```
134
135     %% Determination of the moment of inertia useful for the gait
        condition calculation
136     %Calculation of the moment of inertia in respect of the COG
        through
137     %Hinrichs equation
138     Icog(i)=(6.7508*(lenghtFoot*100)-4.2725*(ankleHeight*100)-105.42)
        *(10^-4); %kg m^2
139
140     %It is needed the moment of inertia in respect of the ankle axis
141     d_ankleCOG=distancePointLine(COG, LM, MM); %function which
        calculate the distance between the point (COG) and the line
        thorugh LM and MM
142     DIST_ankleCOG(i)=mean(d_ankleCOG);
143     %In order to determine the moment of inertia in respect of the
        ankle
144     %axis the Huygens-Stayner theorem has been used
145     Iankle(i)=Icog(i)+mtot.*(DIST_ankleCOG(i).^2);
146
147 end
148
149 value=mean(STIFF_P_BW);
```

```
1  %ESTIMATION OF AFO MINIMUM STIFFNESS IN GAIT
2  % This script has been developed to calculate the minimum stiffness
       in gait conditions, for the
3  % specific patient using its kinematic data
4  close all
5  clear all
6  clc
7
8  %% Caricamento dei dati
9  % Using the csv2mat to create the structure used to obtain the
       trajectories of
10 % the marker and the angle
11
12 load 'data.mat'
13
14 M_tot=[];
15 %The cycle iterates as many times as the number of file selected
16 for i=1:size(data.foot.file, 2);
17     %the patients ID is obtained from the name of the file, where is
18     %reported in specific positions
19     nomeFile=data.foot.file(i).name;
```

```
20    IDpaz=str2num(nomeFile(end-15:end-14));
21
22    %The patient ID numerical order does not respect the order in the
      excel
23    %table
24    if IDpaz == 2;
25        IDpaz=1;
26    elseif IDpaz == 3;
27        IDpaz=2;
28    elseif IDpaz == 4;
29        IDpaz=3;
30    elseif IDpaz == 6;
31        IDpaz=4;
32    elseif IDpaz == 8;
33        IDpaz=5;
34    elseif IDpaz == 9;
35        IDpaz=6;
36    elseif IDpaz == 10;
37        IDpaz=7;
38    elseif IDpaz == 11;
39        IDpaz=8;
40    elseif IDpaz == 13;
41        IDpaz=9;
42    elseif IDpaz == 14;
43        IDpaz=10;
44    end
45
46    %Import of the table with the necessary patients data
47    datiPaz=readtable('info_paz.xlsx');
48    info=table2array(datiPaz);
49    bodyweight=info(IDpaz,2); %kg
50    BW(i)=bodyweight;
51    lenghtFoot=info(IDpaz,3)/1000;
52
53    % The following data are determinated in static conditions
54    ankleWidth=info(IDpaz,4); %m
55    ankleHeight=info(IDpaz,6); %m
56    mfoot=info(IDpaz,8); %kg
57    Iankle=info(IDpaz, 10); %
58
59    %Affected foot
60    if IDpaz == 1 | IDpaz == 3 | IDpaz == 4  | IDpaz == 5 | IDpaz ==
     6 | IDpaz == 7 | IDpaz == 9 | IDpaz == 10;  %left foot affected
```

```
        %find the indices of the position of the necessary markers
        CA=data.foot.file(i).KIN.LT.SWING.MARKER.LCA/1000; %m
        FM=data.foot.file(i).KIN.LT.SWING.MARKER.LFM/1000;
        VM=data.foot.file(i).KIN.LT.SWING.MARKER.LVM/1000;
        LM=data.foot.file(i).KIN.LT.SWING.MARKER.LLM/1000;
        MM=data.foot.file(i).KIN.LT.SWING.MARKER.LMM/1000;
        theta=data.foot.file(i).KIN.LT.SWING.ANGLE.AAngle;
        LMMM=MM-LM;
    else  %rigth foot affected
        CA=data.foot.file(i).KIN.RT.SWING.MARKER.RCA/1000; %m
        FM=data.foot.file(i).KIN.RT.SWING.MARKER.RFM/1000;
        VM=data.foot.file(i).KIN.RT.SWING.MARKER.RVM/1000;
        LM=data.foot.file(i).KIN.RT.SWING.MARKER.RLM/1000;
        MM=data.foot.file(i).KIN.RT.SWING.MARKER.RMM/1000;
        theta=data.foot.file(i).KIN.RT.SWING.ANGLE.AAngle;
        LMMM=LM-MM;
    end

    %The ankle angle is converted into radiants
    theta=(theta*pi)/180;

    %% Determination of the gravity force
    %For this calculation the mass of the foot and the mass of the
   shoe,
    %in this case a lightweight shoe, has been considered
    mshoe=0.164; %kg
    mtot=mfoot+mshoe;
    %We imposed, as convention, that the gravity acceleration is
    %directed downwards
    g=-9.81; %m/s^2
    %Creation of the array with the force of gravity, which has one
    %compenent along the z axis
    Fg=mtot*g; %N
    prova=ones(length(MM),1);
    Fg=Fg.*prova;
    Fgxy=zeros(length(Fg),2);
    Fg=[Fgxy Fg];


    %% Determination of the inertia forces due to accelerations
    %Determination of the COG through a function that calculates the
   mean
    %position of the three markers
```

```
102  COG=GravityCenter(CA, VM, FM); %cambia in ogni istante
103
104  middlepoint=((LM+MM)./2);
105  arm=abs(COG-middlepoint); %lever arm of the force of gravity
106  deltat=0.01; %sampling time
107  %Determination of the acceleration through a function
108  [velocity, acceleration]=difference(COG, deltat);
109
110  %Force due to acceleration
111  F=acceleration.*mtot;  %kg*m/s2 = N
112
113  %This normalization is necessary when calculating the
     acceleration
114  %through
115  %2 consecutive differences the vector reduces its length
116  Fg=normalizeN(Fg, length(acceleration));
117  F=F+Fg;
118
119  %%  Determination of the ankle axis moment due to the two forces
120  arm=normalizeN(arm, length(F));
121  M=cross(arm, F); %cross producte
122
123  %Determination of the unit vector of the ankle axis
124  modLMMM=sqrt((LM(:,1)-MM(:,1)).^2+(LM(:,2)-MM(:,2)).^2+(LM(:,3)-
     MM(:,3)).^2);  %valore che non varia nel tempo
125  for j=1:length(LMMM)   %the unit vector changes its direction
     instant by instant
126      unitvector(j,1:3)=(LMMM(j,1:3)./modLMMM(j));
127  end
128  unitvector=normalizeN(unitvector, length(M));
129
130  M_axis=dot(M, unitvector, 2); %dot product, to calculate the
     component of the moment along the ankle axis
131  M_axis_normalizedweight=M_axis/bodyweight; %Nm/kg
132
133  %% Determination of the component of the ankle moment due to
     acceleration
134  %Determination of the angular acceleration
135  [velocity_ang, acceleration_ang]=difference(theta, deltat);
136  I=acceleration_ang(:,1).*Iankle; %the component of interest is
     along the x axis
137
138  if length(I) < length(M_axis)
```

```
        M_axis=normalizeN(M_axis, length(I));
    else
        I_tot=normalizeN(I, length(M_axis));
    end

    %Reducing computazional cost by deleting NaN values
    vettoreNaNI=isnan(I_tot);
    posI=find(vettoreNaNI);
    I_tot(posI)=[];

    vettoreNaNM=isnan(M_axis);
    posM=find(vettoreNaNM);
    M_axis(posM)=[];

    %% Determination of the total ankle axis moment
    %The moment is a sum of the two component calculated above
    M_ANKLE_AXIS=I_tot'+M_axis;
    M_normalizzato=normalizeN(M_ANKLE_AXIS, 100);

    M_tot(i,:)=M_normalizzato;

    %Plantarfelxion moment
    MIN_PLANTA_MOMENT(i)=min(M_ANKLE_AXIS);
    %DOrsiflexion moment
    MAX_DORSI_MOMENT(i)=max(M_ANKLE_AXIS);
    %Total ankle axis moment normalized on the body weight of the
   patient
    M_ANKLE_AXIS_BW=(I_tot/bodyweight)'+(M_axis/bodyweight);

    %% Determination of the stiffness
    displacement=1; %deg
    STIFF_P(i)=MIN_PLANTA_MOMENT(i)/displacement;

    STIFF_P_BW(i)=STIFF_P(i)/bodyweight;

end

value=mean(STIFF_P_BW);
```

B

Supplementary figures and tables

Static conditions

Patient ID	Moment at the ankle axis [Nm]			
	Affected foot		Non affected foot	
	Lightweight shoe	Safety shoe	Lightweight shoe	Safety shoe
2	-0.64	-0.81	-0.82	-1.04
3	-0.98	-1.20	-0.52	-0.63
4	0.91	-1.11	-1.18	-1.4
6	-0.74	-0.91	-1.13	-1.39
8	-0.91	-1.13	-0.99	-1.22
9	-0.73	-0.91	-0.84	-1.03
10	-0.46	-0.59	-0.70	-0.89
11	-0.78	-0.99	-0.67	-0.84
13	-0.35	-0.44	-0.75	-0.95
14	-0.46	-0.62	-0.51	-0.67
Median (25th, 75th)	-0.74 (-0.91, -0.46)	-0.91 (-1.11, -0.62)	-0.79 (-0.99, -0.67)	-0.99 (-1.22, -0.84)

Table B.1: Moment at the ankle axis calculated in static conditions for both affected and non affected foot, for lightweight and safety shoe for the 10 foot drop patients.

Patient ID	Minimum AFO stiffness [Nm/deg]			
	Affected foot		Non affected foot	
	Lightweight shoe	Safety shoe	Lightweight shoe	Safety shoe
2	0.64	0.81	0.82	1.04
3	0.98	1.20	0.52	0.63
4	0.91	1.11	1.18	1.44
6	0.74	0.91	1.13	1.39
8	0.91	1.13	0.99	1.22
9	0.73	0.91	0.84	1.03
10	0.46	0.59	0.70	0.89
11	0.78	0.99	0.67	0.84
13	0.35	0.44	0.75	0.95
14	0.46	0.62	0.51	0.67
Median (25th, 75th)	0.74 (0.46, 0.91)	0.91 (0.62, 1.11)	0.79 (0.67, 0.99)	0.99 (0.84, 1.22)

Table B.2: Estimated minimum AFO stiffness calculated in static conditions for both affected and non affected foot, for lightweight and safety shoe for the 10 foot drop patients.

Gait conditions

Mean temporal profile (± 1SD) of the ankle moment (Nm) for each of the 10 foot-drop patients in the affected and non affected foot across normalized swing phase duration.

Patient 2

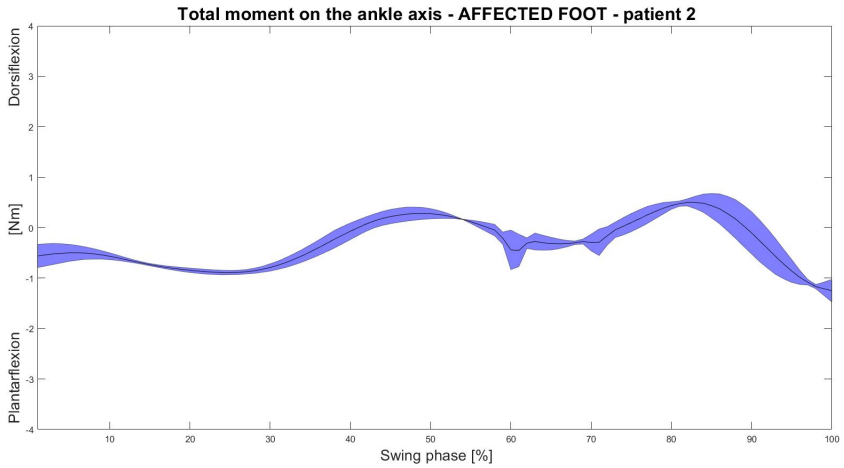

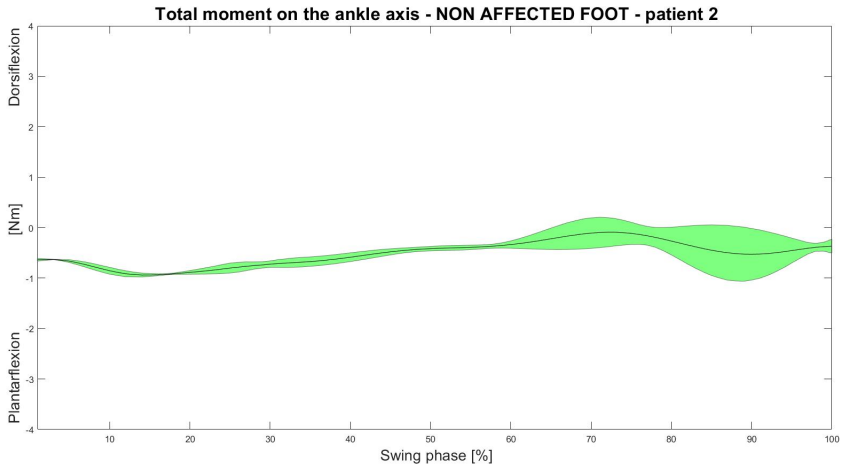

Patient 3

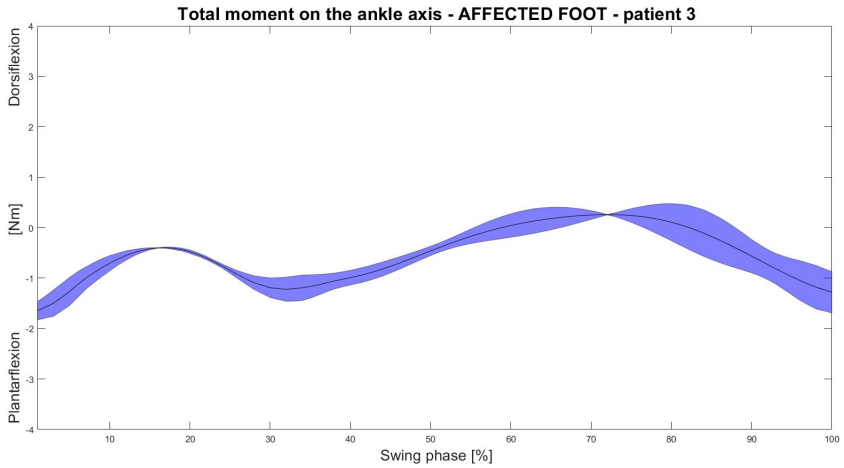
Total moment on the ankle axis - AFFECTED FOOT - patient 3
Dorsiflexion
[Nm]
Plantarflexion
Swing phase [%]

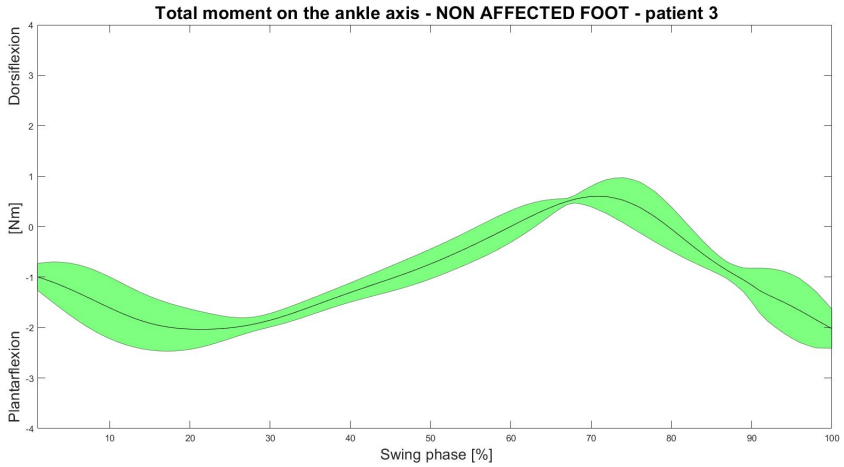
Total moment on the ankle axis - NON AFFECTED FOOT - patient 3
Dorsiflexion
[Nm]
Plantarflexion
Swing phase [%]

Patient 4

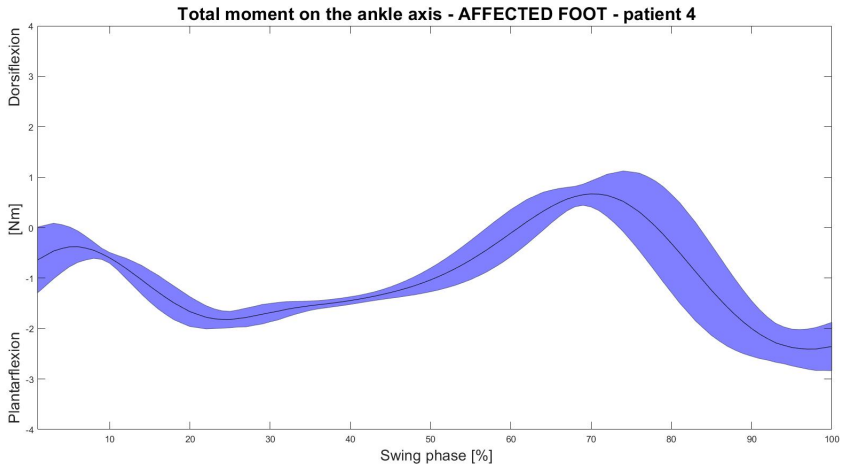
Total moment on the ankle axis - AFFECTED FOOT - patient 4
Dorsiflexion
[Nm]
Plantarflexion
Swing phase [%]

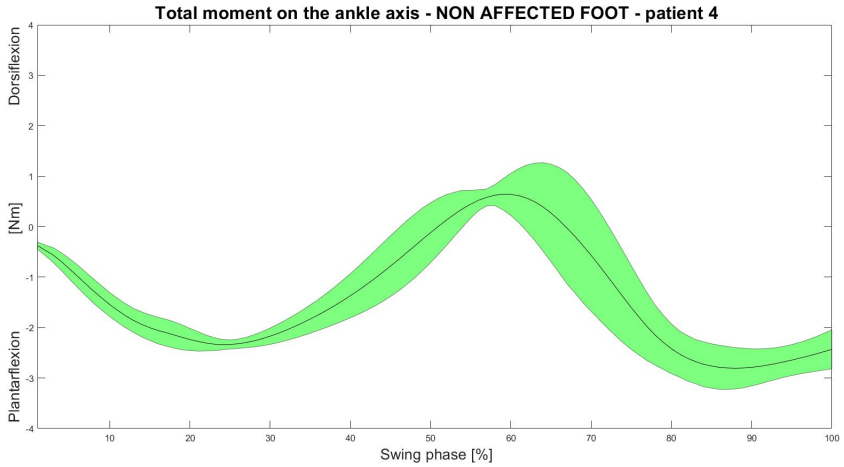
Total moment on the ankle axis - NON AFFECTED FOOT - patient 4
Dorsiflexion
[Nm]
Plantarflexion
Swing phase [%]

Patient 6

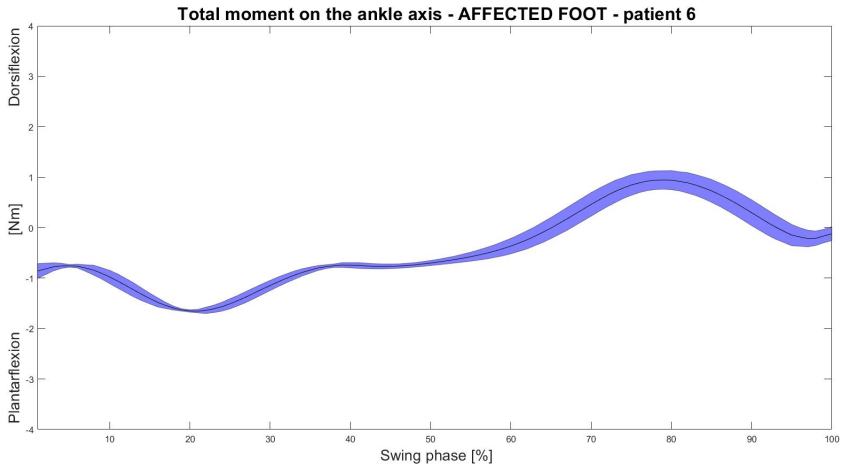
Total moment on the ankle axis - AFFECTED FOOT - patient 6
Dorsiflexion
[Nm]
Plantarflexion
Swing phase [%]

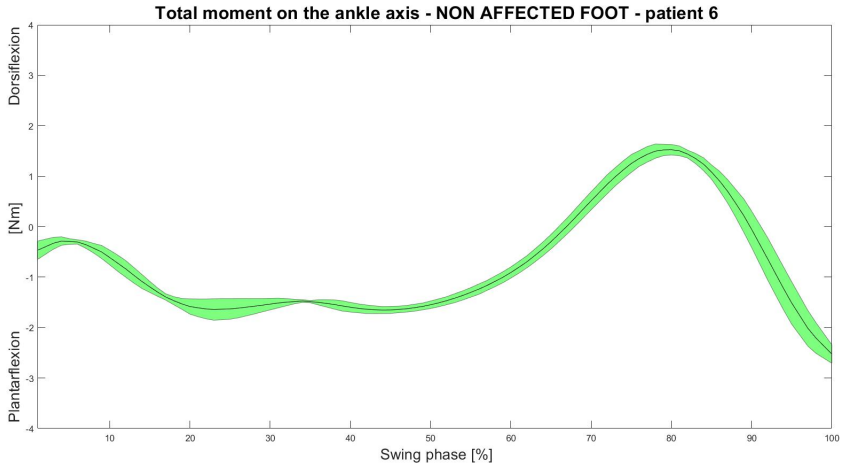
Total moment on the ankle axis - NON AFFECTED FOOT - patient 6
Dorsiflexion
[Nm]
Plantarflexion
Swing phase [%]

Patient 8

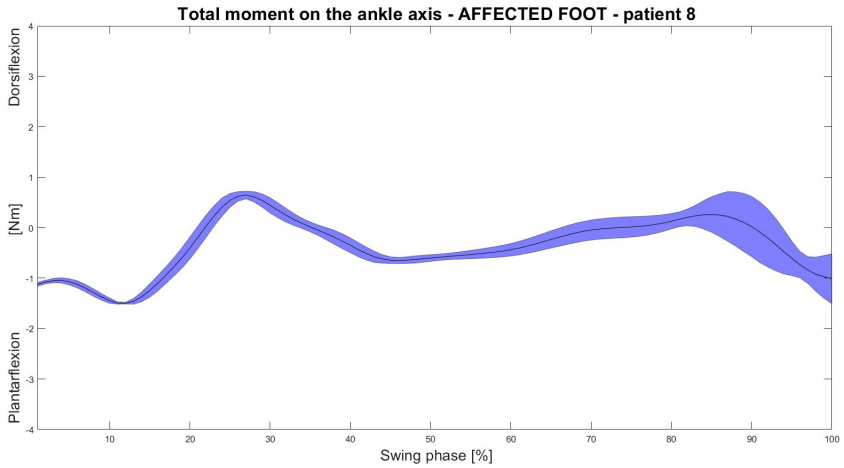
Total moment on the ankle axis - AFFECTED FOOT - patient 8
Dorsiflexion
[Nm]
Plantarflexion
Swing phase [%]

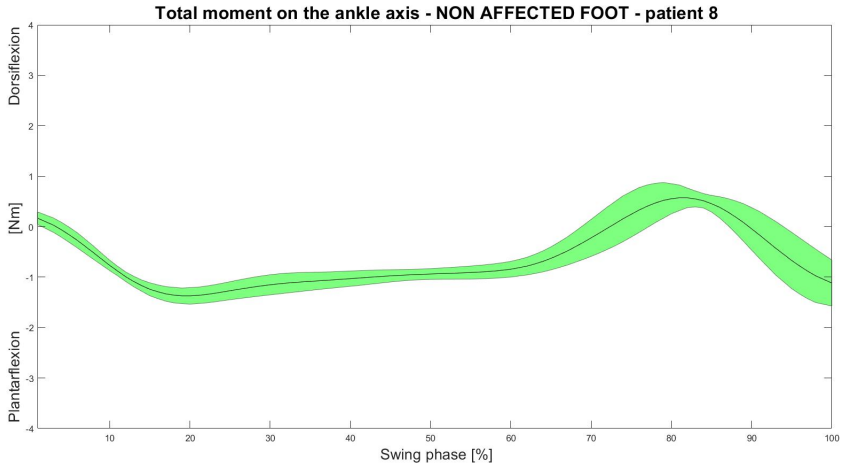
Total moment on the ankle axis - NON AFFECTED FOOT - patient 8
Dorsiflexion
[Nm]
Plantarflexion
Swing phase [%]

Patient 9

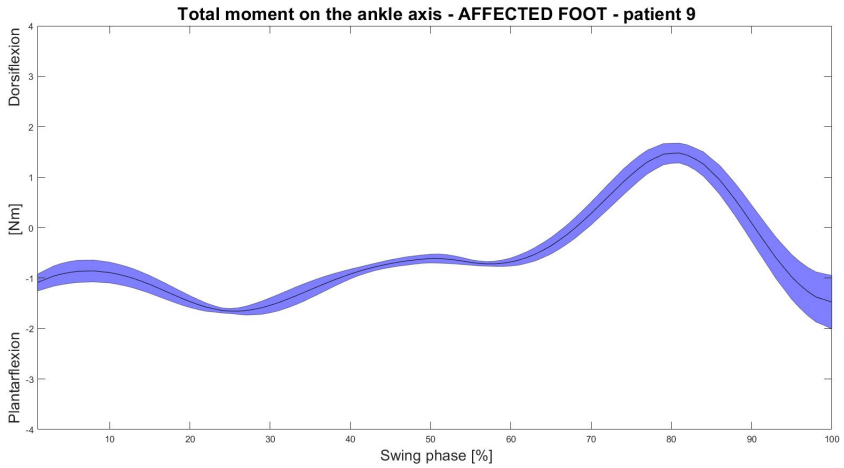
Total moment on the ankle axis - AFFECTED FOOT - patient 9
Dorsiflexion
[Nm]
Plantarflexion
Swing phase [%]

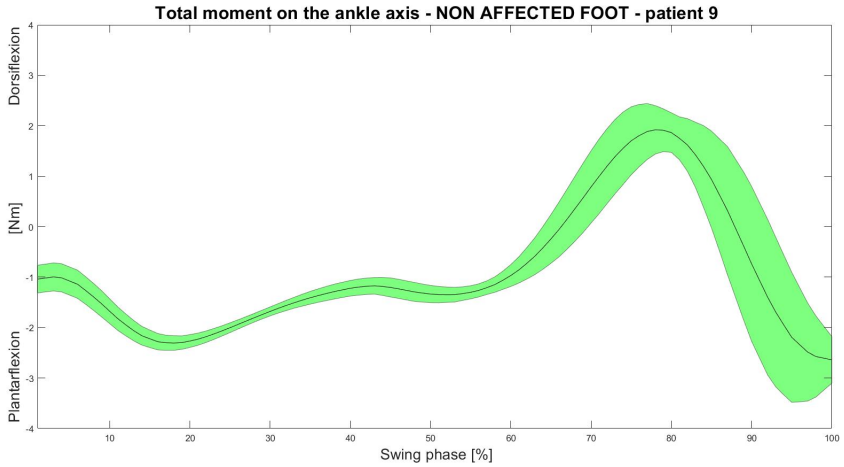
Total moment on the ankle axis - NON AFFECTED FOOT - patient 9
Dorsiflexion
[Nm]
Plantarflexion
Swing phase [%]

Patient 10

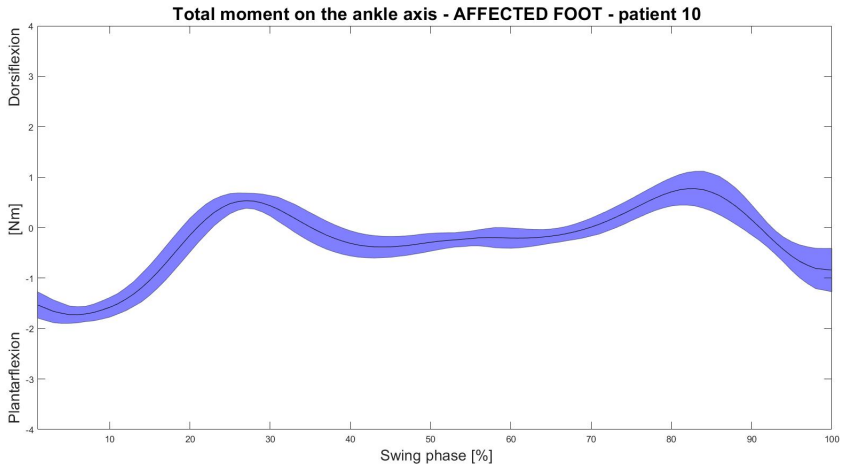
Total moment on the ankle axis - AFFECTED FOOT - patient 10
Dorsiflexion
[Nm]
Plantarflexion
Swing phase [%]

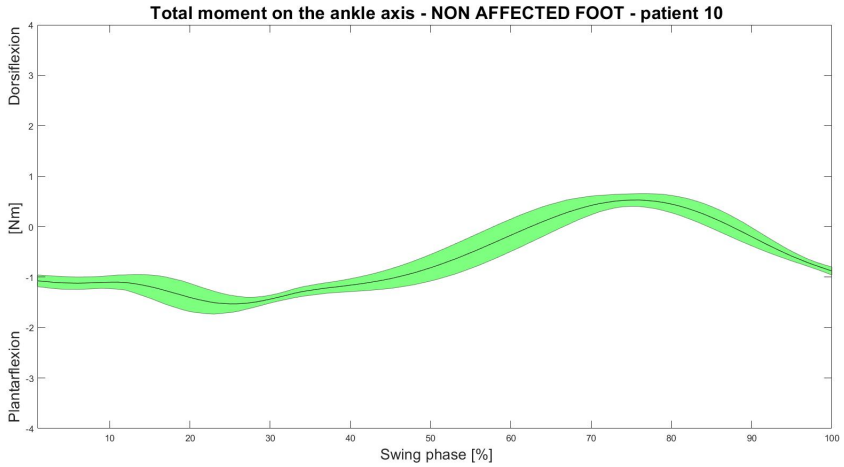
Total moment on the ankle axis - NON AFFECTED FOOT - patient 10
Dorsiflexion
[Nm]
Plantarflexion
Swing phase [%]

Patient 11

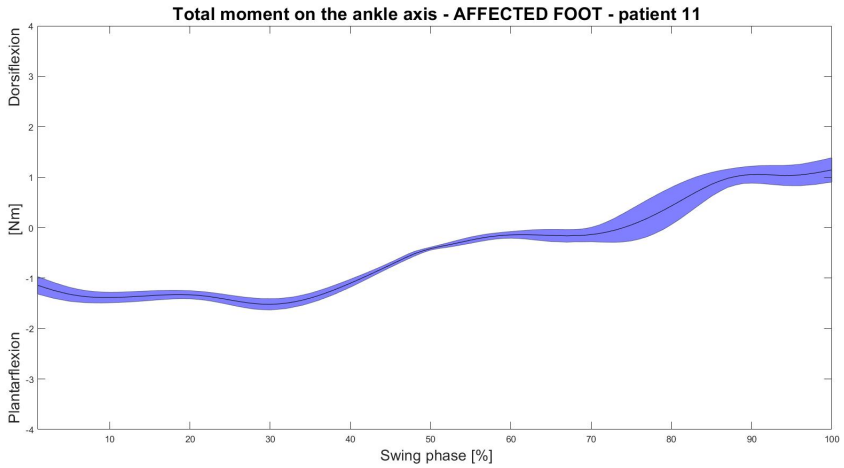
Total moment on the ankle axis - AFFECTED FOOT - patient 11
Dorsiflexion
[Nm]
Plantarflexion
Swing phase [%]

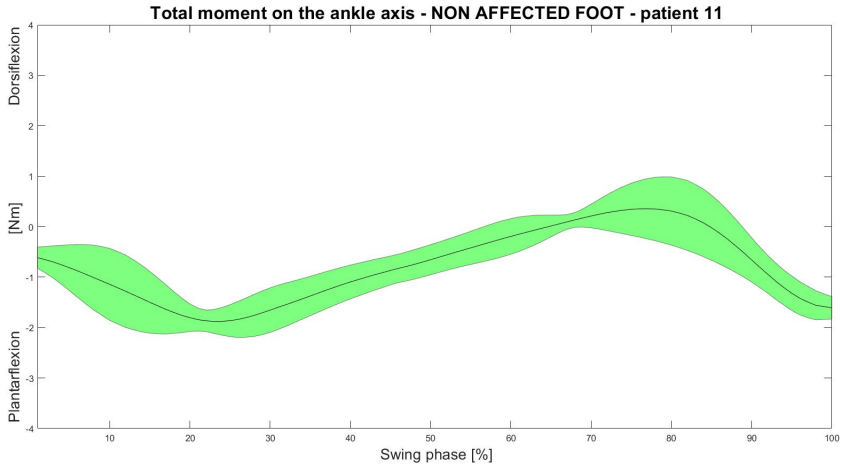
Total moment on the ankle axis - NON AFFECTED FOOT - patient 11
Dorsiflexion
[Nm]
Plantarflexion
Swing phase [%]

Patient 13

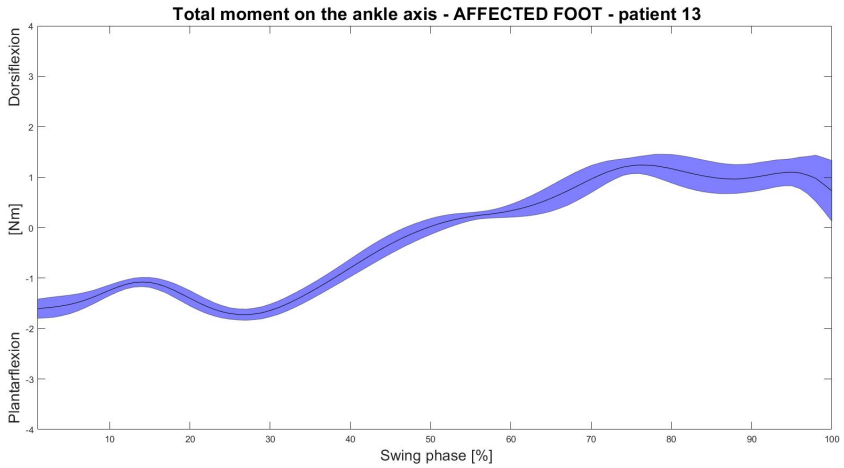
Total moment on the ankle axis - AFFECTED FOOT - patient 13
Dorsiflexion
[Nm]
Plantarflexion
Swing phase [%]

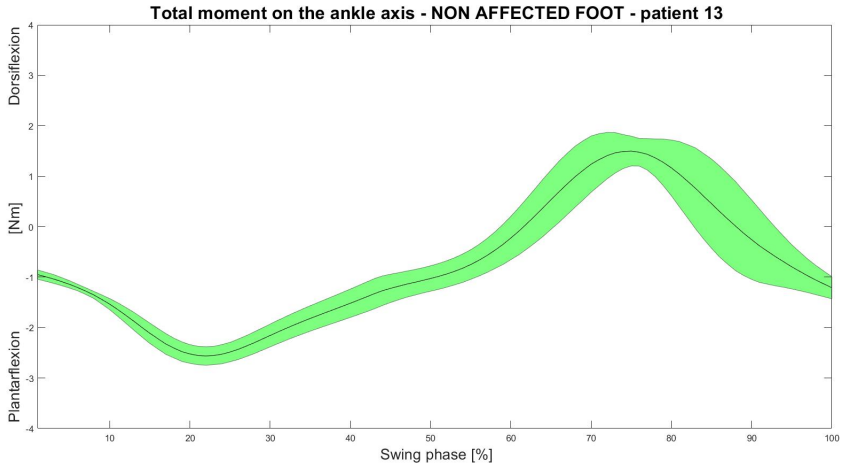
Total moment on the ankle axis - NON AFFECTED FOOT - patient 13
Dorsiflexion
[Nm]
Plantarflexion
Swing phase [%]

Patient 14

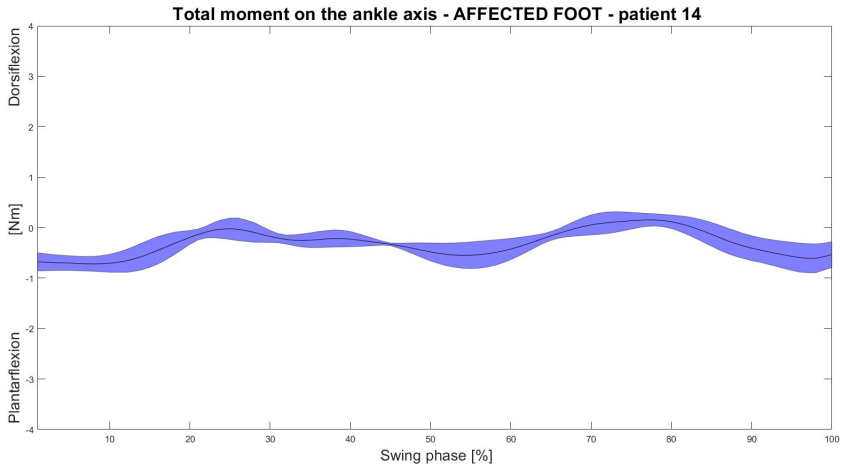
Total moment on the ankle axis - AFFECTED FOOT - patient 14
Dorsiflexion
[Nm]
Plantarflexion
Swing phase [%]

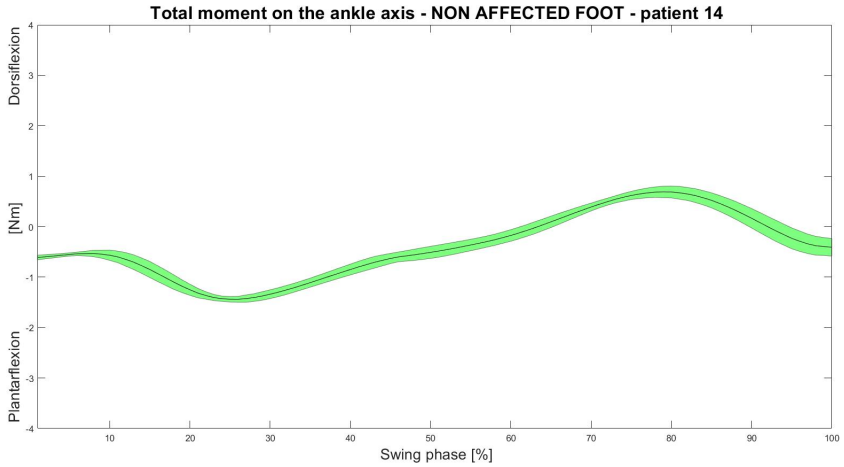
Total moment on the ankle axis - NON AFFECTED FOOT - patient 14
Dorsiflexion
[Nm]
Plantarflexion
Swing phase [%]

Patient ID	Maximum plantarflexion moment [Nm]	
	Affected foot	Non affected foot
	Lightweight shoe	
2	-1.30 ± 0.13	-0.96 ± 0.06
3	-1.66 ± 0.17	-2.15 ± 0.24
4	-2.62 ± 0.23	-2.98 ± 0.30
6	-1.67 ± 0.04	-2.52 ± 0.18
8	-1.52 ± 0.01	-1.43 ± 0.27
9	-1.77 ± 0.18	-2.82 ± 0.38
10	-1.77 ± 0.19	-1.58 ± 0.13
11	-1.52± 0.11	-2.11 ± 0.13
13	-1.74 ± 0.12	-2.58 ± 0.18
14	-0.86 ± 0.15	-1.46 ± 0.07
Meadian (25th, 75th)	-1.66 (-1.77 -1.52)	-2.14 (-2.58, -1.46)

Table B.3: Plantarflexion moment calculated during gait, for both affected and non affected foot, for the 10 foot drop patients. For each patients has been shown the mean of the trials with the standard deviation.

Patient ID	Minimum dorsiflexion moment [Nm]	
	Affected foot	Non affected foot
	Lightweight shoe	
2	0.56 ± 0.08	0.09 ± 0.03
3	0.38 ± 0.04	0.69 ± 0.22
4	0.87 ± 0.16	0.92 ± 0.13
6	0.99 ± 0.19	1.54 ± 0.09
8	0.71 ± 0.11	0.66± 0.25
9	1.52 ± 0.22	2.20 ± 0.31
10	0.85 ± 0.27	0.55 ± 0.14
11	1.19 ± 0.22	0.64 ± 0.26
13	1.32 ± 0.20	1.72 ± 0.33
14	0.26 ± 0.14	0.70 ± 0.11
Median (25th, 75th)	0.86 (0.56, 1.19)	0.70 (0.64, 1.54)

Table B.4: Dorsiflexion moment calculated during gait, for both affected and non affected foot, for the 10 foot drop patients. For each patients has been shown the mean of the trials with the standard deviation.

Patient ID	Minimum AFO stiffness [Nm/deg]	
	Affected foot	Non affected foot
	Lightweight shoe	
2	1.30 ± 0.13	0.96 ± 0.13
3	1.66 ± 0.17	2.15 ± 0.17
4	2.62 ± 0.23	2.98 ± 0.23
6	1.67 ± 0.04	2.52 ± 0.04
8	1.51 ± 0.013	1.43 ± 0.01
9	1.77 ± 0.18	2.82 ± 0.18
10	1.77 ± 0.19	1.58 ± 0.19
11	1.52 ± 0.11	2.11 ± 0.11
13	1.74 ± 0.11	2.58 ± 0.12
14	0.86 ± 0.15	1.46 ± 0.14
Median (25th, 75th)	1.66 (1.52, 1.77)	2.14 (1.46, 2.58)

Table B.5: Estimated minimum AFO stiffness calculated during gait, for both affected and non affected foot, for the 10 foot drop patients. For each patients has been shown the mean of the trials with the standard deviation.

List of Figures

List of Tables

List of Acronyms

AFO Ankle Foot Orthosis

ALS AFO Anterior Leaf Spring Ankle Foot Orthosis

AM Additive manufacturing

ATL Anterior Talofibular Ligament

BRUCE Bi-articular Reciprocating Universal Compliance Estimator

CFL Calcaneofibular Ligament

COG Center of gravity

COP Centre of pressure

EMG Electromyography

FDM Fused Deposition Modeling

GA Gait Analysis

GRF Ground Reaction Force

IOR Rizzoli ORrthopaedic Institute

KST Kentucky Stiffness Tester

LCL Lateral Collateral Ligament

MCL Medial Collateral Ligaments

MJF Multi Jet Fusion

MoCap Motion Capture

MOxFQ Manchester Oxford Foot Questionnaire

MRC Medical Research Council

ODFS Odstock Dropped Foot Stimulator

PD AFO Passive Dynamic AFO

PLS AFO Posterior Leaf Spring Ankle Foot Orthosis

PTFL Posterior Talofibular Ligament

PROM Patient-Recorded Outcome Measure

ROM Range Of Motion

SLA Stereolithography

SLS Selective Laser Sintering

SMApp Stiffness Measurement Apparatus

VAS Visual Analog Scale

Bibliography

[1] Henry Gray et al. "Gray's anatomy: the anatomical basis of clinical practice". In: (2008).

[2] Clare Elizabeth Milner and Roger William Soames. "Anatomy of the collateral ligaments of the human ankle joint". In: *Foot & ankle international* 19.11 (1998), pp. 757–760.

[3] James R Jastifer. "Intrinsic muscles of the foot: Anatomy, function, rehabilitation". In: *Physical Therapy in Sport* (2023).

[4] Claire L Brockett and Graham J Chapman. "Biomechanics of the ankle". In: *Orthopaedics and trauma* 30.3 (2016), pp. 232–238.

[5] Charles E Clauser, John T Mc Conville, and John W Young. *Weight, volume, and center of mass of segments of the human body*. Tech. rep. 1969.

[6] E Harless. "The static moments of the component masses of the human body". In: *Trans. of the Math-Phys., Royal Bavarian Acad. of Sci* 8.1 (1860), pp. 69–96.

[7] W Braune and O Fischer. "The center of gravity of the human body as related to the German infantryman". In: *ATI* 138 (1889), p. 452.

[8] Wilfred Taylor Dempster et al. *Space requirements of the seated operator: geometrical, kinematic, and mechanical aspects of the body with special reference to the limbs*. Vol. 159. Wright Air Development Center Wright-Patterson Air Force Base, Ohio, 1955.

[9] Wilfrid Taylor Dempster and George RL Gaughran. "Properties of body segments based on size and weight". In: *American journal of anatomy* 120.1 (1967), pp. 33–54.

[10] Stanley Plagenhoef, F Gaynor Evans, and Thomas Abdelnour. "Anatomical data for analyzing human motion". In: *Research quarterly for exercise and sport* 54.2 (1983), pp. 169–178.

[11] Rudolfs Drillis and Renato Contini. *Body segment parameters*. New York University, School of Engineering and Science, Research Division, 1966.

[12] A El Helou et al. "Estimating foot inertial parameters: A new regression approach". In: *Clinical biomechanics* 27.3 (2012), pp. 299–305.

[13] Arne Lundberg et al. "The axis of rotation of the ankle joint". In: *The Journal of Bone & Joint Surgery British Volume* 71.1 (1989), pp. 94–99.

[14] Cyril H Barnett and John R Napier. "The axis of rotation at the ankle joint in man. Its influence upon the form of the talus and the mobility of the fibula". In: *Journal of anatomy* 86.Pt 1 (1952), p. 1.

[15] Richard Baker. "Gait analysis methods in rehabilitation". In: *Journal of neuroengineering and rehabilitation* 3 (2006), pp. 1–10.

[16] M.W. Whittle. *Gait Analysis: An Introduction*. Elsevier Science, 2014. ISBN: 9781483183732. URL: https://books.google.it/books?id=dYHiBQAAQBAJ.

[17] Ashutosh Kharb et al. "A review of gait cycle and its parameters". In: *IJCEM International Journal of Computational Engineering & Management* 13 (2011), pp. 78–83.

[18] Giulia Donà et al. "Biomechanical analysis of three different blocking footwork techniques in volleyball: a pilot study". In: *ISBS-Conference Proceedings Archive*. 2006.

[19] Shubham Sharma et al. "Use of motion capture in 3D animation: motion capture systems, challenges, and recent trends". In: *2019 international conference on machine learning, big data, cloud and parallel computing (comitcon)*. IEEE. 2019, pp. 289–294.

[20] Jörg Spörri, Christian Schiefermüller, and Erich Müller. "Collecting kinematic data on a ski track with optoelectronic stereophotogrammetry: A methodological study assessing the feasibility of bringing the biomechanics lab to the field". In: *PLoS One* 11.8 (2016), e0161757.

[21] Alberto Ferrari et al. "Quantitative comparison of five current protocols in gait analysis". In: *Gait & posture* 28.2 (2008), pp. 207–216.

[22] Roy B Davis III et al. "A gait analysis data collection and reduction technique". In: *Human movement science* 10.5 (1991), pp. 575–587.

[23] Aurelio Cappozzo et al. "Position and orientation in space of bones during movement: anatomical frame definition and determination". In: *Clinical biomechanics* 10.4 (1995), pp. 171–178.

[24] C Frigo et al. "Functionally oriented and clinically feasible quantitative gait analysis method". In: *Medical and Biological Engineering and Computing* 36 (1998), pp. 179–185.

[25] M Rabuffetti and P Crenna. "A modular protocol for the analysis of movement in children". In: *Gait Posture* 20 (2004), S77–S78.

[26] Alberto Leardini et al. "Rear-foot, mid-foot and fore-foot motion during the stance phase of gait". In: *Gait & posture* 25.3 (2007), pp. 453–462.

[27] A Leardini et al. "An anatomically based protocol for the description of foot segment kinematics during gait". In: *Clinical biomechanics* 14.8 (1999), pp. 528–536.

[28] Edward S Grood and Wilfredo J Suntay. "A joint coordinate system for the clinical description of three-dimensional motions: application to the knee". In: (1983).

[29] Anne Elisabeth Carolus et al. "The interdisciplinary management of foot drop". In: *Deutsches Ärzteblatt International* 116.20 (2019), p. 347.

[30] John D Stewart. "Foot drop: where, why and what to do?" In: *Practical neurology* 8.3 (2008), pp. 158–169.

[31] Subhadra L Nori and Michael F Stretanski. "Foot drop". In: (2020).

[32] Javad Parvizi. *High yield orthopaedics E-Book*. Elsevier Health Sciences, 2010, pp. 284–285.

[33] Rahul K Nath and Chandra Somasundaram. "Incidence, etiology, and risk factors associated with foot drop". In: *Eplasty* 23 (2023).

[34] Clare Walton et al. "Rising prevalence of multiple sclerosis worldwide: Insights from the Atlas of MS". In: *Multiple Sclerosis Journal* 26.14 (2020), pp. 1816–1821.

[35] Maureen S Durkin et al. "Prevalence of cerebral palsy among 8-year-old children in 2010 and preliminary evidence of trends in its relationship to low birthweight". In: *Paediatric and perinatal epidemiology* 30.5 (2016), pp. 496–510.

[36] Jonathan Morena, Anirudh Gupta, and J Chad Hoyle. "Charcot-Marie-Tooth: from molecules to therapy". In: *International Journal of Molecular Sciences* 20.14 (2019), p. 3419.

[37] Lokesh C Wijesekera and P Nigel Leigh. "Amyotrophic lateral sclerosis". In: *Orphanet journal of rare diseases* 4 (2009), pp. 1–22.

[38] Jessica Forbes, Sunil Munakomi, and Heather Cronovich. *Romberg Test*. StatPearls Publishing, Treasure Island (FL), 2022. URL: http://europepmc.org/books/NBK563187.

[39] Liberson Wt. "Functional electrotherapy: stimulation of the peroneal nerve synchronized with the swing phase of the gait of hemiplegic patients". In: *Arch Phys Med Rehabil* 42 (1961), p. 101.

[40] Paul N Taylor et al. "Patients' perceptions of the Odstock Dropped Foot Stimulator (ODFS)". In: *Clinical rehabilitation* 13.5 (1999), pp. 439–446.

[41] Alfred Adler. *Understanding human nature: The psychology of personality*. General Press, 2020.

[42] Erik B Simonsen et al. "Redistribution of joint moments during walking in patients with drop-foot". In: *Clinical Biomechanics* 25.9 (2010), pp. 949–952.

[43] EB Simonsen et al. "Bone-on-bone forces during loaded and unloaded walking". In: *Cells Tissues Organs* 152.2 (1995), pp. 133–142.

[44] Hasan Kemal Surmen, Nazif Ekin Akalan, and Yunus Ziya Arslan. "Design, manufacture, and selection of Ankle-Foot-Orthoses". In: *Advanced Methodologies and Technologies in Artificial Intelligence, Computer Simulation, and Human-Computer Interaction*. IGI Global, 2019, pp. 250–266.

[45] Bryan S Malas. "What variables influence the ability of an AFO to improve function and when are they indicated?" In: *Clinical Orthopaedics and Related Researchő* 469 (2011), pp. 1308–1314.

[46] DJJ Bregman et al. "Spring-like Ankle Foot Orthoses reduce the energy cost of walking by taking over ankle work". In: *Gait & posture* 35.1 (2012), pp. 148–153.

[47] Morshed Alam, Imtiaz Ahmed Choudhury, Azuddin Bin Mamat, et al. "Mechanism and design analysis of articulated ankle foot orthoses for drop-foot". In: *The Scientific World Journal* 2014 (2014).

[48] Dimas Adiputra et al. "A review on the control of the mechanical properties of ankle foot orthosis for gait assistance". In: *Actuators*. Vol. 8. 1. MDPI. 2019, p. 10.

[49] Arnaud Delafontaine et al. "Rigid ankle foot orthosis deteriorates mediolateral balance control and vertical braking during gait initiation". In: *Frontiers in human neuroscience* 11 (2017), p. 214.

[50] Bi rol Balaban et al. "The effect of hinged ankle-foot orthosis on gait and energy expenditure in spastic hemiplegic cerebral palsy". In: *Disability and rehabilitation* 29.2 (2007), pp. 139–144.

[51] Nancy M Hylton. "Postural and Functional Impact of Dynamic AFOs and FOs in a Pediatric Population." In: *JPO: Journal of Prosthetics and Orthotics* 2.1 (1989), pp. 40–53.

[52] Nancy Hylton. *Dynamic orthotic concepts: background and experiences*. Verlag Orthopädie-Technik, 2000.

[53] Suat Erel et al. "The effects of dynamic ankle-foot orthoses in chronic stroke patients at three-month follow-up: a randomized controlled trial". In: *Clinical rehabilitation* 25.6 (2011), pp. 515–523.

[54] Farah Syazwani Shahar et al. "A review on the orthotics and prosthetics and the potential of kenaf composites as alternative materials for ankle-foot orthosis". In: *Journal of the mechanical behavior of biomedical materials* 99 (2019), pp. 169–185.

[55] Tribedi Sarma et al. "Material selection and development of ankle foot orthotic device". In: *Materials Today: Proceedings* 18 (2019), pp. 2509–2514.

[56] Giulia Rogati, Paolo Caravaggi, and Alberto Leardini. "Design principles, manufacturing and evaluation techniques of custom dynamic ankle-foot orthoses: a review study". In: *Journal of Foot and Ankle Research* 15.1 (2022), p. 38.

[57] Egle Vasiliauskaite et al. "Additive manufacturing of ankle-foot Orthosis with predefined ankle stiffnessa case report". In: *JPO: Journal of Prosthetics and Orthotics* 32.4 (2020), pp. 310–318.

[58] Xianzhong Meng et al. “Application experience and patient feedback analysis of 3D printed AFO with different materials: a random crossover study”. In: *BioMed Research International* 2021 (2021).

[59] Zhen Liu et al. “Additive manufacturing of specific ankle-foot orthoses for persons after stroke: A preliminary study based on gait analysis data”. In: *Math. Biosci. Eng* 16.6 (2019), pp. 8134–8143.

[60] Dong-Sik Chae et al. “The functional effect of 3D-printing individualized orthosis for patients with peripheral nerve injuries: Three case reports”. In: *Medicine* 99.16 (2020).

[61] Yong Ho Cha et al. “Ankle-foot orthosis made by 3D printing technique and automated design software”. In: *Applied bionics and biomechanics* 2017 (2017).

[62] Elisa S Arch and Darcy S Reisman. “Passive-dynamic ankle-foot orthoses with personalized bending stiffness can enhance net plantarflexor function for individuals poststroke”. In: *JPO: Journal of Prosthetics and Orthotics* 28.2 (2016), pp. 60–67.

[63] Constantinos Mavroidis et al. “Patient specific ankle-foot orthoses using rapid prototyping”. In: *Journal of neuroengineering and rehabilitation* 8.1 (2011), pp. 1–11.

[64] Haydar Gök et al. “Effects of ankle-foot orthoses on hemiparetic gait”. In: *Clinical rehabilitation* 17.2 (2003), pp. 137–139.

[65] Jean-Pierre Kruth et al. “Lasers and materials in selective laser sintering”. In: *Assembly Automation* 23.4 (2003), pp. 357–371.

[66] Alida Mazzoli. “Selective laser sintering in biomedical engineering”. In: *Medical & biological engineering & computing* 51 (2013), pp. 245–256.

[67] Omar A Mohamed, Syed H Masood, and Jahar L Bhowmik. “Optimization of fused deposition modeling process parameters: a review of current research and future prospects”. In: *Advances in manufacturing* 3 (2015), pp. 42–53.

[68] Kumaresan Rajan et al. “Fused deposition modeling: process, materials, parameters, properties, and applications”. In: *The International Journal of Advanced Manufacturing Technology* 120.3-4 (2022), pp. 1531–1570.

[69] Ferry PW Melchels, Jan Feijen, and Dirk W Grijpma. "A review on stereolithography and its applications in biomedical engineering". In: *Biomaterials* 31.24 (2010), pp. 6121–6130.

[70] Chao Cai et al. "Comparative study on 3D printing of polyamide 12 by selective laser sintering and multi jet fusion". In: *Journal of Materials Processing Technology* 288 (2021), p. 116882.

[71] Sergio Morales-Planas et al. "Multi Jet Fusion PA12 manufacturing parameters for watertightness, strength and tolerances". In: *Materials* 11.8 (2018), p. 1472.

[72] Deema Totah et al. "The impact of ankle-foot orthosis stiffness on gait: A systematic literature review". In: *Gait & posture* 69 (2019), pp. 101–111.

[73] Nicola Eddison, Miriam Mulholland, and Nachiappan Chockalingam. "Do research papers provide enough information on design and material used in ankle foot orthoses for children with cerebral palsy? A systematic review". In: *Journal of children's orthopaedics* 11.4 (2017), pp. 263–271.

[74] DJJ Bregman et al. "A new method for evaluating ankle foot orthosis characteristics: BRUCE". In: *Gait & posture* 30.2 (2009), pp. 144–149.

[75] Deema Totah et al. "Design and evaluation of the SMApp: a stiffness measurement apparatus for ankle–foot orthoses". In: *Mechatronics* 77 (2021), p. 102572.

[76] Benjamin R Shuman et al. "Comparison of five different methodologies for evaluating ankle–foot orthosis stiffness". In: *Journal of neuroengineering and rehabilitation* 20.1 (2023), pp. 1–9.

[77] G Rogati et al. "A novel apparatus to assess the mechanical properties of Ankle-Foot Orthoses: Stiffness analysis of the Codivilla spring". In: *Journal of Biomechanics* 142 (2022), p. 111239.

[78] Niels FJ Waterval et al. "Precision orthotics: optimising ankle foot orthoses to improve gait in patients with neuromuscular diseases; protocol of the PROOF-AFO study, a prospective intervention study". In: *BMJ open* 7.2 (2017), e013342.

[79] Jill Dawson et al. "A patient-based questionnaire to assess outcomes of foot surgery: validation in the context of surgery for hallux valgus". In: *Quality of life research* 15 (2006), pp. 1211–1222.

[80] Paolo Caravaggi et al. "Development of a Novel Passive-Dynamic Custom AFO for Drop-Foot Patients: Design Principles, Manufacturing Technique, Mechanical Properties Characterization and Functional Evaluation". In: *Applied Sciences* 12.9 (2022), p. 4721.

[81] Giulia Rogati et al. "Validation of a novel Kinect-based device for 3D scanning of the foot plantar surface in weight-bearing". In: *Journal of foot and ankle research* 12 (2019), pp. 1–8.

[82] Dustin Bruening and James G Richards. "Skiing-Skating: Optimal ankle axis position for articulated boots". In: *Sports biomechanics* 4.2 (2005), pp. 215–225.

[83] Jennifer L Durkin and James J Dowling. "Analysis of body segment parameter differences between four human populations and the estimation errors of four popular mathematical models". In: *J. Biomech. Eng.* 125.4 (2003), pp. 515–522.

[84] J Gavin Reid and Robert K Jensen. "Human body segment inertia parameters: a survey and status report". In: *Exercise and sport sciences reviews* 18.1 (1990), pp. 225–242.

[85] Michael J Pavol, Tammy M Owings, and Mark D Grabiner. "Body segment inertial parameter estimation for the general population of older adults". In: *Journal of biomechanics* 35.5 (2002), pp. 707–712.

[86] Richard N Hinrichs. "Regression equations to predict segmental moments of inertia from anthropometric measurements: an extension of the data of Chandler et al.(1975)". In: *Journal of Biomechanics* 18.8 (1985), pp. 621–624.

[87] Giordano Valente et al. "nmsBuilder: Freeware to create subject-specific musculoskeletal models for OpenSim". In: *Computer methods and programs in biomedicine* 152 (2017), pp. 85–92.

[88] Paolo De Leva. "Adjustments to Zatsiorsky-Seluyanov's segment inertia parameters". In: *Journal of biomechanics* 29.9 (1996), pp. 1223–1230.